Three-Zone Modeling of a Mobile Air Conditioning Condenser

M. J. Kempiak and R. R. Crawford

ACRC TR-03 April 1991

For additional information:

Air Conditioning and Refrigeration Center
University of Illinois
Mechanical & Industrial Engineering Dept.
1206 West Green Street
Urbana, IL 61801

(217) 333-3115

Prepared as part of ACRC Project #09
Mobile Air Conditioning Systems
R. R. Crawford, Principal Investigator

The Air Conditioning and Refrigeration Center was founded in 1988 with a grant from the estate of Richard W. Kritzer, the founder of Peerless of America Inc. A State of Illinois Technology Challenge Grant helped build the laboratory facilities. The ACRC receives continuing support from the Richard W. Kritzer Endowment and the National Science Foundation. The following organizations have also become sponsors of the Center.

Acustar Division of Chrysler
Allied-Signal, Inc.
Amana Refrigeration, Inc.
Bergstrom Manufacturing Co.
Caterpillar, Inc.
E. I. du Pont de Nemours & Co.
Electric Power Research Institute
Ford Motor Company
General Electric Company
Harrison Division of GM
ICI Americas, Inc.
Johnson Controls, Inc.
Modine Manufacturing Co.
Peerless of America, Inc.
Environmental Protection Agency
U. S. Army CERL
Whirlpool Corporation

For additional information:

Air Conditioning & Refrigeration Center
Mechanical & Industrial Engineering Dept.
University of Illinois
1206 West Green Street
Urbana IL 61801

217 333 3115

TABLE OF CONTENTS

LIST OF TABLES

Page

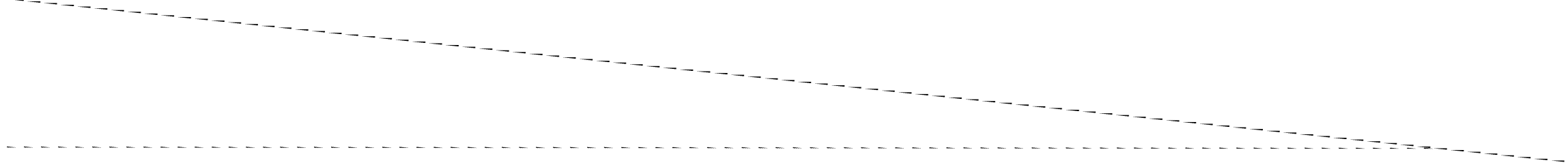

LIST OF FIGURES

Page

LIST OF SYMBOLS

A	cross-sectional area of tube	ft^2 [m^2]
C	capacitance term for refrigerant and wall	Btu/lb_m-°F [kJ/kg-K]
d	inner tube diameter	ft [m]
E	stored energy	Btu [kJ]
f	friction factor	[-]
f_i	fraction of total tube length	[-]
F_f	surface forces in control volume	lb_f [N]
g	gravity	ft/s^2 [m/s^2]
h	enthalpy	Btu/lb_m [kJ/kg]
h_f	friction-head loss	ft [m]
L	total tube length	ft [m]
m	mass	lb_m [kg]
P	pressure	psia [kPa]
Q	rate of heat transfer	Btu/h [kW]
R	residual equation	[-]
t	time	[s]
T	temperature	°F [K]
U	overall heat transfer coefficient per tube length	Btu/h-ft-°F [kW/m-K]
v	fluid velocity	ft/s [m/s]
$\dot{V}$	volumetric flow rate	ft^3/min [m^3/s]
w	mass flow rate	lb_m/s [kg/s]
δt	time step	[s]
ρ	density	lb_m/ft^3 [kg/m^3]
ω	humidity ratio	$lb_{m\ water}/lb_{m\ dry\ air}$ [$kg_{water}/kg_{dry\ air}$]

SUBSCRIPTS

air	air side
cond	condensing section
cv	control volume
dsh	desuperheating section
f	outlet of condensing section and inlet of subcooling section or outlet of incomplete condensing section
g	outlet of superheated section and inlet of condensing section
in	inlet of superheated section or inlet of control volume
k	number of time steps
out	outlet of subcooling section or outlet of control volume
ref	refrigerant side
sc	subcooling section

SUPERSCRIPTS

'	average of the inlet and outlet values of the control volume

CHAPTER 1
OVERVIEW

1.1. Objectives

Due to environmental concerns, R-12 (dichlorodifluoromethane), a refrigerant commonly used in mobile air conditioning, is being replaced with R-134a (1,1,1,2-tetrafluoroethane). This new refrigerant requires numerous changes in equipment design to be as reliable and efficient as R-12 which has been developed over several decades. But mobile systems differ from many other air conditioning systems since they operate under additional transient conditions. Some of these transients include the engine speed, passenger compartment air temperature, air flow rates across the evaporator and condenser, and the cycling of the compressor to prevent evaporator frosting. With the increased use of microprocessors in automobiles, advanced adaptive and optimal control algorithms can be employed to improve the overall system performance.

The objectives of this study are to develop and test a transient condenser model for use in a mobile air conditioning system simulation to study optimal control algorithms. Since the system simulation time must be held to a minimum to allow a reasonable time between testings of the control algorithms, the condenser model was developed to achieve desired accuracy without the complexity of a finite-difference method. Incorporated in this model are calculations to determine the pressure drop within the condenser. Also, this model has physical parameters that can be varied to analyze potential design changes without exhaustive experimental efforts. The test facility described in this document was used to generate the necessary data for developing and verifying the condenser model. The test facility is part of the automotive air conditioning section of the Air Conditioning and Refrigeration Center at the University of Illinois.

1.2. Literature Review

This section contains the reviews obtained from the literature search on transient vapor-compression cycles. The chapter begins with a few steady-state models to obtain simpler model

equations. Since this paper is particularly interested in the condenser transients, an extensive search on crossflow heat exchanger transients was also performed. Experimental studies of transient vapor-compression cycles are included which emphasize the determination of the mass flow rate within each component. The section continues with reports on the special topics of transient studies during start-up and shutdown, and then transient models of the entire system. The system model reviews concentrate on the condenser transients since this is the component under consideration.

1.2.1. Modeling of Vapor-Compression Systems

Ellison, Creswick, Rice, Jackson, and Fisher [1] from Oak Ridge National Laboratory present a system model of a heat pump based solely on the underlying physical principles. The model is intended to aid in the understanding of the interactions between the components and the changes in system performance based on changes in individual components. For the condenser, the model first calculates the fraction of the condenser required for desuperheating. The fraction of the coil in the two-phase section is then calculated. The remaining coil length is in the subcooled region. If the sum of the two-phase and desuperheated fractions is greater than one, an exit quality is calculated. Heat transfer rates are determined from these calculations and the exit air temperature is a weighted average of the three sections. The paper contains useful suggestions on component and system modeling based on the experiences of the authors. Also included in the paper are experimental results to support the model.

Davis and Scott [2] describe a model built for the evaluation of off-design conditions, optimization of components within the system, and estimation of the effects of different refrigerants. Since the designer would use this model frequently, it was desirable to achieve reasonable accuracy with low computing time. This was accomplished with models based on fundamental principles coupled with carefully chosen empirical parameters based on relatively simple component testing. Great detail is given to the compressor model and the empirical parameters within this model.

Davis, Chianese, and Scott [3] outline the basic theory and techniques used to develop the Air-Conditioning Analytical Simulation Package (A/CASP). The condenser model portion of this system analysis computes the performance of the condenser based on a given geometry at specified refrigerant and gas inlet states and flow rates. The overall heat transfer coefficient was allowed to be modified to account for dirt buildup on the condenser. Once again, the condenser was divided into three sections and treated as three separate heat exchangers. The solution process first assumes a constant pressure within each section to determine the length of the section and then adjusts for the pressure drop. Convergence with this approach is believed to be quite rapid. The other components are also described in this paper. The results of the model are also incorporated into a vehicle pull-down simulation. All of the models are compared and necessary parameters are adjusted to assure model accuracy to system tests.

Martin [4] describes the approach employed in a digital computer simulation of water-source heat pump performance. The paper details the curve fits used in the model to properly simulate the system components. The condenser is divided into three sections and evaluated as three individual heat exchangers. Pressure drops are not considered on the refrigerant side. Many simulation runs are presented showing the effects of refrigerant flow rates, condenser size, air flow rates, etc. This model incorporates a Newton-Raphson technique to solve for a set of non-linear equations which can be solved simultaneously for a steady-state operating condition.

1.2.2. Transient Response of Crossflow Heat Exchangers

Kays and London [5] dedicate an entire chapter to the transient response of heat exchangers, condensers, and evaporators. Fifteen solutions are given for two-fluid heat exchangers and an insulated duct through which fluid is flowing. These solutions are based on step inputs of either or both of the fluid temperatures. The nondimensional parameters are defined and described on a physical basis. Reference sources are provided for those interested in periodic or sinusoidal inputs for control applications. An example is given to clarify the solution technique.

Dusinberre [6] solves the transient response for a gas to air single-pass crossflow heat exchanger in a gas-turbine regenerator. Digital computer programming is considered as a solution technique along with hand calculations. The heat exchanger is subdivided into several sections and the temperature of the gas and metal surface are calculated by numerical methods. Every step in the solution process is shown providing a detailed analysis of the transients in heat exchangers.

Myers, Mirchell, and Norman [7] simulate the behavior of a single-phase crossflow heat exchanger with one fluid mixed. An approximate integral technique was used to obtain the solution to the governing differential equations for a step change in the mixed fluid temperature, assuming the wall capacitance is large. Design curves are included for calculating the transient as a function of time for a step change in the condensing and noncondensing fluid. Also, new parameters for transient analysis are suggested which allow greater insight into the transient problem.

Myers, Mitchell, and Linderman [8] discuss transient response of evaporators or condensers to a step change in the temperature of the infinite capacitance rate fluid temperature. Also considered are intermediate and large values of wall capacitance. Analytical and finite-difference methods are used to obtain solutions. These equations are presented and guidelines for which solution to be used are set forth. An approximate solution also exists for hand calculations.

Yamashita, Izumi, and Yamaguchi [9] use finite-difference methods to calculate the exit fluid temperature responses for evaporators and condensers in crossflow with neither fluid mixed. A transient is initiated by a step change in the inlet temperature. The effects of the governing parameters are illustrated by varying one parameter and fixing all other parameters to the same constant values. The data presented is limited but is not restricted to large wall capacitance.

Romie [10] determines the transient mixed mean temperature of two gases leaving a crossflow heat exchanger due to a unit step temperature increase in either of the two gases. The solutions are determined using Laplace transform methods. These results are then plotted to give temperature responses for a specified range of parameters and responses are given for all values of the governing equations. Any type of input can be simulated by applying methods of linear

analysis. This method is believed to be shorter than the time required to use a finite-difference method.

Gvozdenaz [11] presents a detailed analytical solution to the energy equations governing convective heat transfer between a heat exchanger core. The core is at an arbitrary spatial temperature distribution with incoming fluids at constant mass velocities with arbitrary time varying temperatures. The thermal capacitance of the two fluids in the heat exchanger are assumed negligibly small relative to the thermal capacity of the heat exchanger core. Presented are the mean mixed fluid temperatures at the exit and temperature distributions of both fluids. Solutions are found by using Laplace transform methods and special functions in the form of series of modified Bessel equations.

Spiga and Spiga [12] determine the two-dimensional transient behavior of a gas-to-gas crossflow heat exchanger. The analytical method used determines the transient distribution of temperatures in the core wall and in the unmixed gases. Large wall capacitance is assumed allowing the general solutions to be deduced by Laplace transform methods and presented as integrals of modified Bessel functions. Inputs such as step, ramp, and exponential responses have been simulated with little computer time. The results are presented graphically for a wide range of the number of transfer units.

Wedekind, Bhatt, and Beck [13] use system mean void fraction modeling to convert a two-phase condensing flow into a type of lumped parameter system. This method allows for simple closed form solutions in terms of the important system parameters. The system mean void fraction is assumed to be time-invariant. This allows the problem to be uncoupled from the transient form of the momentum equation. Transients are considered for changes in the inlet flow rate. Experimental data is presented to substantiate the model accuracy.

Gartner and Harrison [14] express the dynamic characteristics of a water-to-air crossflow heat exchanger in terms of transfer functions. These functions are modified resulting in excellent correlations throughout the frequency range and the functions are reduced to a rational form. A discussion is then given on the experimental apparatus used to verify the model. Model results

were compared to the experimental results. Limitations in the model accuracy are either corrected through parameter adjustments or explained by the assumptions assumed for the initial analysis.

Schoenberg [15] describes a mathematical model to predict the dynamic behavior of a single-tube condenser. The model uses transfer functions derived from linearized forms of the fundamental heat-transfer and flow equations. This model relates the condensing pressure and varying liquid-vapor interface to various disturbance variables. Experimental frequency responses of a gas-cooled mercury condenser are compared to the model for verification. Additional investigations are made into the effects of model predictions due to uncertainties in evaluating some of the transfer functions. Simplifications to the model were made through evaluations of the coefficients of the transfer functions influence on the predicted frequency responses.

1.2.3. Experimental Studies of Transients

Neckowitz, Murphy, Goldschmidt, and Johnston [16] present their findings on the transient response of air conditioners due to the time required for flooding upstream of the throttling device. A hot wire anemometer was placed in the liquid line of an air conditioner and was shown to give a measure of the state of the refrigerant. This state corresponds to an anemometer signal representing the presence of vapor. Data are shown for tests, with analysis and conclusions drawn form these runs.

Tanaka, Ikeuchi, and Yamanaka [17] performed an experimental study of the dynamics of a 1-ton (3.5 KW) heat pump. The pressures and temperatures were recorded continuously. The mass in each section of the system was determined by closing valves at the section boundaries simultaneously, transferring the refrigerant between these valves at set time intervals into a separate cylinder and weighing the refrigerant in the cylinder. Then the system was recharged and ran until the next time interval. Two cases were discussed: pull-down during start-up and start-up within a cycling period. Four system changes were evaluated based on the findings of these tests. The schemes included changing the accumulator size, installing a magnetic valve between the condenser

and capillary tube to cycle on and off in conjunction with the compressor operation, and use of a reverse cycle.

Mulroy and Didion [18] perform a similar experiment to Tanaka, et al. but use a 3 ton (10.5 KW) system. These test were evaluated for a 6-minute-on and 24-minute-off cycle, which is a typical dynamic period for air conditioning operation. The results from these tests were compared to single and double time constant regressive approximations and to the time constant calculated from the evaporator mass and heat transfer coefficient. Concluding remarks state that for the dynamics of a given unit to be characterized with less burden, all of the components must be considered individually and then lumped as a group. When comparing this paper to Tanaka et al., the difference in results are believed to be explained by the different systems under consideration.

Miller [19] reported on the results of a single-speed cycling test conducted on a nominal three-ton, split-system air-to-air heat pump. Continuous measurements of the weight of the refrigerant in the outdoor section, the coil, the accumulator, and the compressor, were made with a counterbalanced force transducer arrangement. The conclusion discusses observable improvements in cycling COP and capacity by controlling off-cycle refrigerant migration.

Belth and Tree [20] describe the system designed, major problems encountered, and give preliminary results of a system to continuously measure change in refrigerant mass in the evaporator, condenser, accumulator, and compressor of a heat pump. By measuring the weight of these individual components with balance beams during start-up and shutdown, the change in mass in the liquid line was calculated. The results are then compared with previous experiments conducted by Tanaka et al. and Mulroy and Didion.

1.2.4. Start-Up and Shutdown Transient Models

Josiassen [21] simulates the start-up sequence of a traditional evaporation refrigerating system with hermetic compressor and capillary tube. The model uses a "pot" to describe the compressor housing, condenser, and evaporator. In this system, the "pot" has the following features: only the compressor "pot" has oil, the shell of the "pot" is at the same temperature as the

charge, the "pot" is assumed to have an average external heat transfer coefficient, and loss-free inlet and outlet tubes. Pressure drops were ignored in all components except the orifice to make the calculations simpler. Also, simple mass and energy balances were used in the model. A simple Euler integration method is used for the solution routine. When compared to experimental data, the simulation is believed to contain the important trends but requires improved component models.

Murphy and Goldschmidt [22] model the start-up transients in a residential air conditioner. The condenser is divided into sections to allow for equally divided refrigerant flow rates through parallel flow paths to simplify pressure drop calculations. A steady-state energy balance is performed on the air-side. Coupled with the heat transfer equation for the superheated section, the length of the superheated section is determined assuming a constant mass flow rate for this section. With an energy balance on the heat exchanger wall, the future temperature of the wall is computed explicitly. The subcooled section is computed similar to the superheated section except discrete temperatures are considered instead of a mean temperature. This can be done since the two-phase region is assumed to be under constant saturated conditions. With the lengths known for each section, the pressure drop is determined. The condenser model gives good results when compared to the test unit data but lacks generality since an evaporator model is not included.

Murphy and Goldschmidt [23] also looked at shutdown transients. These transients are driven by the pressure difference within the system. Energy transfer and flow regimes exist as a result of the pressure imbalance. Assuming no backflow of refrigerant through the compressor discharge, a lumped orifice equation is used from the condenser to the evaporator to predict the pressure drop. The condenser and evaporator are treated as tanks containing two-phase mixtures with either net inflow or outflow where the tanks and two-phase mixtures are in thermal equilibrium. An explicit continuity equation is used to determine the outlet mass flow rate. The application of the first law of thermodynamics to the tank determines the new tank temperature iteratively since the refrigerant properties depend on this temperature. The model is compared to test results and included is a discussion of the results and physical interpretations.

1.2.5. General Transient Models

Dhar and Soedel [24, 25] present a two-part paper: Part 1 describes the development of a quasi-steady model, and Part 2 explains the computational technique used and some model results. The model separates the condenser into three cases: fully superheated, mixed, and mixed with subcooled refrigerant. The mixed region is defined as the volume of the condenser that contains the superheated vapor and the saturated refrigerant. Since the saturated refrigerant occupies most of the mixed region, the condenser is characterized by a saturation temperature . The bulk liquid and bulk vapor states are evaluated as a saturated vapor and saturated liquid at the saturation temperature. The superheated, mixed, and subcooled regions are considered as control volumes. Each control volume is modeled as a "stirred tank" in which the outlet conditions from the control volume are equal to the bulk conditions in the control volume and the size of the control volume is allowed to vary between time steps. Conservation of mass and energy are used to establish the state of the refrigerant in the control volume.

A simultaneous solution technique is employed solving for algebraic and ordinary differential equations where the differential equations are solved using an explicit Euler method. The time step was determined by interval halving. For each time step, pressure drops are neglected and then calculated at the end of each cycle. Empirical parameters were chosen for two-phase heat transfer coefficients, oil transportation, etc.

Chi and Didion [26] simulate the transient performance of a heat pump. Their model divides the heat exchanger into small elements. Analysis of the element starts from a set of governing differential equations defining mass, momentum, and energy balances for transient one-dimensional flow of the air and refrigerant streams. Each equation is reduced to a lumped parametric form. An energy balance is performed on the heat exchanger wall where the solution technique is an explicit, first-order, Euler method. The momentum equation is used to determine refrigerant pressure drops in the heat exchanger. Using this method, the time step was determined by interval halving. All fluid properties and coefficients for single-phase and two-phase fluid heat, mass, and momentum transfer were determined by correlations in the open literature.

MacArthur [27] uses a first principles formulation to simulate transients in vapor-compression heat pumps. The heat exchanger is discretized into a series of control volumes. Energy and continuity equations are applied to the control volume for the refrigerant and air sides. Also considered is the energy balance on the heat exchanger wall. The time-dependent momentum equation and associated pressure drop calculations are not considered. The equations are integrated with respect to time and distance. With the flow assumed constant, there are three fully implicit coupled energy equations for a control volume in terms of the heat exchanger wall, refrigerant fluid, and secondary fluid.

The solution technique starts by solving for all the energy balances in terms of the refrigerant consecutively for each control volume. These balances are based on unknown values. Next, the secondary fluid is evaluated consecutively for each control volume. Similarly, the energy balance for the heat exchanger wall is evaluated. This process is repeated until the new calculated values are within a given percentage of the old values. Then the next time step is performed in a similar manner. The time increment and grid spacing are arbitrary since the method is implicit but accuracy of the solutions is still a function of these values. The only curve-fit data is that concerning the physical properties of the refrigerant and correlations defining the surface coefficients.

1.3. Model Approach

To keep computational time to a minimum, a finite-difference approach or a numerical integration technique were considered inappropriate for the transient condenser model. This eliminates many of the crossflow heat exchanger models discussed in the literature review. Also, all of the models discussed in the section on transient response of crossflow heat exchangers (1.2.2.) were only concerned within an increase in the inlet temperature of either fluid. Since the model needed to simulate a mobile air conditioning system, a change in the inlet refrigerant pressure, refrigerant temperature, refrigerant mass flow rate, air temperature, and air mass flow rate were all considered to be possible varying conditions within the heat exchanger.

Dhar and Soedel determined the response of a condenser under transient conditions by dividing the condenser into two sections: mixing, and subcooling. By only having two sections, the computational time would be much smaller when compared to a finite-difference computation time. But the desuperheating section is lumped with the condensing section and saturated conditions are used to describe these two processes. Murphy and Goldschmidt [22] determined that the desuperheating section represents about 25% of the total condenser heat transfer. A better approach would be to divide the condenser into three sections: desuperheating, condensing, and subcooling. Martin [4] used this method in a steady-state analysis and solved the set of equations using a Newton-Raphson method. Also, Dhar and Soedel used the outlet state of the refrigerant to describe the mixing or subcooling section. A simple analysis will be performed to determine if the inlet, outlet, or average value under consideration best represents the control volume. The momentum equation will be included in the model to determine pressure drops in the heat exchanger.

CHAPTER 2

TRANSIENT CONDENSER MODEL

The dynamic model of the condenser is described in this chapter. A general description is included on the mass, energy, and momentum equations with relation to any section of the condenser under consideration. Specifics are then introduced for the four different possible sections of the heat exchanger, namely: desuperheating, condensing, subcooling, and partial condensing. The solution technique is described. Then, some of the specifics required to implement the computer program are addressed as well as the physical parameters incorporated in the model to analyze potential design changes without exhaustive experimental studies.

2.1. General Model Description

The condenser is simulated as a single length tube and fin heat exchanger. This model divides the condenser into three sections as shown in Figure 2.1: the desuperheating (dsh), condensing (cond), and subcooling (sc) regimes. The refrigerant enters the tube at a pressure P_{in}, a temperature T_{in}, and a mass flow rate w_{in}. It exists the desuperheating section as a saturated vapor at a temperature T_g which corresponds to a saturation pressure P_g. Mass stored in the desuperheating section is represented by m_{dsh} and w_g is the mass flow rate of refrigerant exiting this section. The length of the desuperheating section is $f_{dsh}L$ where L is the total tube length and f_{dsh} is the fraction of the condenser in the desuperheating regime. A similar labeling process is used on the condensing and subcooling regimes. The only difference is that the subscript for the outlet state of the condensing section is f and the subcooling section is out. The inlet and outlet air temperatures, $T_{air,in}$ and $T_{air,out}$, are temperatures representing the average air temperature of the inlet and outlet streams, respectively.

By subdividing the condenser, a complex heat exchanger is divided into three simple heat exchangers (liquid-to-gas, gas-to-gas, and simple condenser). Although the subdivisions of the condenser introduced new intermediate variables (w_{ref}, T_{ref}, P_{ref}, f_i) between sections, pressure

and temperature are no longer independent at these points since the refrigerant is by definition, either a saturated liquid or saturated vapor. The general mass, energy rate, and momentum equations applied to each of these sections for the refrigerant side are

$$w_{in} = w_{out} + \frac{dm_{cv}}{dt} \qquad \text{(mass)} \tag{2.1}$$

$$Q_{in} + w_{in}h_{in} = w_{out}h_{out} + \frac{dE_{cv}}{dt} \qquad \text{(energy)} \tag{2.2}$$

$$P_{in}A_{in} + w_{in}V_{in} = P_{out}A_{out} + w_{out}V_{out} + F_f + \frac{d(mV)_{cv}}{dt} \qquad \text{(momentum)} \tag{2.3}$$

where

A = cross-sectional flow area

E_{cv} = stored energy within the control volume

F_f = frictional forces on the refrigerant in the control volume

h = refrigerant enthalpy

m_{cv} = refrigerant mass in control volume

P = refrigerant pressure

Q_{in} = rate of heat transfer to the control volume

t = time

V = refrigerant velocity

w = mass flow rate

The subscripts "in" and "out" indicate variables associated with the inlet and outlet refrigerant streams and "cv" indicates that the specified variable is the total value for the control volume. The control volume terms in the time derivatives use values based on the inlet and outlet states of the section which best represent the entire control volume. This evaluation is discussed in the next section.

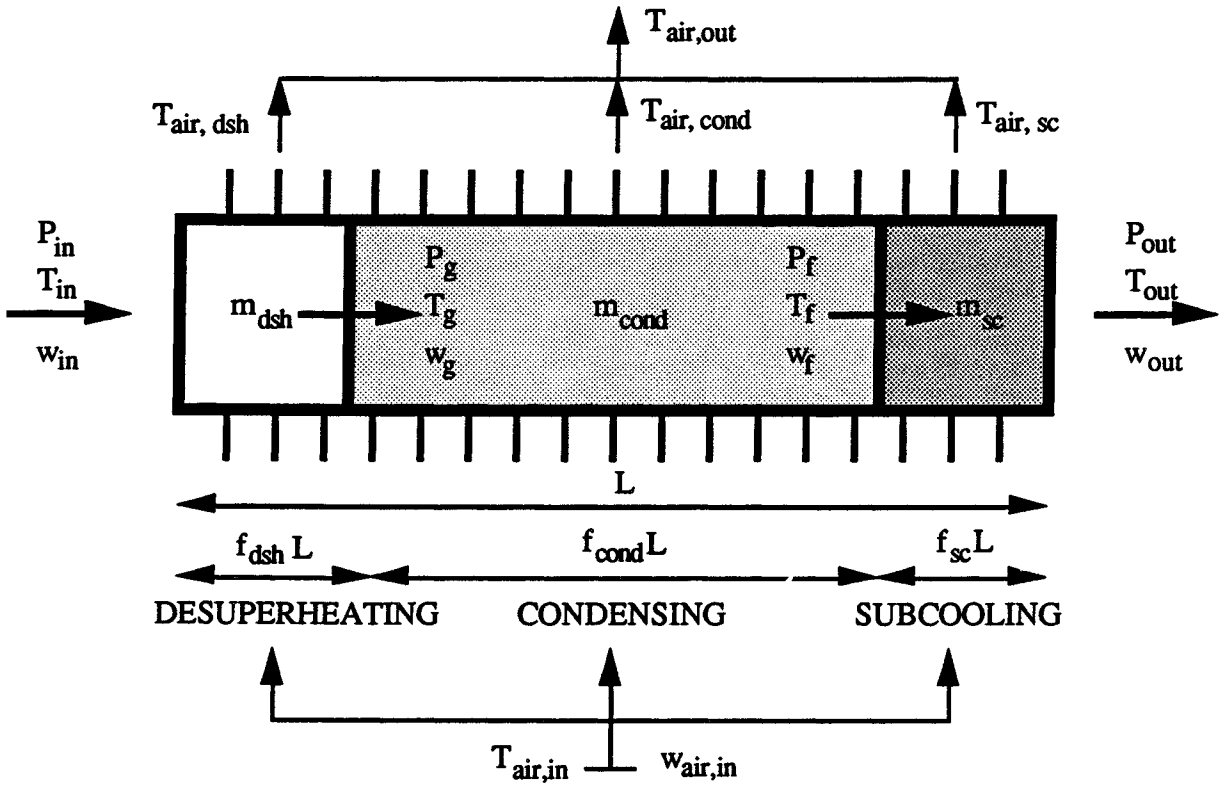

Figure 2.1. Labeling Diagram for Transient Condenser Model.

The momentum equation is included in the model to determine the pressure drop due to friction within the heat exchanger. The friction term, F_f, for a given section is expressed in terms of the friction-head loss by the Darcy-Weisbach equation [28]:

$$h_{f,i} = f \frac{f_i L}{d} \frac{V^2}{2} \tag{2.4}$$

where

d = inner tube diameter

f = Darcy friction factor

f_i = fraction of total heat exchanger for section i

$h_{f,i}$ = pipe head loss for section i

L = total tube length

V = refrigerant velocity

By expressing the velocity in terms of a mass flow rate, the Darcy-Weisbach equation may be written

$$h_{f,i} = f\frac{f_i L}{d}\frac{w^2}{2\rho^2 A^2} \tag{2.5}$$

The pressure drop for a tube is calculated based on the pipe-head loss, gravity, and density of the refrigerant:

$$\Delta P_i = \rho g_c h_{f,i} \tag{2.6}$$

where

ΔP_i = pressure drop in section i

The pressure drop is then related to the frictional force:

$$F_f = f\frac{f_i L}{d}\frac{w^2}{2\rho A} \tag{2.7}$$

Equation 2.3 may now be written:

$$P_{in}A_{in} + w_{in}V_{in} = P_{out}A_{out} + w_{out}V_{out} + f\frac{f_i L}{d}\frac{w^2}{2\rho A} + \frac{d(mV)_{cv}}{dt} \tag{2.8}$$

The heat transfer term for each section of the heat exchanger is expressed as

$$Q_i = f_i L U_i (T'_{air} - T'_{ref}) \tag{2.9}$$

where

f_iL = tube length of section i

T_{air} = average of the inlet and outlet air temperatures

T_{ref} = average of the inlet and outlet refrigerant temperatures

U_i = overall heat transfer coefficient per tube length for section i

The air side energy rate analysis results in the relation

$$Q_{in} = w_{air}C_{p,air}(T_{air,in} - T_{air,out}) \tag{2.10}$$

where

$C_{p,air}$ = air specific heat

For the modeling procedure, the inlet refrigerant pressure, temperature, and mass flow rate to the condenser are assumed to be known from the outlet state of the compressor. The inlet air temperature and mass flow rate are also assumed to be known. All sections receive inputs into the control volume from the outlets of the previous section.

2.2. Property Data

McLinden et al. [29] have determined the property data for R-134a. The property information needed to evaluate the governing equations was curve-fitted over the range of operating conditions for a typical automotive condenser. These data include density and enthalpy for the saturated vapor and saturated liquid regimes in terms of temperature. Also needed is the saturation temperature in terms of pressure and the saturation pressure in terms of temperature. The enthalpy and density of the superheated refrigerant are defined by pressures and temperatures. The specifics of these fits can be found in Appenedix A.

2.3. Control Volume Identification

To determine the best method for representing the control volume terms in Equations 2.1 to 2.3 (m_{cv}, E_{cv}, and $(mV)_{cv}$), a simple analysis is considered for a condenser operating under steady-state conditions with a constant heat flux. Figure 2.2 represents a typical temperature profile of R-12 passing through a condenser coil [30]. The desuperheating (0-5%), condensing (5-90%), and subcooling (90-100%) zones will vary 5 to 10 percent depending on the entering gas temperature and pressure, and leaving liquid temperature. The drop in temperature during the condensing process is the result of the friction loss through the condenser coil. From a visual interpretation of Figure 2.2, an average temperature based on the inlet and outlet temperatures of each of the three condensing sections properly represents these sections.

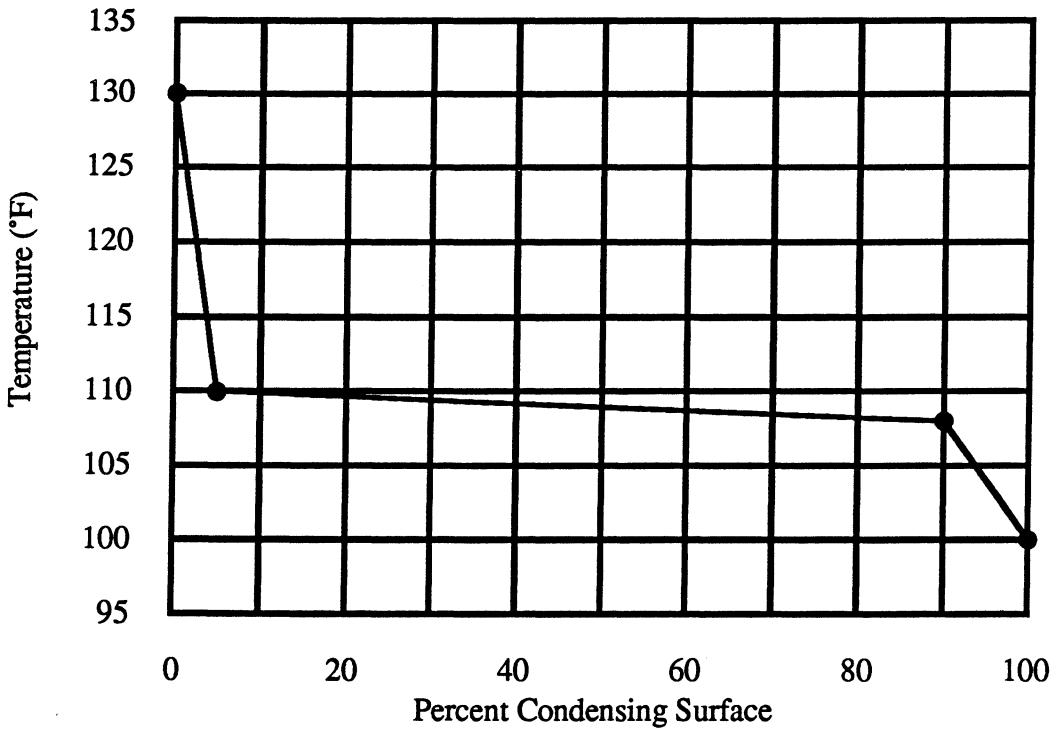

Figure 2.2. Temperature Versus Percent Condensing Surface for a Typical Condenser.

Based on the property data contained in Reference 30, the specific heat of the refrigerant as a function of the condenser surface is determined and is presented in Figure 2.3. If the heat flux is assumed constant, the quality varies linearly throughout the condenser. With the specific heat being an intensive property, the specific heat also varies linearly throughout the condensing process. The desuperheating and condensing sections are represented by an average specific heat determined with the inlet and outlet specific heats. The specific heat in the subcooling section is only a function of the saturated liquid specific heat but varies linearly since the temperature of the subcooled section is assumed to vary linearly. This section is also represented by the mean value of the inlet and outlet specific heats.

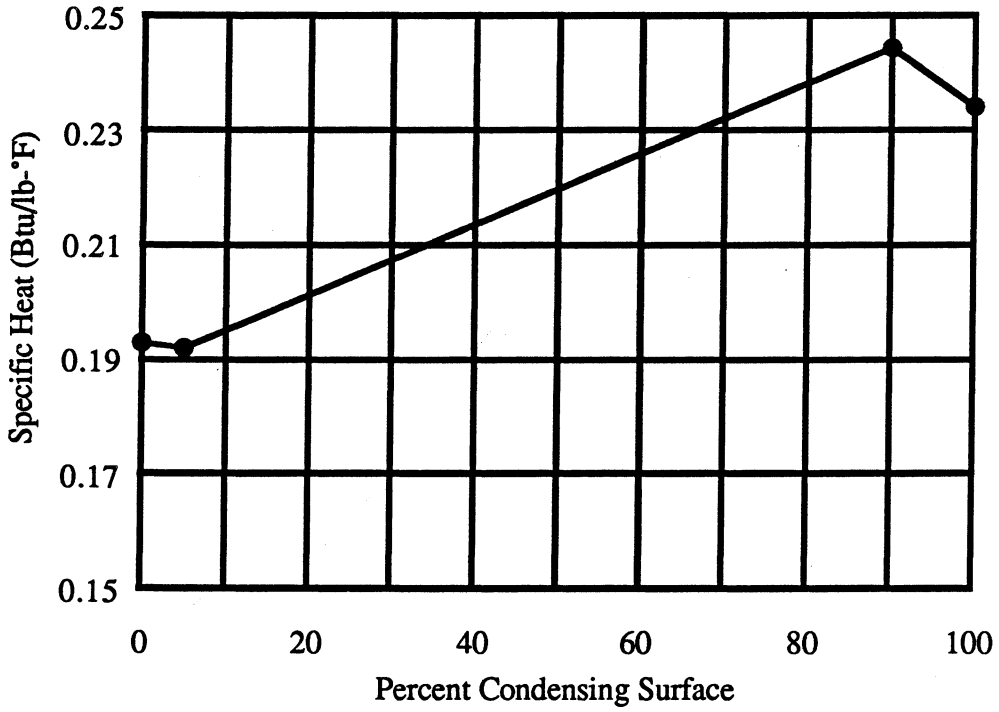

Figure 2.3. Specific Heat Versus Percent Condensing Surface for a Typical Condenser.

Figure 2.4 shows the density as a function of percent condensing surface. Based on the graph, an average value of the inlet and outlet densities can be used to identify the desuperheating and subcooling sections. Since the specific volume is an intensive property, the specific volume is

linear with respect to the quality. Therefore, the density, which is the inverse of the specific volume, follows an increasing trend. The condensing section is then best represented by the inlet (saturated vapor) density, rather than the outlet (liquid) or average of the inlet and outlet densities.

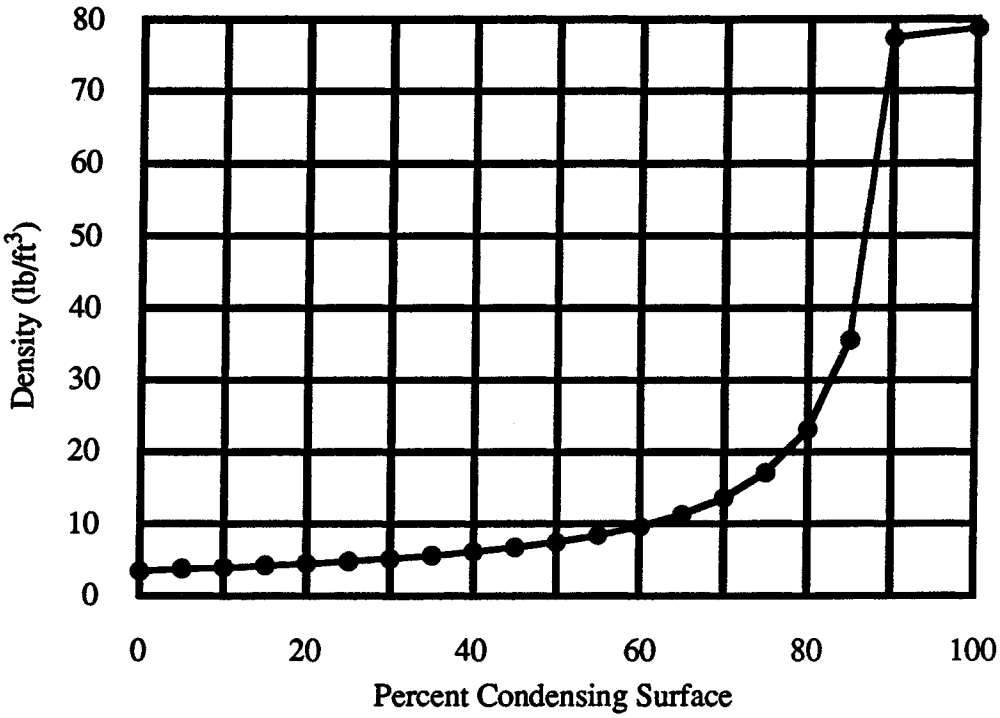

Figure 2.4. Density Versus Percent Condensing Surface for a Typical Condenser.

The control volume term from the mass equation (Equation 2.1) for section i of the condenser is written:

$$m_{cv,i} = Af_iL(\rho')_i \tag{2.11}$$

where

A = cross-sectional flow area

f_iL = tube length of section i

$(\rho')_i$ = average density based on the inlet densities for the subcooled and superheated sections. For the condensing section, density of the saturated vapor at the inlet.

The control volume term from the energy equation (Equation 2.2) for section i of the condenser is written:

$$E_{cv,i} = m_{cv,i} C_i (T'_{ref})_i \tag{2.12}$$

where

C_i = capacitance term for refrigerant and wall of section i

$(T'_{ref})_i$ = average temperature based on the inlet and outlet temperatures of section i

The control volume term from the momentum equation (Equation 2.3) for section i of the condenser in terms of a mass flow rate is written:

$$(mV)_{cv,i} = f_i L (w')_i \tag{2.13}$$

where

$(w')_i$ = average mass flow rate based on the inlet and outlet mass flow rates of section i

When these terms are substituted into the governing equations, only the cross-sectional flow area, A, and total tube length, L, are constants not evaluated with the derivative term. The remaining variables are inside the derivative term since these values vary with time. Even the fraction of heat exchanger in section i, f_i, is placed inside the derivative since the fraction will also vary with respect to time during transient conditions.

2.4. Desuperheating Section

The desuperheating section is defined as the fraction of the condenser from the entrance of the condenser to the state where the refrigerant is a saturated vapor. This defined control volume means all property values relative to the control volume are averaged based on the inlet conditions and the saturated vapor outlet conditions. It should be noted that thermodynamic data such as density and enthalpy are a function of two properties. With the curve fits used from Section 2.2, these data are a function of pressure and temperature.

The continuity equation is written:

$$w_g = w_{in} - AL\frac{d(f\rho')_{dsh}}{dt} \tag{2.14}$$

The energy rate equation for the refrigerant side, air side, and total heat exchanger is written as follows:

$$AL\frac{d(f\rho' CT'_{ref})_{dsh}}{dt} = Q_{dsh} - w_g h_g + w_{in} h_{in} \tag{2.15}$$

$$T_{air,dsh} = T_{air,in} - \frac{Q_{dsh}}{(w_{air} C'_{p,air})_{dsh}} \tag{2.16}$$

$$Q_{dsh} = f_{dsh} L U_{dsh} (T'_{air} - T'_{ref})_{dsh} \tag{2.17}$$

The momentum equation is written as

$$P_g A = P_{in} A + \frac{w_{in}^2}{A\rho_{in}} - \frac{w_g^2}{A\rho_g} - F_{f,dsh} - L\frac{d(fw')_{dsh}}{dt} \tag{2.18}$$

Knowing the inlet conditions to the condenser from the compressor outlet state, the above equations are used, with the air inlet information, to determine the outlet state of the refrigerant. The continuity equation determines the outlet mass flow rate of the refrigerant (w_g). Since the outlet state is a saturated vapor, the outlet pressure (P_g), evaluated with the momentum equation, completely defines the state of the refrigerant. This allows the energy rate equation, in terms of the refrigerant, to be evaluated for the fraction of heat exchanger (f_{dsh}) in the vapor regime. Finally, the energy rate equation, with respect to the air side, is used to determine the outlet temperature of the air ($T_{air,dsh}$).

2.5. Condensing Section

The condensing section is defined as the fraction of the condenser where the refrigerant enters as a saturated vapor and leaves as a saturated liquid. All property values used to characterize the control volume terms, except density, are based on an average value of the outlet and inlet states of the refrigerant in this section. The density for the control volume term is based on the saturated vapor density. The thermodynamic data are determined with the curve fits based on the saturated liquid or saturated vapor temperature or pressure. The equations used for this analysis are similar to those listed for the desuperheating section (2.14 - 2.18). Only the subscripts change to represent the new inlet, outlet, and sectional labels.

$$w_f = w_g - AL\frac{d(f\rho')_{cond}}{dt} \tag{2.19}$$

$$AL\frac{d(f\rho' CT'_{ref})_{cond}}{dt} = Q_{cond} - w_f h_f + w_g h_g \tag{2.20}$$

$$T_{air,cond} = T_{air,in} - \frac{Q_{cond}}{(w_{air}C'_{p,air})_{cond}} \tag{2.21}$$

$$Q_{cond} = f_{cond}LU_{cond}(T'_{air} - T'_{ref})_{cond} \tag{2.22}$$

$$P_f A = P_g A + \frac{w_g^2}{A\rho_g} - \frac{w_f^2}{A\rho_f} - F_{f,cond} - L\frac{d(fw')_{cond}}{dt} \tag{2.23}$$

The inlet conditions are defined by the outlet values of the superheated section of the condenser. The outlet pressure (P_f) is determined by these values with the momentum equation. Since the outlet condition is a saturated liquid, the refrigerant state is completely defined. With the refrigerant state known, the refrigerant side energy rate equation is used to determine the fraction of the condenser in two-phase flow (f_{cond}). This leaves the outlet mass flow rate (w_f) to be determined by the conservation of mass equation and the outlet air temperature ($T_{air,cond}$) to be solved with the air side energy rate equation.

2.6. Subcooling Section

The subcooling section is defined as the fraction of the condenser where the refrigerant enters as a saturated liquid and leaves as a liquid. All property values used to characterize the control volume terms are based on an average value of the outlet and inlet states of the refrigerant in this section. The thermodynamic data are determined with curve fits based on temperature. The equations used for this analysis are similar to those listed for the desuperheating section (2.14-2.18). Only the subscripts change to represent the new inlet, outlet, and sectional labels.

$$w_{out} = w_f - AL\frac{d(f\rho')_{sc}}{dt} \tag{2.24}$$

$$AL\frac{d(f\rho' CT'_{ref})_{sc}}{dt} = Q_{sc} - w_{out}h_{out} + w_f h_f \tag{2.25}$$

$$T_{air,sc} = T_{air,in} - \frac{Q_{sc}}{(w_{air}C'_{p,air})_{sc}} \tag{2.26}$$

$$Q_{sc} = f_{sc} L U_{sc} (T'_{air} - T'_{ref})_{sc} \tag{2.27}$$

$$P_{out}A = P_f A + \frac{w_f^2}{A\rho_f} - \frac{w_{out}^2}{A\rho_{out}} - F_{f,sc} - L\frac{d(fw')_{sc}}{dt} \tag{2.28}$$

The inlet conditions to the subcooling section are defined by the outlet conditions of the condensing section. Using this information in the continuity equation, the outlet mass flow rate (w_{out}) is determined. With the air side energy rate equation, the outlet air temperature ($T_{air,sc}$) is evaluated. The momentum equation is used to solve for the outlet pressure (P_{out}). Since two properties are required to define the refrigerant state, the refrigerant temperature (T_{out}) is evaluated with the refrigerant side energy rate equation. Previously, the refrigerant side energy rate equation was employed to solve for the fraction of heat exchanger in a given regime. Now, the fraction is a function of the remaining heat exchanger volume:

$$f_{sc} = 1 - f_{sh} - f_{cond} \tag{2.29}$$

Figure 2.5 summarizes the analysis required to determine the outlet state of the condenser.

2.7. Partial Condensing Section

The partial condensing section is defined as the fraction of the condenser where the refrigerant enters as a saturated vapor and leaves as a two-phase mixture. All property values used to characterize the control volume terms, except density, are based on an average value of the outlet and inlet states of the refrigerant in this section. The density for the control volume term is based on the saturated vapor density. The equations used for this analysis are identical to those listed for the desuperheating section (2.14-2.18).

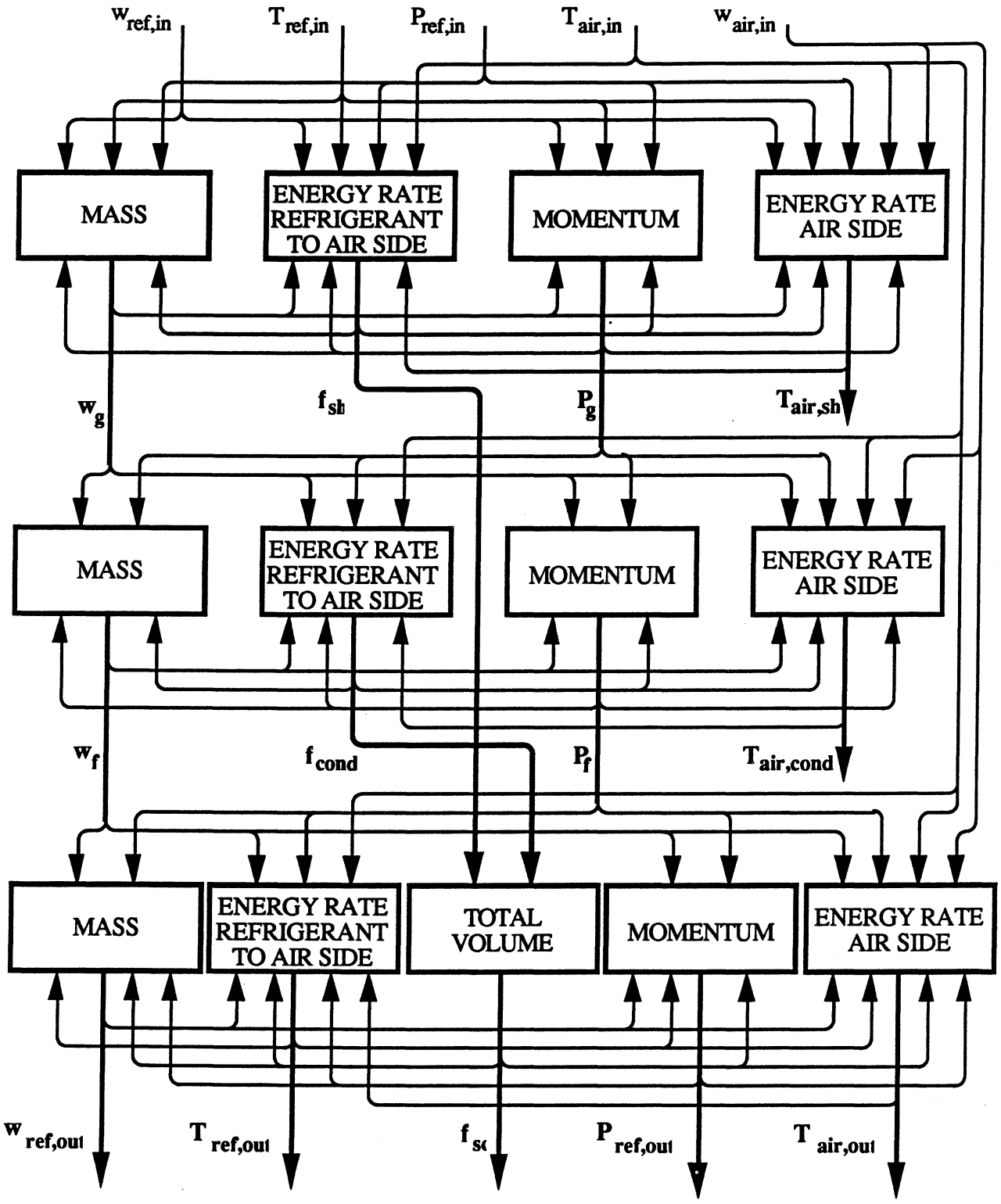

Figure 2.5. Block Diagram of Information Flow Between the Superheated and Subcooled Sections.

The inlet conditions to the partial condensing section are defined by the outlet conditions of the superheated section. The equations used for this analysis are identical to those listed for the desuperheating section (2.19-2.23). With the continuity equation, the outlet mass flow rate (w_{out}) is determined. With the air side energy rate equation, the outlet air temperature ($T_{air,out}$) is evaluated. The momentum equation is used to solve for the outlet pressure (P_{out}). Since two properties are required to define the refrigerant state and the refrigerant temperature is a function of the two-phase pressure, the quality (x) is evaluated by the refrigerant side energy rate equation. The fraction of the heat exchanger in the two-phase regime is a function of the remaining heat exchanger volume:

$$f_{cond} = 1 - f_{sh} \tag{2.30}$$

Figure 2.6 summarizes the procedure used to determine the outlet state of the condenser when the refrigerant is partially condensed.

2.8. Solution Technique

The equations for the heat exchanger sections described above must be solved simultaneously. Two possible configurations existed: the outlet of the condenser is subcooled or the outlet is in the two-phase regime. For the subcooled outlet condition, twelve equations are solved simultaneously, four equations for each section. With the outlet of the condenser in the two-phase state, eight equations must be solved simultaneously, four for the superheated section and four for the partial condensing section.

Since the equations are dependent on time, the set of equations are solved for each time step. A simple implicit Euler method is used. The resolution of the answer using this method relies on the selection of the proper time step.

A Newton-Raphson [31] technique is used to solve the set of equations. This method requires all of the equations to be rewritten in a residual form such that all terms appear on one side

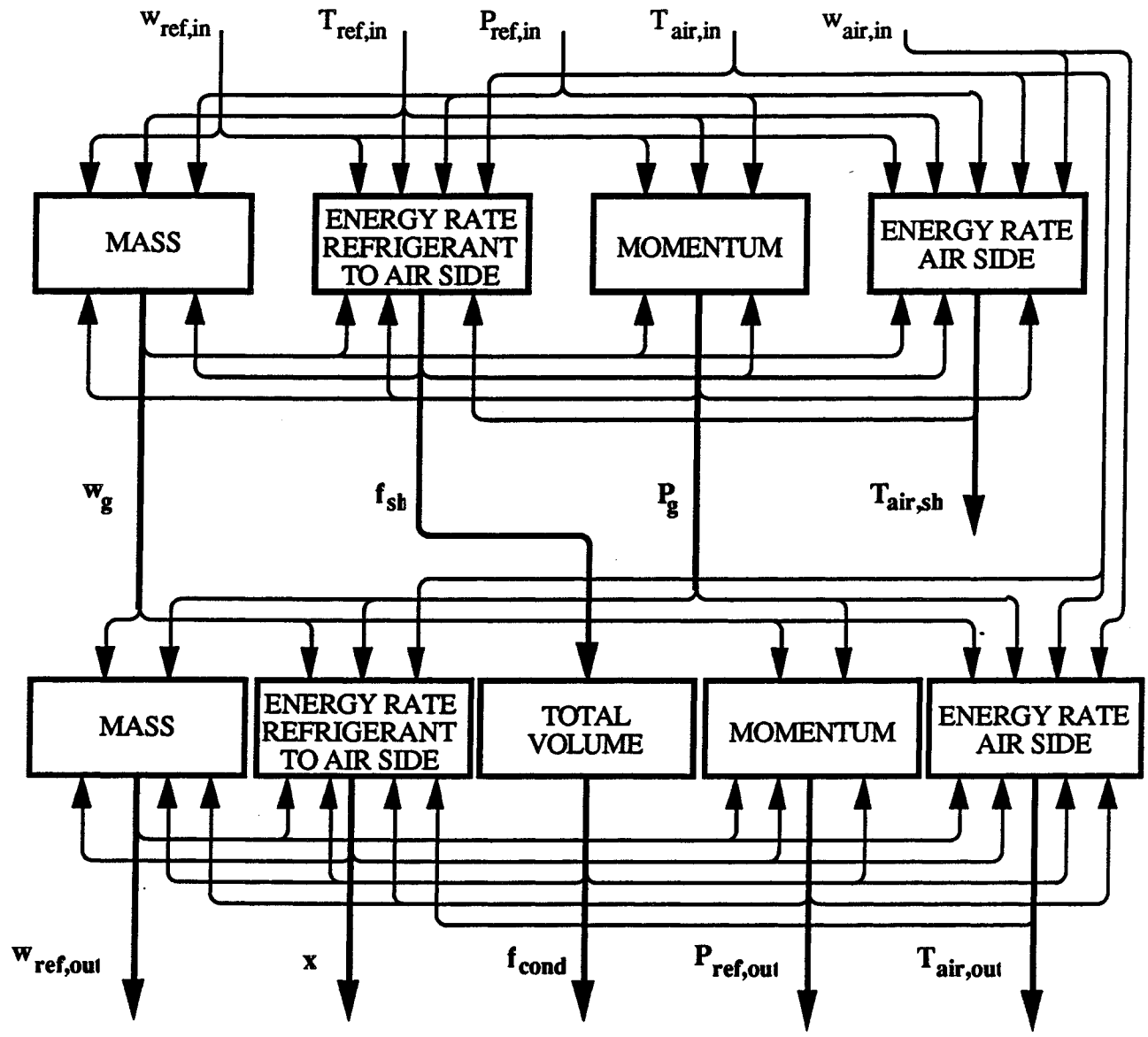

Figure 2.6. Block Diagram of Information Flow Between the Superheated and Partial Condensing Sections.

of the equality sign. Values are assumed for each unknown and then the residuals are calculated. The partial derivatives are computed with respect to all variables. A Taylor-Series expansion is used with these partial derivatives to establish a set of linear simultaneous equations. This set of linear simultaneous equations determines the change in a given unknown. A new value for the unknown is determined by the computed change in a given unknown. With this new value for the

unknown, the residuals are tested for convergence. If the residuals are close to zero within a given percentage, the procedure has converged. Otherwise, the process is repeated until the procedure does converge.

The residual equations that described the condenser when the outlet is subcooled are

$$R_1 = [w_{in}]_k - [w_g]_k - AL\frac{([f\rho']_k - [f\rho']_{k-1})_{dsh}}{\delta t} \tag{2.31}$$

$$R_2 = [w_g h_g]_k - [w_{in} h_{in}]_k + AL\frac{([f\rho' CT'_{ref}]_k - [f\rho' CT'_{ref}]_{k-1})_{dsh}}{\delta t}$$

$$- [w_{air,dsh}]_k [C'_{p,air,dsh}]_k ([T_{air,in}]_k - [T_{air,out,dsh}]_k) \tag{2.32}$$

$$R_3 = [w_g h_g]_k - [w_{in} h_{in}]_k + AL\frac{([f\rho' CT'_{ref}]_k - [f\rho' CT'_{ref}]_{k-1})_{dsh}}{\delta t}$$

$$- [f_{dsh}]_k LU_{dsh}([T'_{air}]_k - [T'_{ref}]_k)_{dsh} \tag{2.33}$$

$$R_4 = [P_{in}]_k A + \frac{[w_{in}^2]_k}{A[\rho_{in}]_k} - [P_g]_k A - \frac{[w_g^2]_k}{A[\rho_g]_k} - [F_{f,dsh}]_k$$

$$- L\frac{d([fw']_k - [fw']_{k-1})_{dsh}}{\delta t} \tag{2.34}$$

$$R_5 = [w_g]_k - [w_f]_k - AL\frac{([f\rho_g]_k - [f\rho_g]_{k-1})_{cond}}{\delta t} \tag{2.35}$$

$$R_6 = [w_f h_f]_k - [w_g h_g]_k + AL\frac{([f\rho_g CT'_{ref}]_k - [f\rho_g CT'_{ref}]_{k-1})_{cond}}{\delta t}$$

$$- [w_{air,cond}]_k[C'_{p,air,cond}]_k([T_{air,in}]_k - [T_{air,out,cond}]_k) \quad (2.36)$$

$$R_7 = [w_f h_f]_k - [w_g h_g]_k + AL\frac{([f\rho_g CT'_{ref}]_k - [f\rho_g CT'_{ref}]_{k-1})_{cond}}{\delta t}$$

$$- [f_{cond}]_k LU_{cond}([T'_{air}]_k - [T'_{ref}]_k)_{cond} \quad (2.37)$$

$$R_8 = [P_g]_k A + \frac{[w_g^2]_k}{A[\rho_g]_k} - [P_f]_k A - \frac{[w_f^2]_k}{A[\rho_f]_k} - [F_{f,cond}]_k$$

$$- L\frac{d([fw']_k - [fw']_{k-1})_{cond}}{\delta t} \quad (2.38)$$

$$R_9 = [w_f]_k - [w_{out}]_k - AL\frac{([f\rho']_k - [f\rho']_{k-1})_{sc}}{\delta t} \quad (2.39)$$

$$R_{10} = [w_{out}h_{out}]_k - [w_f h_f]_k + AL\frac{([f\rho' CT'_{ref}]_k - [f\rho' CT'_{ref}]_{k-1})_{sc}}{\delta t}$$

$$- [w_{air,sc}]_k[C'_{p,air,sc}]_k([T_{air,in}]_k - [T_{air,out,sc}]_k) \quad (2.40)$$

$$R_{11} = [w_{out}h_{out}]_k - [w_f h_f]_k + AL\frac{([f\rho' CT'_{ref}]_k - [f\rho' CT'_{ref}]_{k-1})_{sc}}{\delta t}$$

$$- [f_{sc}]_k LU_{sc}([T'_{air}]_k - [T'_{ref}]_k)_{sc} \quad (2.41)$$

$$R_{12} = [P_f]_k A + \frac{[w_f^2]_k}{A[\rho_f]_k} - [P_{out}]_k A - \frac{[w_{out}^2]_k}{A[\rho_{out}]_k} - [F_{f,sc}]_k$$

$$- L\frac{d([fw']_k - [fw']_{k-1})_{sc}}{dt} \tag{2.42}$$

The mass flow rates determined by the continuity equations are w_g, w_f, and w_{out}. The momentum equations evaluate the pressures P_g, P_f, and P_{out}. The air side energy rate balances determine the outlet air temperatures $T_{air,out,dsh}$, $T_{air,out,cond}$, and $T_{air,out,sc}$. The refrigerant side energy rate balance determines the heat exchanger fraction for the superheated and two-phase regions, f_{dsh} and f_{cond}, and the outlet refrigerant temperature, T_{out}.

The residual equations that describe the condenser when the outlet is in the two-phase regime are similar to equations 2.31 to 2.38. The mass flow rates determined by the continuity equations are w_g and w_{out}. The momentum equations evaluate the pressures P_g, and P_{out}. The air side energy rate balances determine the outlet air temperatures $T_{air,out,dsh}$ and $T_{air,out}$. While the refrigerant side determines the heat exchanger fraction for the superheated region, f_{dsh}, and the outlet refrigerant quality, x.

2.9. Computer Program Considerations

The main model is written in SI units. The model included the option of entering data in IP or SI units as well as displaying output in either of the two systems of units.

The model of the condenser is simulated as a single length of tube and fin heat exchanger. This allows for the study of various heat exchanger lengths on condenser performance. Also, the inner diameter of the tube may be altered to simulate different tube sizes.

Since the inlet conditions to the condenser can be defined by the computer model, any type of input can be simulated. These include step, sinusoidal, ramp, and other programmable inputs. The controllable inputs are inlet refrigerant temperature, pressure, and mass flow rate. The air side inlet temperature and mass flow rate are control variables.

The overall heat transfer coefficient for the total heat exchanger may also be varied. Through experimental tests, this value is determined for a given condenser. But new heat

exchanger designs can be easily incorporated into the test stand to determine the heat transfer coefficient or calculated values based on theoretical considerations can determine the new heat transfer coefficient. The condenser model can then be used to perform exhaustive tests on the new condenser configurations.

Figure 2.7 is a flow chart of the data streams within the computer program along with the file names of the data sets. Files are used in the program to facilitate the large amount of data inherent in a transient analysis. The file PARAM contains the estimated parameters in the model. These are the total tube length (L), tube diameter (d), friction factors for the three sections (f_i), overall heat transfer coefficient per unit length (U_i), and the specific heat of the refrigerant and tube wall (C_i). INITIAL contains the data from an experimental run that will be used as inputs to the model. These are the condenser inlet refrigerant temperature (T_{in}) and pressure (P_{in}), inlet mass flow rate of refrigerant (w_{in}), inlet air temperature ($T_{air,in}$), and mass flow rate of the air (w_{air}). The calculated model values are the outlet refrigerant temperature (T_{out}) and pressure (P_{out}), and the outlet air temperature ($T_{air,out}$). The calculated values are store in MODEL while the actual experimental values are stored in TEST. The intermediate values calculated by the program are placed in a file titled RESULTS.

For a given time step, data stored in the file INITIAL is input into the model. Based on the parameters in the file PARAM, intermediate values are calculated and stored in RESULTS. The final output results are stored in MODEL. These results are then compared to the experimental findings stored in TEST. The PARAM file is adjusted at the end of a model run until the model accuracy is sufficient.

It was decided that the model would be written in the computer programming language True BASIC™ since this structured language has built in matrix subroutines. The actual True BASIC™ code can be found in appendix B.

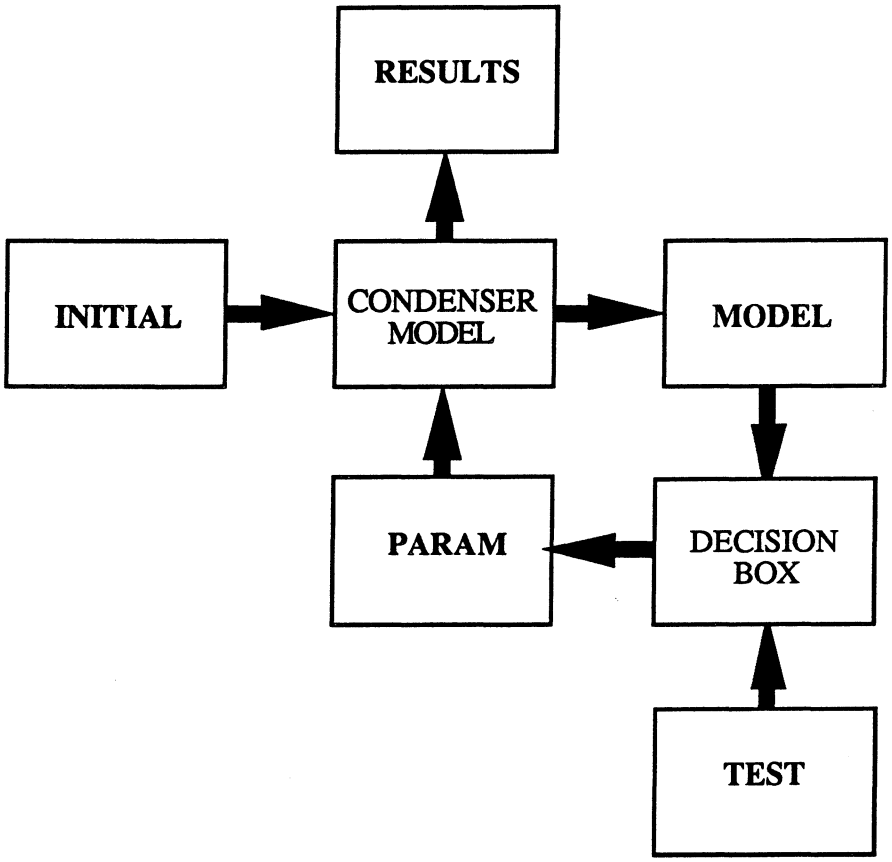

Figure 2.7. Data Flow for Transient Condenser Model.

The model is designed to operate either with the condenser outlet as a two-phase mixture or a subcooled liquid. For some modeling conditions, there would be a transition between either one of these states. The transition between the two-phase outlet state to the subcooled liquid state is detected by monitoring the fraction of the total heat exchanger in the subcooled state. When this parameter becomes so small that it would not enter into the total heat exchanger calculation, the model would then switch to the residual equations for the two-phase outlet state. If a transition occurs between the two-phase state to the subcooled state, the exit quality of the refrigerant is monitored. If this quantity approaches zero within a certain percentage, the residual equations for the subcooled outlet state would be evaluated.

The program enables a graphical display of the computed values to be overlaid onto the actual results from the experiment. This allows for a visual interpretation of the model

performance. With this "on-line" verification, model parameters can be evaluated during the actual model run instead of after the entire run time.

CHAPTER 3

ANALYSIS OF CONDENSER PARAMETERS

To determine the unknown condenser parameters for each of the three sections (overall heat transfer coefficient U and friction factor F), steady-state data were collected from a mobile air conditioning test stand. With a least-squares fit of the test data based on the governing steady-state equations, these parameters were determined. The test stand description can be found in Appendix C and D. The programs used to execute the least-squares fit are contained in Appendices E and F.

3.1. Test Plan

The condenser used in the test was a design for a Ford Taurus automobile. It consists of tubes that are brazed to the plate fins. The condenser face dimensions are 15-3/8" x 24-5/8" (39.1 cm x 62.6 cm) resulting in a condenser face area of 2.63 ft^2 (0.244 m^2). The tube used in the heat exchanger was a 3/8" (9.5 mm) OD, 1/4" (6.4 mm) ID aluminum tube with a total tube length of 70 feet (21 m). The fin thickness is 0.0156 in (0.396 mm) with 9 fins per inch (0.35 fins per mm). Figure 3.1 shows a simplified drawing of the circuiting used on this particular heat exchanger. The refrigerant enters at the top of the heat exchanger and divides into two parallel streams. These streams continue in a serpentine pattern halfway down the condenser and then join together again. The combined stream then follows a similar serpentine pattern along the backside of the condenser where the backside is defined as the exit air side of the condenser. The tubing then runs along the front side of the condenser and exits at the center of the condenser face area.

Parallel circuits are used in the heat exchanger to reduce the amount of pressure drop inherent in the vapor section of the condenser due to its higher velocity. The streams are then joined so that the increase in mass flow will result in a higher heat transfer coefficient for the refrigerant. The subcooling section is placed on the air side entrance of the heat exchanger to assure that the coolest possible air will aid in the subcooling process.

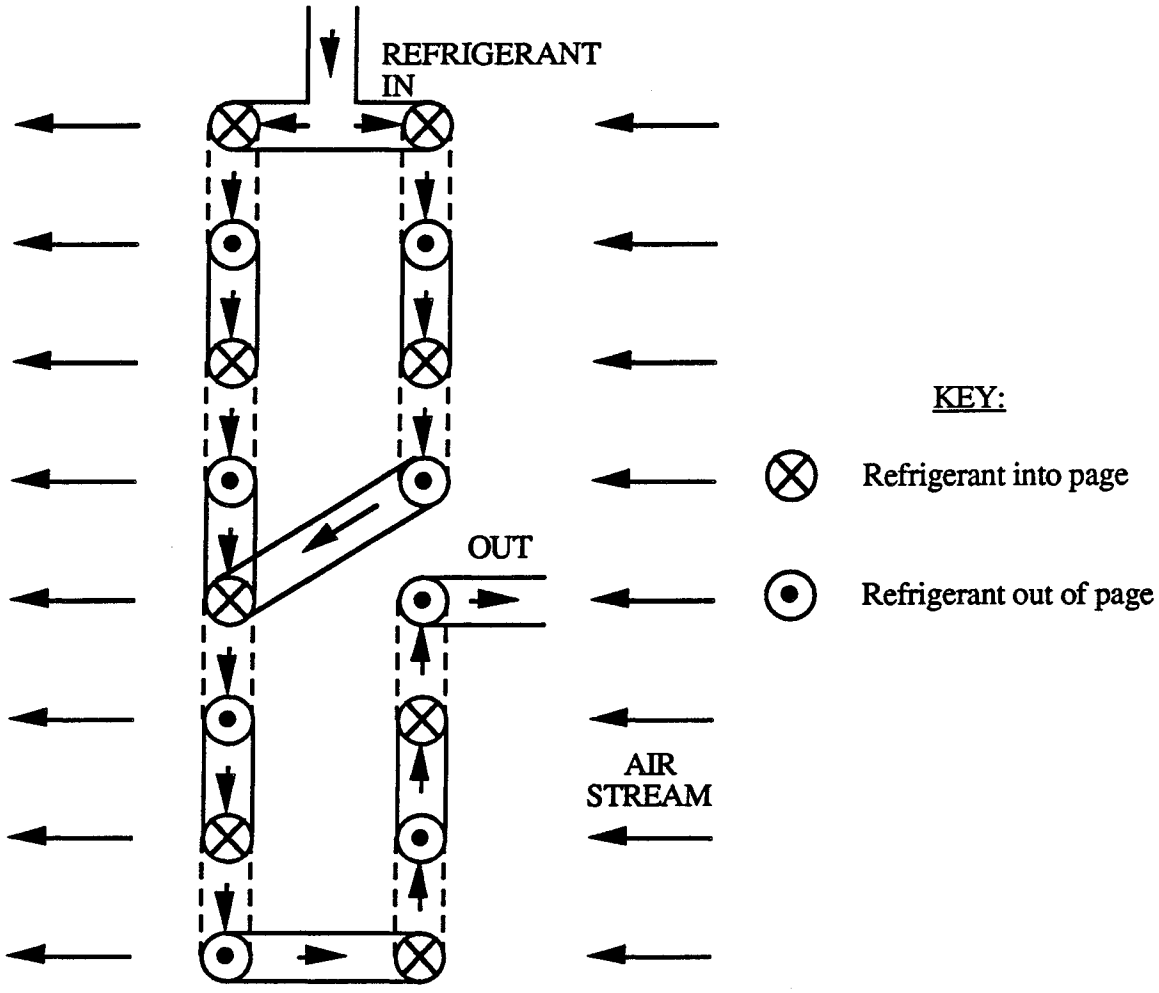

Figure 3.1. Schematic of Condenser .

Two test matrices were formed to encompass a wide range of conditions that might be experienced by a mobile air conditioner. The first test matrix was composed of low air flow rates through the condenser (590, 710, 825, 945, and 1060 SCFM) and various compressor speeds (1150, 1725, 2300, 2875, and 3450 RPM). The second test matrix contained higher air flow rates through the condenser (600, 1200, 1500, and 1800 SCFM) and similar compressor speeds (1000, 1500, 2000, 2500, 3000, 3500, and 4000 RPM). The inlet air conditions to the evaporator and condenser were determined by the ambient laboratory environment.

This analysis used a total of 53 test runs. With each test run, the inlet and outlet air temperatures ($T_{air,in}$ and $T_{air,out}$) were recorded as well as the wet bulb temperature (T_{wet}). The

humidity ratio (ω), determined by the inlet air temperature and the inlet wet bulb temperature, was assumed constant at the inlet and outlet air conditions. The volumetric air flow rate was recorded at the outlet of the condenser and then calculated as a mass flow rate (w_{air}). On the refrigerant side, the inlet and outlet temperatures (T_{in} and T_{out}) and pressures (P_{in} and P_{out}) were measured. The mass flow rate (w_{in}) was determined with a turbine meter based on an R12 calibration and then was corrected for the density difference between R134a and R12 to reflect the mass flow rate of R134a.

With the given information above, an energy balance was performed on the air and refrigerant streams to verify the experimental results. On the air side, the energy balanced reduces to

$$Q_{air} = w_{air}(h_{air,in} - h_{air,out}) \tag{3.1}$$

where

$$h_{air,out} = f(T_{air,out} \text{ and } \omega)$$

$$h_{air,in} = f(T_{air,in} \text{ and } \omega)$$

The refrigerant side is written as

$$Q_{ref} = w_{in}(h_{out} - h_{in}) \tag{3.2}$$

where

$$h_{out} = f(P_{out} \text{ and } T_{out})$$

$$h_{in} = f(P_{in} \text{ and } T_{in})$$

Figure 3.2 shows the comparison between the air and refrigerant side energy balances. Based on the graph, the air side energy calculation is generally greater than the refrigerant side calculation. The few points above the the 45 degree line are believed to be a result of improper turbine readings. The 45 degree line on the graph represents the points where the energy exchange between the refrigerant and air streams are equivalent. Since most of the points fall far below this

line, this left the experimental data to be suspected of error. The biggest error was believed to occur at the turbine meter which measured the flow rate. Since the meter was calibrated using R12 and not R134a, a density correction was done to correct for the different fluids. This correction factor is believed to not adequately correct for the fluid differences. Therefore, the refrigerant mass flow rate was calculated from an energy balance between the air and refrigerant sides. With all the necessary quantities known for air and the refrigerant enthalpies determined from pressure and temperature measurements, the mass flow rate of refrigerant was calculated. This forced a perfect energy balance between the air and refrigerant streams.

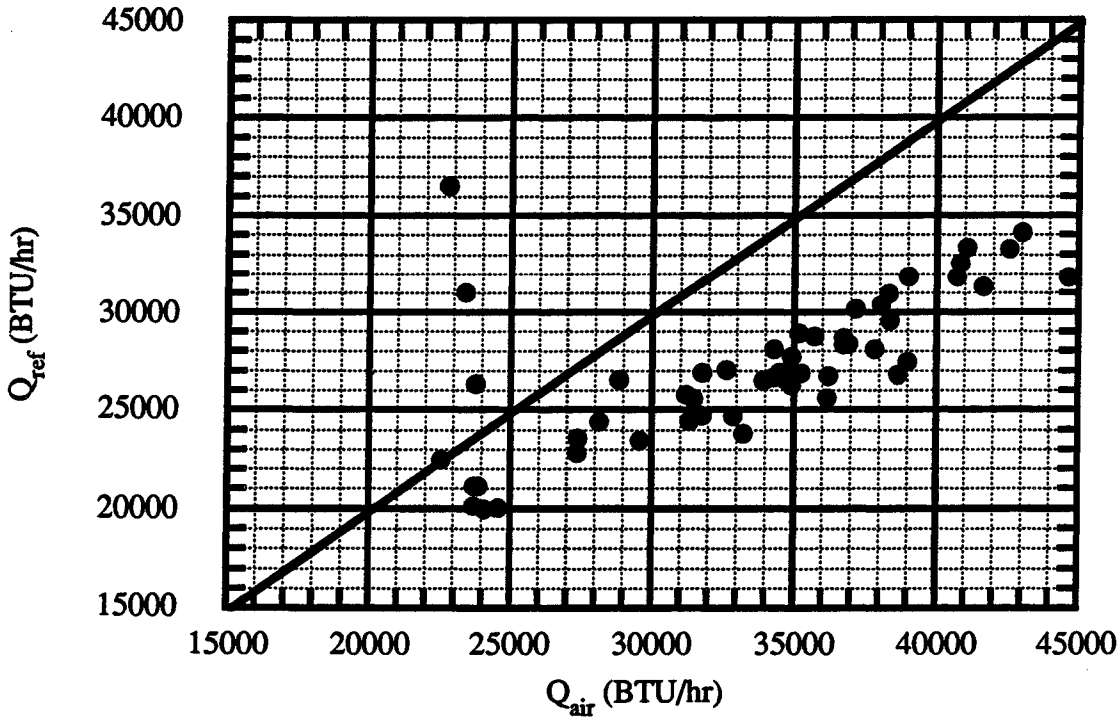

Figure 3.2. Comparison of Air and Refrigerant Energy Balances.

3.2. Parameter Estimations Using Energy Balances

Using the steady-state energy equations based on the refrigerant side and the overall heat transfer coefficient, the fraction of each section can be determined in terms of the overall heat transfer coefficient. Based on the refrigerant side:

$$Q_{dsh} = w_{in}(h_g - h_{in}) \tag{3.3}$$

$$Q_{cond} = w_{in}(h_f - h_g) \tag{3.4}$$

$$Q_{sc} = w_{in}(h_{out} - h_f) \tag{3.5}$$

The heat transfer term for each section of the heat exchanger is expressed as

$$Q_{dsh} = f_{dsh}LU_{dsh}(T_{air,in} - T'_{ref})_{dsh} \tag{3.6}$$

$$Q_{cond} = f_{cond}LU_{cond}(T_{air,in} - T'_{ref})_{cond} \tag{3.7}$$

$$Q_{sc} = f_{sc}LU_{sc}(T_{air,in} - T'_{ref})_{sc} \tag{3.8}$$

where

T'_{ref} = average of the inlet and outlet refrigerant temperatures of the specified section

Solving for the fractions of the heat exchanger in each of the three sections:

$$f_{dsh} = \frac{1}{LU_{dsh}} \frac{w_{in}(h_g - h_{in})}{(T_{air,in} - T'_{ref})_{dsh}} \tag{3.9}$$

$$f_{cond} = \frac{1}{LU_{cond}} \frac{w_{in}(h_f - h_g)}{(T_{air,in} - T'_{ref})_{cond}} \tag{3.10}$$

$$f_{sc} = \frac{1}{LU_{sc}} \frac{w_{in}(h_{out} - h_f)}{(T_{air,in} - T'_{ref})_{sc}} \tag{3.11}$$

Realizing that the sum of the fractions must equate to one, the final equation used in the least-squares analysis is

$$1 = \frac{1}{LU_{dsh}} \frac{w_{in}(h_g - h_{in})}{(T_{air,in} - T'_{ref})_{dsh}} + \frac{1}{LU_{cond}} \frac{w_{in}(h_f - h_g)}{(T_{air,in} - T'_{ref})_{cond}} +$$

$$\frac{1}{LU_{sc}} \frac{w_{in}(h_{out} - h_f)}{(T_{air,in} - T'_{ref})_{sc}} \qquad (3.12)$$

The only terms in Equation 3.12 that are unknown are h_f and h_g. These terms are first evaluated by using the inlet pressure as the saturated vapor pressure and the outlet pressure as the saturated liquid pressure to determine the saturation temperatures. Then the saturation temperatures determine the saturated liquid and vapor properties. The momentum equations for each heat exchanger section, discussed in the next section, evaluate the pressure drop. Then the new pressure drop terms are used to evaluate the total resistance. This successive substitution process is continued until the pressure terms evaluated with the momentum equations in each of the three heat exchanger sections balances.

The inverse of the overall heat transfer coefficient times the total tube length ($\frac{1}{LU_i}$) for each section are the unknowns evaluated with the least-squares fit. Using all 53 data points, the three terms were determined. This analysis produced a negative quantity for the subcooling section. This is not a rational solution to the problem since a negative quantity reflects a negative resistance. Also, this solution technique produced a maximum error of 35% percent between the expected value of the heat exchanger fractions and the curve-fitted values.

With this large error and a negative quantity computed for the subcooling resistance, a new approach was considered. Wilson [32] determined that the total resistance of the heat exchanger should approximately vary linearly with the inverse of the square root of the volumetric flow rate of air ($\dot{V}$), if the internal resistance of the refrigerant stream does not vary. This can be written:

$$\frac{1}{U_i L} = a_i + \frac{b_i}{\dot{V}^{0.5}} \tag{3.13}$$

But, the air side heat transfer coefficient is approximately the same for all three sections since the coefficient primarily depends on the air velocity, thus b is assumed constant for all three sections. Therefore, the overall heat transfer coefficients are determined with a least-squares analysis using the following equation which is derived from Equation 3.12.

$$1 = a_{dsh}\frac{w_{in}(h_g - h_{in})}{(T_{air,in} - T'_{ref})_{dsh}} + a_{cond}\frac{w_{in}(h_f - h_g)}{(T_{air,in} - T'_{ref})_{cond}} +$$

$$a_{sc}\frac{w_{in}(h_{out} - h_f)}{(T_{air,in} - T'_{ref})_{sc}} + \frac{b}{\dot{V}^{0.5}}\left\{\frac{w_{in}(h_g - h_{in})}{(T_{air,in} - T'_{ref})_{dsh}} + \right.$$

$$\left.\frac{w_{in}(h_f - h_g)}{(T_{air,in} - T'_{ref})_{cond}} + \frac{w_{in}(h_{out} - h_f)}{(T_{air,in} - T'_{ref})_{sc}}\right\} \tag{3.14}$$

After a least-squares fit, the largest error was determined to only be 3%. But, the subcooling term (a_{sc}) still remained a negative quantity. Therefore, the assumption of a constant internal convective resistance with respect to the refrigerant flow rate was believed to be false for this analysis. Heat transfer correlations were examined for use in the analysis of the internal resistance. These correlations were simplified since the condenser operates over a limited temperature and pressure range.

For a refrigerant in a single-phase, the Dittus-Boelter Correlation [33] can be used where

$$h_{sp} = 0.023 Re^{0.8} Pr^{0.4} \frac{k}{D} \tag{3.15}$$

where

D = inner tube diameter

h_{sp} = single-phase heat transfer coefficient

k = single-phase thermal conductivity of the refrigerant

Pr = single-phasePrandtl number = $\frac{c_p \mu}{k}$

Re = single-phase Reynolds number = $\frac{4w}{\pi \mu D}$

Since this analysis is only concerned with the range of conditions experienced by a mobile condenser, the only varying term in Equation 3.15 is the mass flow rate (w). The other terms such as viscosity (μ), specific heat (c_p), and thermal conductivity (k) are assumed to be constant for the operating conditions considered. Therefore, Equation 3.15 may now be written as

$$h_{sp} = cw^{0.8} \tag{3.16}$$

where

c = constant

w = mass flow rate of refrigerant

For a refrigerant that is condensing, the Cavallini-Zecchin Correlation [33] may be used to express an average heat transfer coefficient for the condensing process where

$$h_c = 0.05 Re_{eq}^{0.8} Pr_f^{0.33} \frac{k_f}{D} \tag{3.17}$$

where

$$Re_{eq} = Re_f + \left(\frac{\mu_g}{\mu_f}\right)\left(\frac{\rho_f}{\rho_g}\right)^{0.5} Re_g$$

D = inner tube diameter

k_f = liquid thermal conductivity of the refrigerant

Pr_f = liquid Prandtl number = $\frac{(c_{p,f}\,\mu_f)}{k_f}$

Re_g = gas Reynolds number = $\frac{4w}{\pi \mu_g D}$

$$Re_f = \text{liquid Reynolds number} = \frac{4w}{\pi \mu_f D}$$

Once again, only the refrigerant mass flow is believed to vary significantly when compared to the other refrigerant properties used to evaluate the heat transfer coefficeint at the condenser operating conditions. The condensing refrigerant heat transfer coefficient is written

$$h_c = c w^{0.8} \tag{3.18}$$

where

c = constant

Now the heat transfer terms for each refrigerant section are combined with the heat transfer coefficient for the air side and substituted into Equation 3.14:

$$1 = \frac{c_{dsh}}{\left(\frac{w_{in}}{2}\right)^{0.8}} \frac{w_{in}(h_g - h_{in})}{(T_{air,in} - T'_{ref})_{dsh}} + \frac{c_{cond}}{w_{in}^{0.8}} \frac{w_{in}(h_f - h_g)}{(T_{air,in} - T'_{ref})_{cond}} +$$

$$\frac{c_{sc}}{w_{in}^{0.8}} \frac{w_{in}(h_{out} - h_f)}{(T_{air,in} - T'_{ref})_{sc}} + \frac{b}{\dot{V}^{0.5}} \left\{ \frac{w_{in}(h_g - h_{in})}{(T_{air,in} - T'_{ref})_{dsh}} + \right.$$

$$\left. \frac{w_{in}(h_f - h_g)}{(T_{air,in} - T'_{ref})_{cond}} + \frac{w_{in}(h_{out} - h_f)}{(T_{air,in} - T'_{ref})_{sc}} \right\} \tag{3.19}$$

It should be noted that the refrigerant mass flow rate in the desuperheating section is divided by two. Since the refrigerant entering the condenser is divided into two streams, (see Figure 3.1), the mass flow rate used to determine the heat transfer coefficient for this section must be half of the total mass flow rate. This will not change the mass flow rate used in Equation 3.3 to determine the heat exchange for the desuperheating section since the control volume is placed around the parallel tubes. Also, the condensing section may start in the parallel tube portion of the condenser.

Assuming the majority of the condensing regime will be in the single tube section, the mass flow rate is not changed.

After the least-squares fit, the largest error between the actual value of one and the curve fit value for any given data point was 4%. Still, the subcooling coefficient (c_{sc}) was negative. A reasonable explanation for the negative value is found in the model assumption of expressing the air temperature as the inlet air temeprature ($T_{air,in}$) only. Therefore, the air temperature is expressed as the average value of the inlet and outlet air temperatures (T'_{air}). The least-squares analysis was done by solving for the inverse of the overall heat transfer coefficient times the total tube length ($\frac{1}{LU_i}$), similar to Equation 3.12:

$$1 = \frac{1}{LU_{dsh}} \frac{w_{in}(h_g - h_{in})}{(T'_{air} - T'_{ref})_{dsh}} + \frac{1}{LU_{cond}} \frac{w_{in}(h_f - h_g)}{(T'_{air} - T'_{ref})_{cond}} +$$

$$\frac{1}{LU_{sc}} \frac{w_{in}(h_{out} - h_f)}{(T'_{air} - T'_{ref})_{sc}} \qquad (3.20)$$

Since these results still produced a negative number for the subcooling heat transfer coefficient ($\frac{1}{LU_{sc}}$), a least-squares fit was done for an equation similar to Equation 3.14. With the air temperatures averaged:

$$1 = a_{dsh} \frac{w_{in}(h_g - h_{in})}{(T'_{air} - T'_{ref})_{dsh}} + a_{cond} \frac{w_{in}(h_f - h_g)}{(T'_{air} - T'_{ref})_{cond}} +$$

$$a_{sc} \frac{w_{in}(h_{out} - h_f)}{(T'_{air} - T'_{ref})_{sc}} + \frac{b}{\dot{V}^{0.5}} \left\{ \frac{w_{in}(h_g - h_{in})}{(T'_{air} - T'_{ref})_{dsh}} + \right.$$

$$\left. \frac{w_{in}(h_f - h_g)}{(T'_{air} - T'_{ref})_{cond}} + \frac{w_{in}(h_{out} - h_f)}{(T'_{air} - T'_{ref})_{sc}} \right\} \qquad (3.21)$$

This also resulted in a negative value for the subcooling heat transfer coefficient (a_{dsh}). Finally, an equation similar to Equation 3.19 was used in the analysis. With the air temperature as an average of the inlet and outlet air temperatures:

$$1 = \frac{c_{dsh}}{\left(\frac{w_{in}}{2}\right)^{0.8}} \frac{w_{in}(h_g - h_{in})}{(T'_{air} - T'_{ref})_{dsh}} + \frac{c_{cond}}{w_{in}^{0.8}} \frac{w_{in}(h_f - h_g)}{(T'_{air} - T'_{ref})_{cond}} +$$

$$\frac{c_{sc}}{w_{in}^{0.8}} \frac{w_{in}(h_{out} - h_f)}{(T'_{air} - T'_{ref})_{sc}} + \frac{b}{\dot{V}^{0.5}} \left\{ \frac{w_{in}(h_g - h_{in})}{(T'_{air} - T'_{ref})_{dsh}} + \right.$$

$$\left. \frac{w_{in}(h_f - h_g)}{(T'_{air} - T'_{ref})_{cond}} + \frac{w_{in}(h_{out} - h_f)}{(T'_{air} - T'_{ref})_{sc}} \right\} \qquad (3.22)$$

The results show that all the coefficients of Equation 3.22 are positive. The largest error associated with the fit versus the actual result for the first iteration is about 4%. All the results are presented in Chapter 4 since this chapter presents the procedure used to obtain the results.

3.3. Parameter Estimations Using Momentum Balances

Since the parallel tubes must have the same amount of pressure drop, a single tube could represent the pressure drop in the two tubes. Only, the mass flow rate would be half of the total mass flow rate for the single tube. When determining the momentum equations for each section of the heat exchanger, the condensing section is divided into two sections since the condensing process will take place in the parallel and single tube sections. Still, the condensing friction factor times the total length is modeled as one lumped parameter. Since 1/3 of the total flow length has parallel tubes and the desuperheating section might fill this entire section, the percentage of condensing length in the parallel tubes was calculated. The momentum equations are then written:

$$P_{in} + \frac{\left(\frac{w_{in}}{2}\right)^2}{A^2\rho_{in}} = P_g + \frac{\left(\frac{w_{in}}{2}\right)^2}{A^2\rho_g} + F_{dsh}L\,\frac{f_{dsh}}{d}\,\frac{\left(\frac{w_{in}}{2}\right)^2}{2\rho_{in}A^2} \tag{3.23}$$

$$P_g + \frac{\left(\frac{w_{in}}{2}\right)^2}{A^2\rho_g} = P_x + \frac{w_{in}^2}{A^2\rho_g} + F_{cond}L\,\frac{(\frac{1}{3} - f_{dsh})}{d}\,\frac{\left(\frac{w_{in}}{2}\right)^2}{2\rho_g A^2} \tag{3.24}$$

$$P_x + \frac{w_{in}^2}{A^2\rho_g} = P_f + \frac{w_{in}^2}{A^2\rho_f} + F_{cond}L\,\frac{(f_{cond} - (\frac{1}{3} - f_{dsh}))}{d}\,\frac{w_{in}^2}{2\rho_g A^2} \tag{3.25}$$

$$P_f + \frac{w_{in}^2}{A^2\rho_f} = P_{out} + \frac{w_{in}^2}{A^2\rho_{out}} + F_{sc}L\,\frac{f_{sc}}{d}\,\frac{w_{in}^2}{2\rho_f A^2} \tag{3.26}$$

By adding Equations 3.23 through 3.26, a new equation results where the friction factor and total tube length, F_iL, for each section was evaluated with a least-squares fit using all of the test data:

$$P_{in} + \frac{\left(\frac{w_{in}}{2}\right)^2}{A^2\rho_{in}} - P_{out} - \frac{w_{in}^2}{A^2\rho_{out}} = F_{dsh}L\,\frac{f_{dsh}}{d}\,\frac{\left(\frac{w_{in}}{2}\right)^2}{2\rho_{in}A^2} + F_{sc}L\,\frac{f_{sc}}{d}\,\frac{w_{in}^2}{2\rho_f A^2} +$$

$$F_{cond}L\left\{\frac{(\frac{1}{3} - f_{dsh})}{d}\,\frac{\left(\frac{w_{in}}{2}\right)^2}{2\rho_g A^2} + \frac{(f_{cond} - (\frac{1}{3} - f_{dsh}))}{d}\,\frac{w_{in}^2}{2\rho_g A^2}\right\} \tag{3.27}$$

This method determined a negative value for the subcooling section ($F_{sc}L$). But these friction factors were never dependent on any test parameters. Therefore, a correlation was needed so that the friction factor could be expressed as some function of the test such as the mass flow in the case of the heat transfer coefficient evaluation. For smooth conduit walls, an empirical correlation gives [34]

$$F = \frac{0.3164}{Re^{0.25}} \qquad \text{for Re up to } 10^5$$

$$F = 0.0032 + \frac{0.221}{Re^{0.237}} \qquad \text{for } 10^5 < Re < 3 \times 10^6 \qquad (3.28)$$

Once again, the Reynolds number is assumed to only vary according to the mass flow rate since the condenser operates over a small temperature range. A constant is included in one of the friction factor expressions to adjust for the constant 0.0032 in Equation 3.28. Equation 3.28 is now written

$$F = \frac{c}{w^{0.25}} \qquad \text{for Re up to } 10^5$$

$$F = b + \frac{c}{w^{0.237}} \qquad \text{for } 10^5 < Re < 3 \times 10^6 \qquad (3.29)$$

The condensing section is modeled as a vapor as a result of the analysis done in Chapter 2. Since the friction factor is expressed as a function of the mass flow rate, the condensing friction factor analysis is divided into two sections although the constant remains the same for each section. The Reynolds number in the liquid range is less than 10^5 and the vapor range is greater than this value. Also, all the constants are lumped into one term. Now Equation 3.27 may be written

$$P_{in} + \frac{\left(\frac{w_{in}}{2}\right)^2}{A^2\rho_{in}} - P_{out} - \frac{w_{in}^2}{A^2\rho_{out}} = \left(b + \frac{c_{dsh}}{\left(\frac{w_{in}}{2}\right)^{0.237}}\right) L \frac{f_{dsh}}{d} \frac{\left(\frac{w_{in}}{2}\right)^2}{2\rho_{in}A^2} +$$

$$\left(b + \frac{c_{cond}}{\left(\frac{w_{in}}{2}\right)^{0.237}}\right) L \frac{\left(\frac{1}{3} - f_{dsh}\right)}{d} \frac{\left(\frac{w_{in}}{2}\right)^2}{2\rho_g A^2} +$$

$$(b + \frac{c_{cond}}{w^{0.237}})L\frac{(f_{cond} - (\frac{1}{3} - f_{dsh}))}{d}\frac{w_{in}^2}{2\rho_g A^2} +$$

$$(\frac{c_{sc}}{w^{0.25}})L\frac{f_{sc}}{d}\frac{w_{in}^2}{2\rho_f A^2} \qquad (3.30)$$

The above equation is solved for the four unknowns ($c_{dsh}L$, $c_{cond}L$, $c_{sc}L$, and bL) with a least-squares fit. All the coefficients are in terms of the total length (L). Therefore, an analysis may be done on varying tube lengths or condenser sizes. The b constant was determined to be negative. This is believed to occur as a result of modeling the two-phase portion of the condenser as a vapor. The largest error for any one data point and the calculated quantity was 30% of the overall pressure drop.

3.4. Determination of Pressure Drop

To adjust for the pressure drop recorded in the actual test data, Equations 3.23 through 3.26 are modified to determine the pressure drop in each section:

$$\Delta P_{dsh} = \frac{(\frac{w_{in}}{2})^2}{A^2\rho_g} - \frac{(\frac{w_{in}}{2})^2}{A^2\rho_{in}} + (b + \frac{c_{dsh}}{(\frac{w_{in}}{2})^{0.237}})L\frac{f_{dsh}}{d}\frac{(\frac{w_{in}}{2})^2}{2\rho_{in}A^2} \qquad (3.31)$$

$$\Delta P_{cond} = \frac{w_{in}^2}{A^2\rho_f} - \frac{(\frac{w_{in}}{2})^2}{A^2\rho_g} + (b + \frac{c_{cond}}{(\frac{w_{in}}{2})^{0.237}})L\frac{(\frac{1}{3} - f_{dsh})}{d}\frac{(\frac{w_{in}}{2})^2}{2\rho_g A^2} +$$

$$(b + \frac{c_{cond}}{w^{0.237}})L\frac{(f_{cond} - (\frac{1}{3} - f_{dsh}))}{d}\frac{w_{in}^2}{2\rho_g A^2} \qquad (3.32)$$

$$\Delta P_{sc} = \frac{w_{in}^2}{A^2\rho_{out}} - \frac{w_{in}^2}{A^2\rho_f} + (\frac{c_{sc}}{w^{0.25}})L\frac{f_{sc}}{d}\frac{w_{in}^2}{2\rho_f A^2} \qquad (3.33)$$

The actual pressure at the saturated interfaces are determined by

$$P_g = P_{in} - \frac{\Delta P_{dsh}}{\Delta P_{tot}} (P_{in} - P_{out}) \tag{3.44}$$

$$P_f = P_{out} + \frac{\Delta P_{sc}}{\Delta P_{tot}} (P_{in} - P_{out}) \tag{3.45}$$

where

$$\Delta P_{tot} = \Delta P_{dsh} + \Delta P_{cond} + \Delta P_{sc}$$

The new pressures were now used in the analysis of the energy balance to determine the condenser resistances. New pressures, based upon the relative error, were calculated. The iteration process was usually completed after two iterations.

CHAPTER 4

STEADY-STATE RESULTS

This chapter presents the steady-state results. Table 4.1 is presented to give a test number to each test along with the test data used in the analysis. The letter A in the test number represents a low air temperature entering the evaporator and an inlet condenser air temperature between 80°F and 90°F. The letter B in the test number represents a higher air temperature entering the evaporator and an inlet condenser air temperature between 70°F and 76°F. The first number represents the volumetric air flow grouping. The last number represents the lowest to highest compressor speed for the specified volumetric air flow grouping where one is the lowest compressor speed.

Table 4.1. Steady-State Test Runs.

TEST NUMBER	$\dot{V}$ SCFM	$\dot{w}$ $\frac{lb}{hr}$	$T_{air,in}$ °F	$T_{air,out}$ °F	T_{wet} °F	$T_{ref,in}$ °F	$P_{ref,in}$ psia	$T_{ref,out}$ °F	$P_{ref,out}$ psia
A-590-1	588	329.6	85.6	125.0	70	189.9	260.9	136.9	255.3
A-590-2	591	447.8	84.2	137.0	73	218.6	319.8	150.4	312.7
A-590-3	590	469.9	83.0	140.7	70	236.3	336.3	154.5	328.4
A-590-4	600	496.4	83.2	144.1	69	246.9	351.5	158.2	343.4
A-590-5	591	475.8	80.0	142.4	66	257.3	343.2	156.6	334.7
A-710-1	711	312.4	86.7	118.7	70	186.6	242.6	130.5	236.6
A-710-2	709	428.4	85.3	128.8	73	212.2	296.2	142.5	288.3
A-710-3	714	430.5	83.8	129.9	70	230.5	300.3	144.2	292.0
A-710-4	703	440.3	83.4	132.0	69	239.0	308.5	146.4	299.9
A-710-5	713	440.4	81.3	131.5	66	251.6	308.0	146.4	299.3
A-825-1	820	301.2	88.0	115.3	70	184.9	232.8	126.6	226.6
A-825-2	828	401.8	87.3	123.4	73	208.6	276.4	136.5	268.7
A-825-3	829	420.5	85.5	125.1	70	226.6	285.4	139.4	276.3
A-825-4	823	413.3	84.2	124.6	69	235.2	282.6	138.9	273.6
A-825-5	822	417.1	83.0	125.6	66	249.3	287.8	140.3	278.7
A-945-1	949	297.9	89.3	112.9	70	184.3	225.8	124.5	219.9
A-945-2	942	390.3	89.1	120.4	73	206.4	265.8	133.2	258.3
A-945-3	940	407.9	87.6	122.0	70	225.5	274.7	135.9	265.7
A-945-4	945	399.8	85.5	120.3	69	233.6	268.7	134.5	259.8
A-945-5	946	408.4	84.6	121.5	66	247.0	274.6	136.2	265.5

Table 4.1. (cont.).

TEST NUMBER	$\dot{V}$ SCFM	w $\frac{lb}{hr}$	$T_{air,in}$ °F	$T_{air,out}$ °F	T_{wet} °F	$T_{ref,in}$ °F	$P_{ref,in}$ psia	$T_{ref,out}$ °F	$P_{ref,out}$ psia
A-1060-1	1054	296.7	90.4	111.8	70	184.4	222.1	122.9	215.9
A-1060-2	1056	355.7	90.2	116.5	73	207.5	247.3	129.0	239.4
A-1060-3	1055	397.8	89.8	120.2	70	225.9	267.0	133.9	258.6
A-1060-4	1067	388.6	87.2	117.7	69	233.7	258.9	131.6	250.1
A-1060-5	1062	401.5	86.8	119.6	66	248.0	267.2	133.7	257.9
B-600-1	604	319.3	69.9	105.0	68	128.4	206.8	112.1	200.8
B-600-2	606	399.2	69.9	112.3	68	139.8	239.8	120.6	232.3
B-600-3	606	471.7	70.2	119.0	68	152.2	273.1	128.7	264.6
B-600-4	609	530.6	70.3	124.2	68	163.8	300.8	135.0	291.7
B-600-5	609	591.8	71.2	130.4	69	175.2	332.1	141.3	322.4
B-600-6	610	644.2	70.9	135.0	69	188.6	362.4	147.1	351.9
B-600-7	614	700.0	71.1	139.5	69	199.3	392.5	152.7	381.8
B-1200-1	1206	309.3	71.5	89.7	68	114.6	169.1	94.7	163.2
B-1200-2	1206	374.0	71.1	93.0	68	123.1	187.3	98.9	179.7
B-1200-3	1204	422.8	71.1	95.9	68	131.9	203.7	102.9	194.6
B-1200-4	1209	465.2	71.4	98.7	68	142.2	218.9	106.8	208.8
B-1200-5	1210	498.3	71.3	100.9	68	152.5	232.8	109.9	222.2
B-1200-6	1215	528.5	71.4	102.9	68	161.1	244.0	112.7	232.6
B-1200-7	1212	548.5	71.5	104.6	68	168.2	254.0	114.9	241.9
B-1500-1	1514	313.9	74.9	89.7	69	115.0	169.4	94.5	163.2
B-1500-2	1500	382.0	75.0	93.1	69	123.9	187.6	98.7	179.6
B-1500-3	1503	430.3	75.0	95.4	69	132.7	202.3	101.7	193.2
B-1500-4	1500	466.4	75.0	97.4	69	142.1	214.8	104.6	204.4
B-1500-5	1498	494.6	75.2	99.2	69	151.7	227.0	107.2	215.9
B-1500-6	1502	522.8	75.4	101.0	69	159.5	237.3	109.7	225.7
B-1500-7	1500	545.9	75.3	102.3	69	166.7	247.1	111.7	234.9
B-1800-1	1822	296.7	74.8	86.6	69	110.8	159.4	90.4	153.4
B-1800-2	1826	355.7	75.1	89.2	68	120.0	175.3	94.0	167.5
B-1800-3	1828	402.0	75.1	91.2	68	129.3	188.5	96.4	179.6
B-1800-4	1826	435.3	75.3	93.0	68	139.3	200.0	98.8	189.9
B-1800-5	1830	463.9	75.6	94.7	68	150.4	210.3	101.6	199.3
B-1800-6	1817	482.0	75.4	95.6	68	157.0	218.3	103.0	206.6
B-1800-7	1824	501.2	75.6	96.8	68	164.6	225.6	104.7	213.9

4.1. Least-Squares Analysis with the Energy Equations

Based upon the energy equations and the fact that the sum of the fractions of the condenser must equate to one, the sectional overall heat transfer coefficients could be determined. The least squares analysis determined the coefficients expressed in Equation 3.22 which minimized the sum of the squared errors (e):

$$1 = \frac{c_{dsh}}{\left(\frac{w_{in}}{2}\right)^{0.8}} \frac{w_{in}(h_g - h_{in})}{(T'_{air} - T'_{ref})_{dsh}} + \frac{c_{cond}}{w_{in}^{0.8}} \frac{w_{in}(h_f - h_g)}{(T'_{air} - T'_{ref})_{cond}} +$$

$$\frac{c_{sc}}{w_{in}^{0.8}} \frac{w_{in}(h_{out} - h_f)}{(T'_{air} - T'_{ref})_{sc}} + \frac{b}{\dot{V}^{0.5}} \left\{ \frac{w_{in}(h_g - h_{in})}{(T'_{air} - T'_{ref})_{dsh}} + \right.$$

$$\left. \frac{w_{in}(h_f - h_g)}{(T'_{air} - T'_{ref})_{cond}} + \frac{w_{in}(h_{out} - h_f)}{(T'_{air} - T'_{ref})_{sc}} \right\} + e \qquad (4.1)$$

where

$$c_{dsh} = 216.202 \frac{^{\circ}F\text{-sec}}{Btu} \left(\frac{lb}{hr}\right)^{0.8}$$

$$c_{cond} = 110.637 \frac{^{\circ}F\text{-sec}}{Btu} \left(\frac{lb}{hr}\right)^{0.8}$$

$$c_{sc} = 463.107 \frac{^{\circ}F\text{-sec}}{Btu} \left(\frac{lb}{hr}\right)^{0.8}$$

$$b = 115.287 \frac{^{\circ}F\text{-sec}}{Btu} \left(\frac{ft^3}{min}\right)^{0.5}$$

The results of the fit are graphically displayed in Figure 4.1. The exact solution would be one and the sum of the fractions of the condenser calculated with Equation 4.1 is displayed based upon the mass flow rate of the test. The scatter in the data is less than 5%.

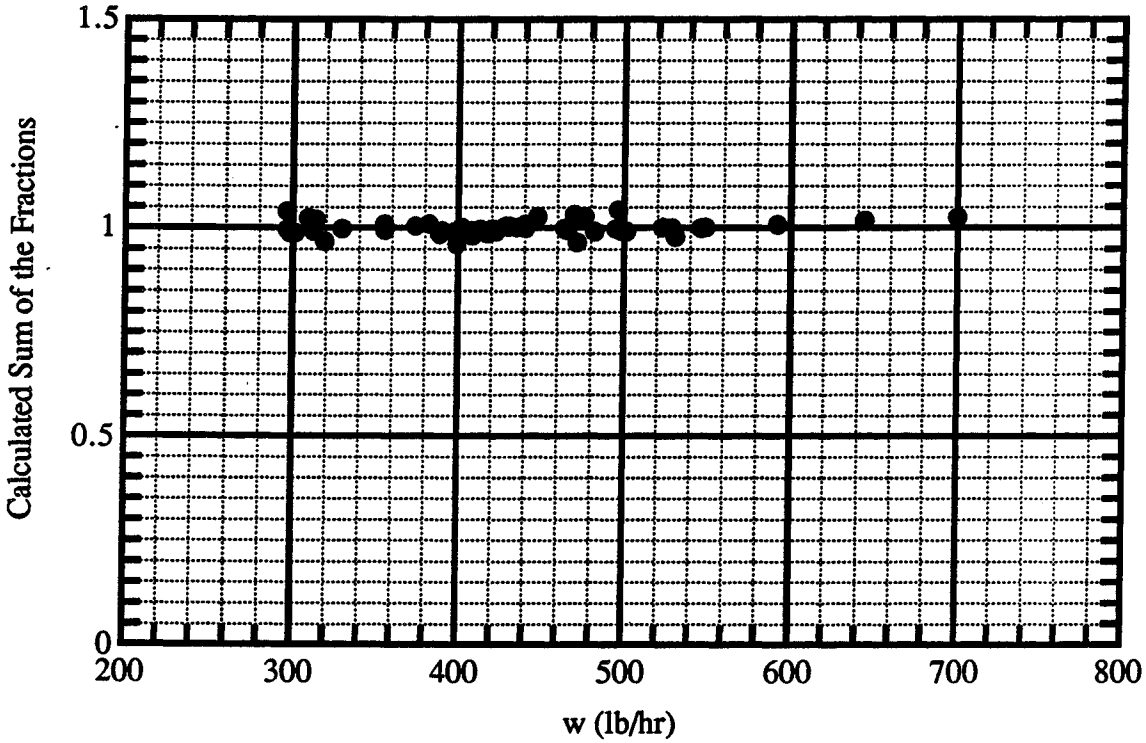

Figure 4.1. Calculated Sum of the Fractions Versus the Refrigerant Mass Flow Rate.

The fit was also compared based on the volumetric flow rate of air to determine if any trends existed. Figure 4.2 shows the sum of the fractions of the condenser calculated with Equation 4.1 versus the volumetric flow rate of air. No apparent trends in error can be determined with the volumetric air flow rate. Similar plots were constructed for all the data listed in Table 4.1. The results showed no obvious trends.

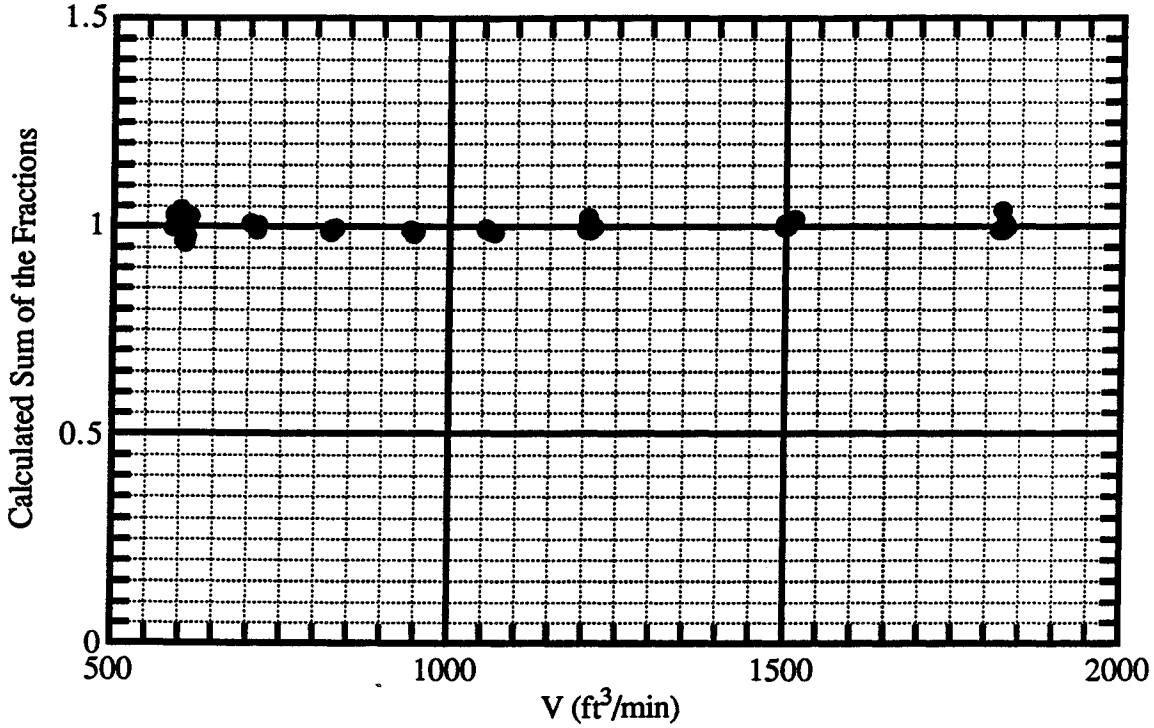

Figure 4.2. Calculated Sum of the Fractions Versus the Volumetric Air Flow Rate.

4.2. Least-Squares Analysis with the Momentum Equations

With the overall heat transfer coefficients known for each section, the fraction of the condenser in each section can be determined. This will be shown later when the final answer reflects the convergence of the pressure drop terms. The fractions of the condenser used in the least-squares analysis determined the coefficients expressed in Equation 3.30 to determine the friction factors for the three sections:

$$P_{in} + \frac{\left(\frac{w_{in}}{2}\right)^2}{A^2\rho_{in}} - P_{out} - \frac{w_{in}^2}{A^2\rho_{out}} = \left(b + \frac{c_{dsh}}{\left(\frac{w_{in}}{2}\right)^{0.237}}\right) L \frac{f_{dsh}}{d} \frac{\left(\frac{w_{in}}{2}\right)^2}{2\rho_{in}A^2} +$$

$$(b + \frac{c_{cond}}{(\frac{w_{in}}{2})^{0.237}})L \frac{(\frac{1}{3} - f_{dsh})}{d} \frac{\left(\frac{w_{in}}{2}\right)^2}{2\rho_g A^2} +$$

$$(b + \frac{c_{cond}}{w^{0.237}})L \frac{(f_{cond} - (\frac{1}{3} - f_{dsh}))}{d} \frac{w_{in}^2}{2\rho_g A^2} +$$

$$(\frac{c_{sc}}{w^{0.25}})L \frac{f_{sc}}{d} \frac{w_{in}^2}{2\rho_f A^2} + e \qquad (4.2)$$

where

$$Lc_{dsh} = 0.227253 \left(\frac{lb}{s}\right)^{0.237} ft$$

$$Lc_{cond} = 0.137762 \left(\frac{lb}{s}\right)^{0.237} ft$$

$$Lc_{sc} = 0.271552 \left(\frac{lb}{s}\right)^{0.25} ft$$

$$Lb = -0.108633 \text{ ft}$$

Figure 4.3 shows the total measured pressure drops from experimental data ($\Delta P_{actual} = P_{in} - P_{out}$) on the ordinate and the calculated pressure drops based on the least-squares analysis on the abscissa. The 45 degree line is superimposed on the plot to visually clarify the scatter of the fit.

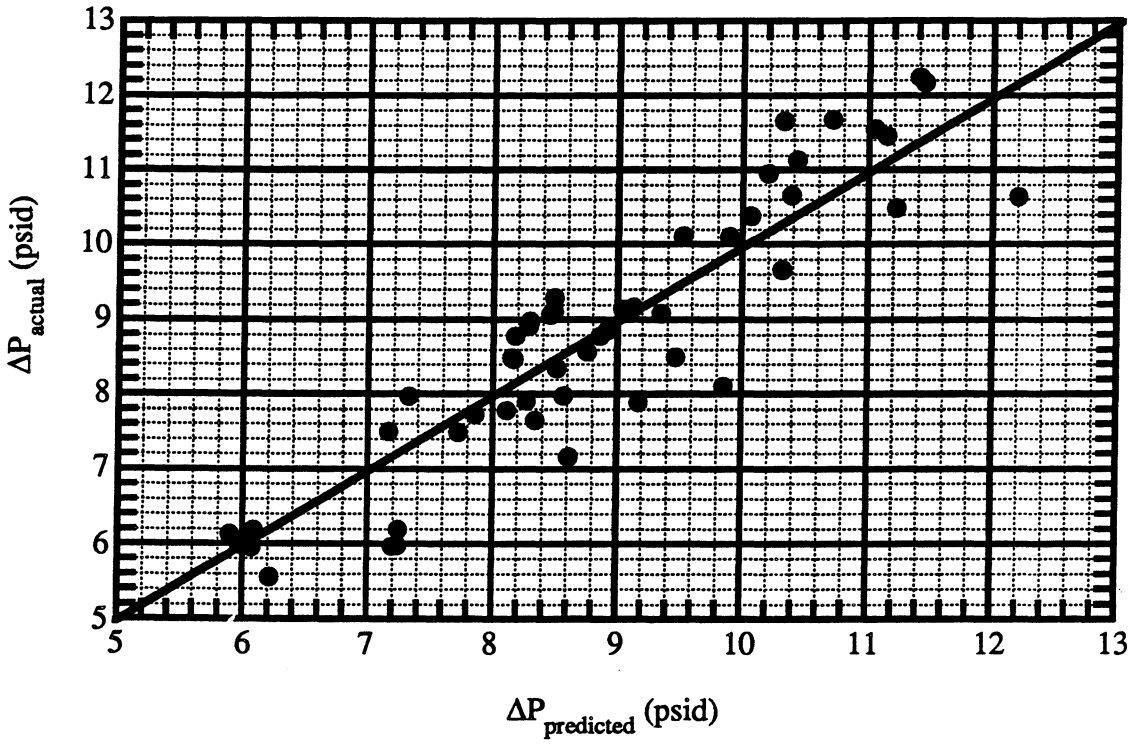

Figure 4.3. Experimentally Measured Values of Equation 4.2 Versus the Least-Squares Calculated Values.

Figure 4.3 presents the error between the actual and predicted pressure drop values. The maximum error is 2 psid. Figure 4.4 is pressure drop error versus the refrigerant mass flow rate. This graph does not appear to have any trends that would suggest a relation between the pressure drop error and the refrigerant mass flow rate.

To be consistent with the least-squares energy balance analysis, the errors of the measured and least-squares calculated pressure drops versus the volumetric air flow rate are shown in Figure 4.5. This graph also does not appear to have any trends that would suggest a relation between the pressure drop error and the refrigerant mass flow rate.

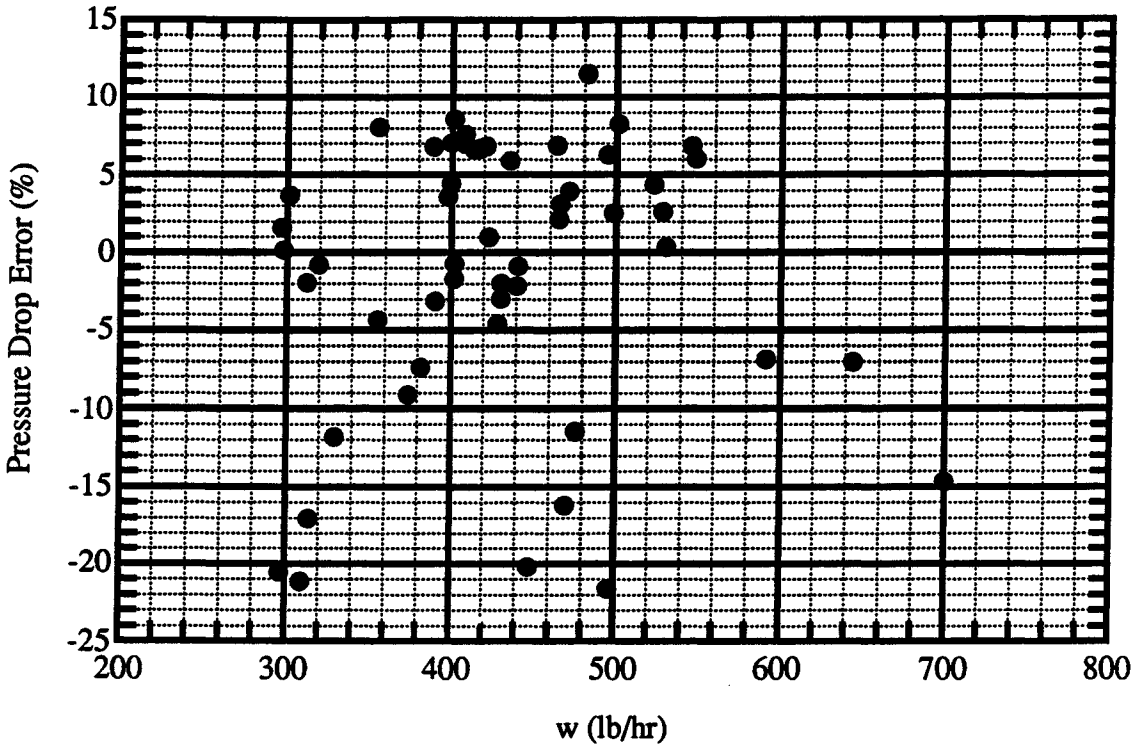

Figure 4.4. Error of Measured and Least-Squares Calculations Versus the Refrigerant Mass Flow Rate.

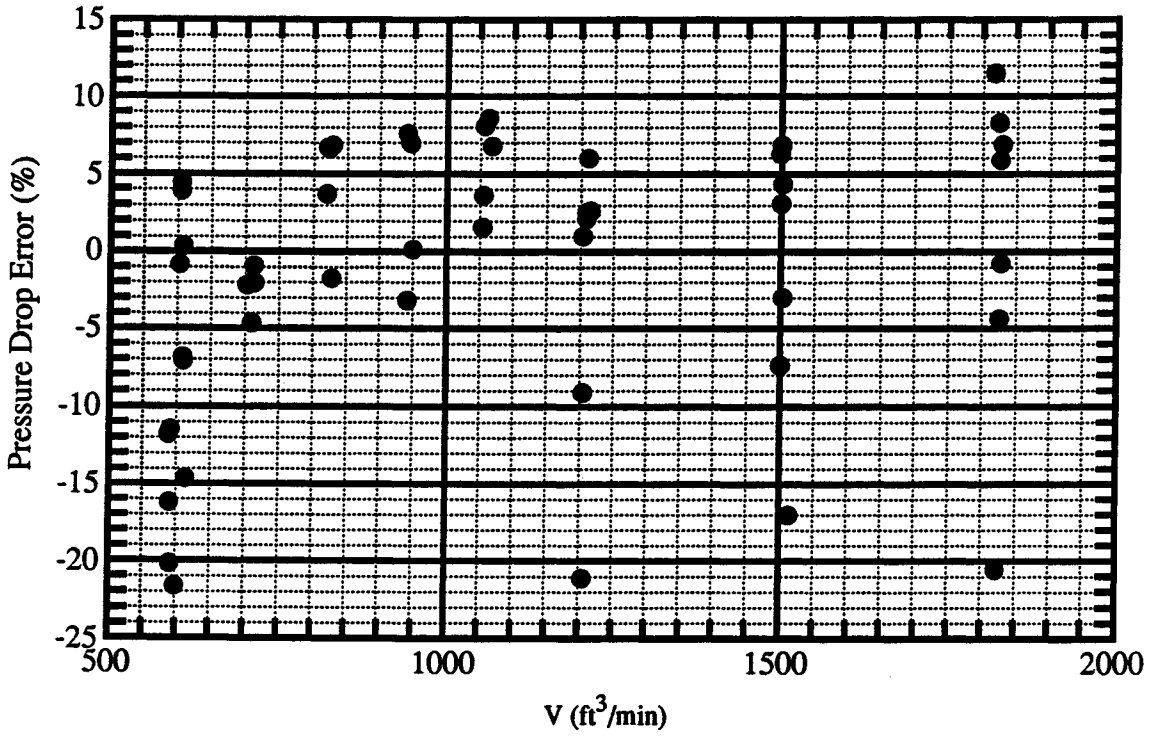

Figure 4.5. Pressure Drop Error Versus the Volumetric Air Flow Rate.

Similar plots were constructed for all the data listed in Table 4.1. When the error was plotted against the condenser inlet ($T_{ref,in}$) and outlet refrigerant ($T_{ref,in}$) temperatures and pressures, a trend similar to Figure 4.6, pressure drop error versus outlet refrigerant temperature, was observed for all cases. The largest error always occurred at the highest and lowest temperature or pressure. This suggests that at the larger and smaller pressure and temperature values the model may need to be modified to properly represent this region. This is especially true of the A-590 case where the air flow and compressor speeds are very low compared to the other data points.

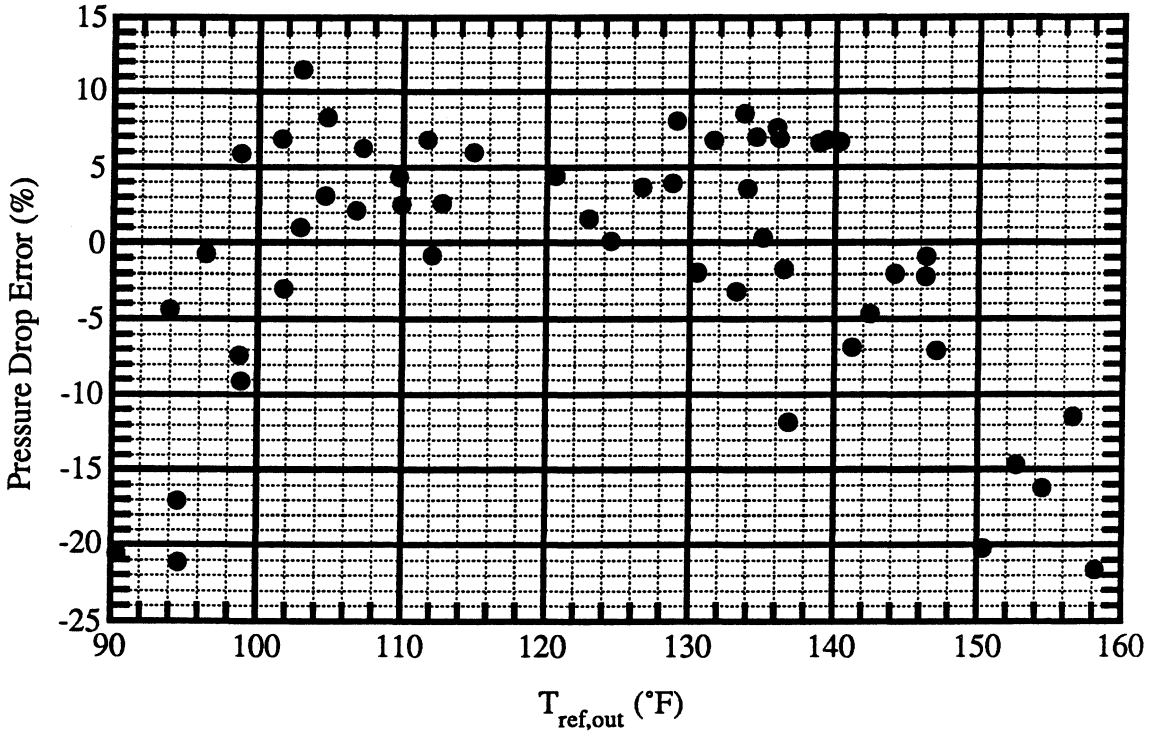

Figure 4.6. Pressure Drop Error Versus the Outlet Refrigerant Temperature.

4.3. Condenser Characteristics During Steady-State

The iteration process to determine the pressure drops was completed after two iterations. The overall heat transfer coefficients calculated for each section were determined with the constants found in Equation 4.1. Figure 4.7 shows the desuperheating overall heat transfer coefficient times

the tube length ($U_{dsh}L$) for a given volumetric air flow rate versus the refrigerant mass flow rate. In general, as the refrigerant mass flow rate increases the overall heat transfer coefficient also increases. Also, as the air volume flow rate increases, the overall heat transfer coefficient increases.

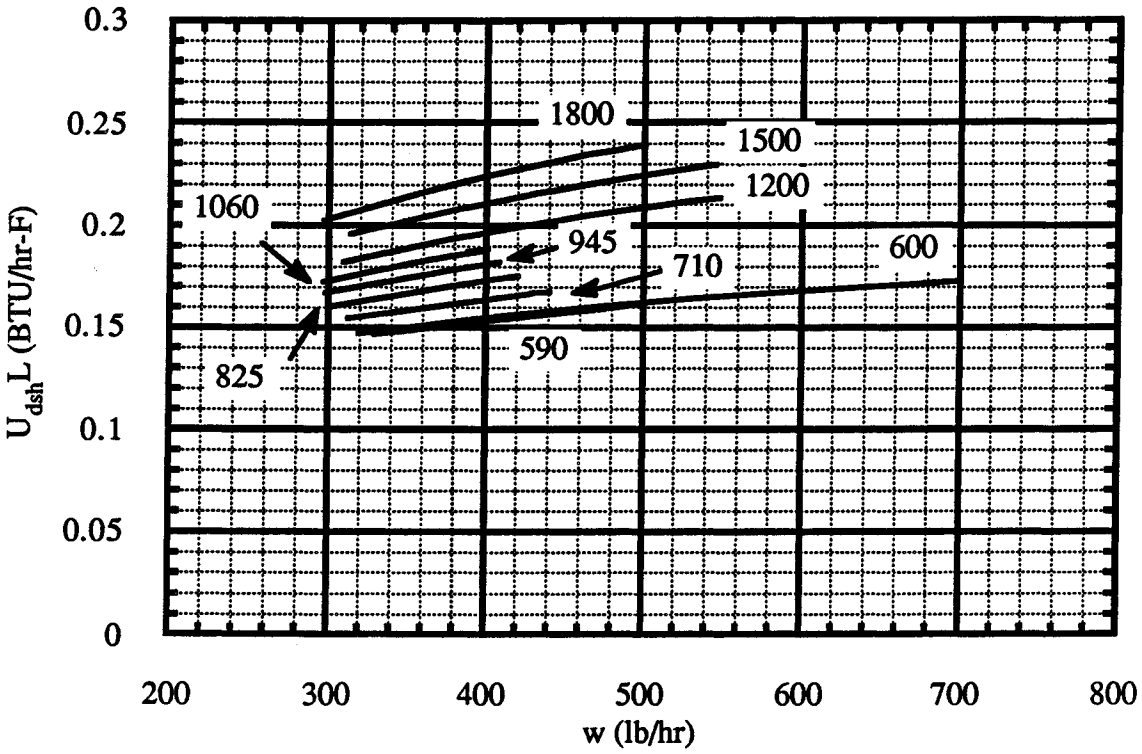

Figure 4.7. Desuperheating Overall Heat Transfer Coefficient Times Tube Length Versus the Refrigerant Mass Flow Rate For a Volumetric Air Flow (SCFM).

Figure 4.8 shows the condensing overall heat transfer coefficient times the tube length ($U_{cond}L$) for a given volumetric air flow rate versus the refrigerant mass flow rate. Once again, the overall heat transfer coefficient increases with increasing refrigerant mass flow rate. The overall heat transfer coefficient increases with increasing volumetric air flow rates.

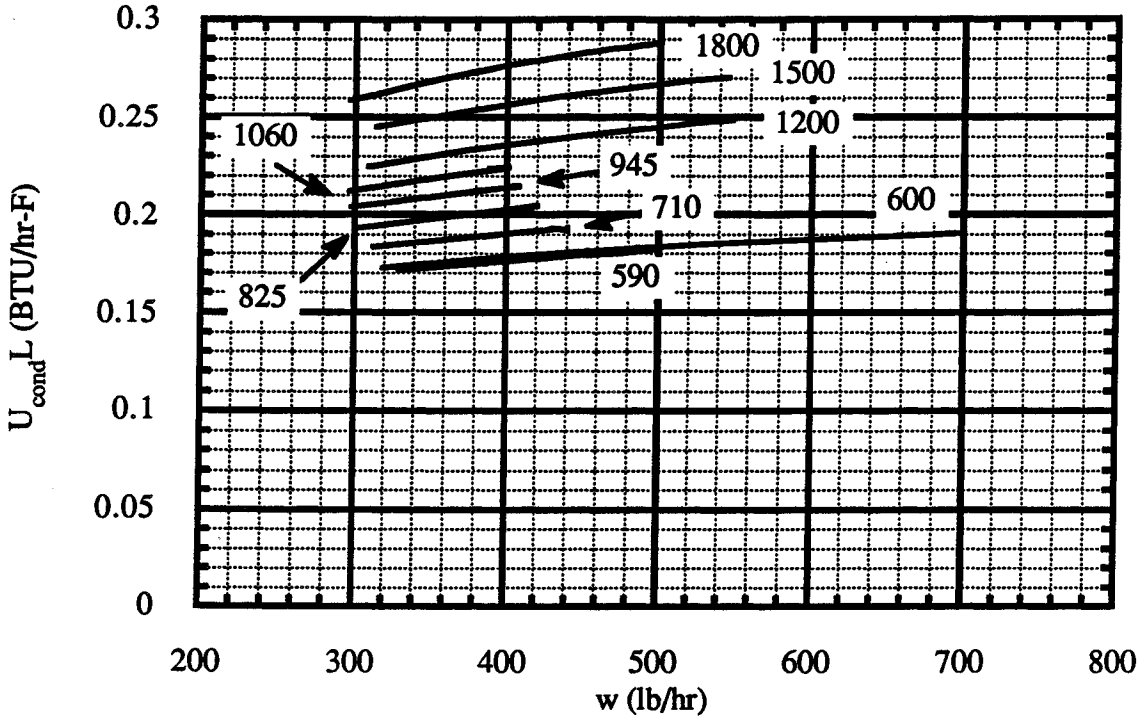

Figure 4.8. Condensing Overall Heat Transfer Coefficient Times Tube Length Versus the Refrigerant Mass Flow Rate For a Volumetric Air Flow (SCFM).

Figure 4.9 shows a similar trend for the subcooling section. The magnitudes of the overall heat transfer coefficient times the tube length show the condensing section being the largest, then the desuperheating section, and finally the subcooling section being the smallest. It should be noted that the magnitude of the desuperheating and condensing overall heat transfer coefficients are almost similar. Also, the desuperheating section has a mass flux that is half the mass flux of the subcooling section and the condensing section has two sections, one at half the subcooling flow rate and the other at the subcooling flow rate. This may explain why the condensing section does not have a higher overall heat transfer coefficient when compared to the desuperheating section.

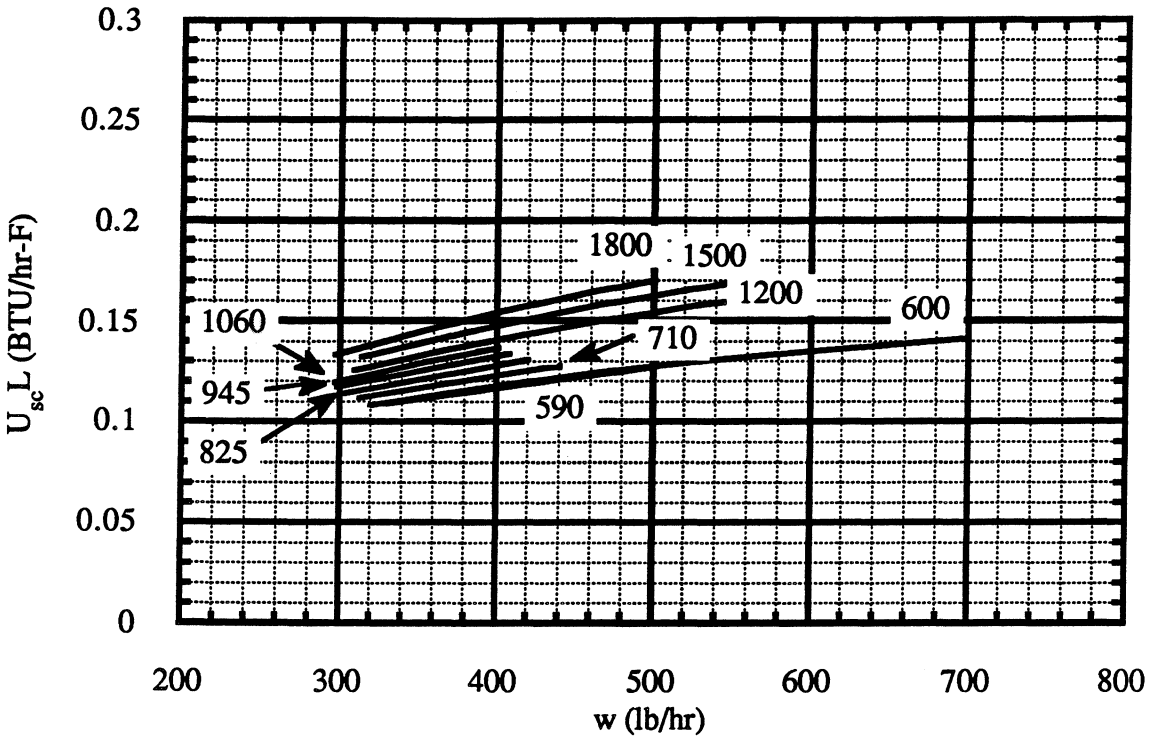

Figure 4.9. Subcooling Overall Heat Transfer Coefficient Times Tube Length Versus the Refrigerant Mass Flow Rate For a Volumetric Air Flow (SCFM).

Figure 4.10 shows the desuperheating fraction of the condenser as a function of the desuperheating temperature ($\Delta T_{desuperheating} = T_{in} - T_g$). The data appears to be clustered in two sections based on the inlet evaporator and inlet condenser air temperatures. In general, the fraction increases as the air volumetric flow rate decreases. Also, as the desuperheating temperature increases, the fraction also increases.

Figure 4.11 shows the subcooling fraction versus the subcooling temperature ($\Delta T_{subcooling} = T_f - T_{out}$). Once again the data is clustered based on the evaporator inlet air temperature. At the low evaporator loading (Grouping A), the subcooling fraction appears to be independent of the volumetric air flow rate. The fraction only increases as the subcooling temperature increases. The high evaporator loading (grouping B) shows the subcooling fraction increasing with increasing volumetric air flow and increasing with the subcooling temperature.

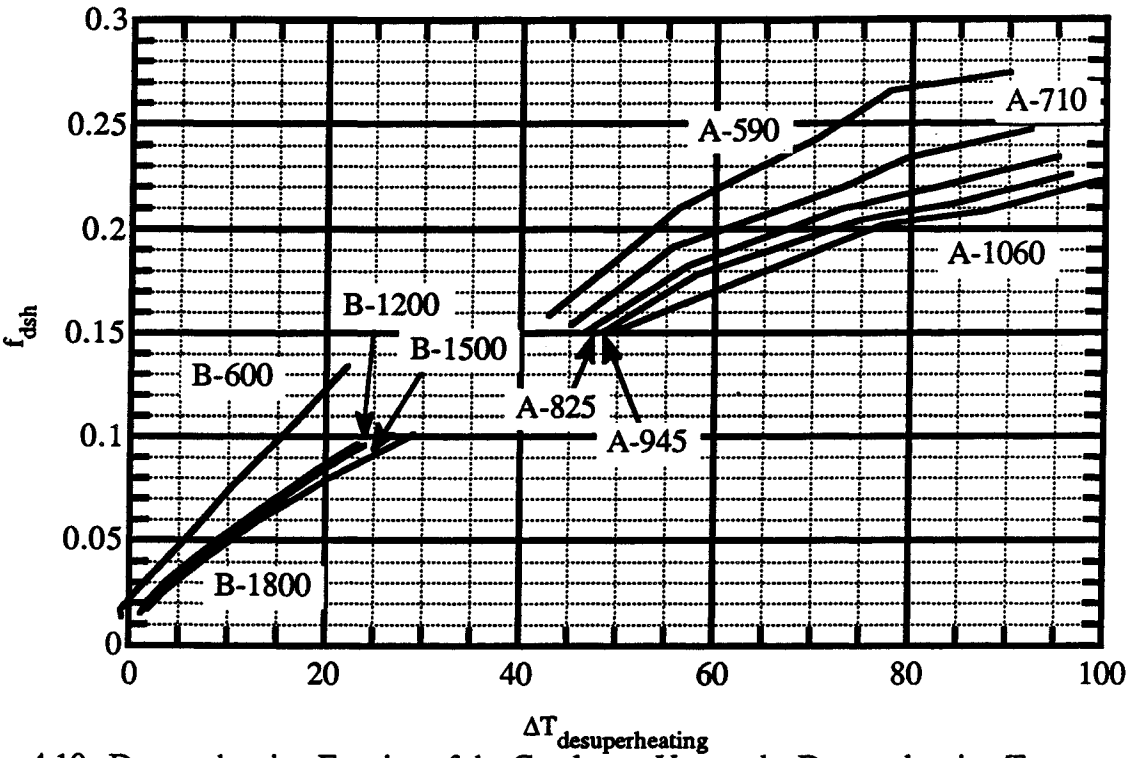

Figure 4.10. Desuperheating Fraction of the Condenser Versus the Desuperheating Temperature.

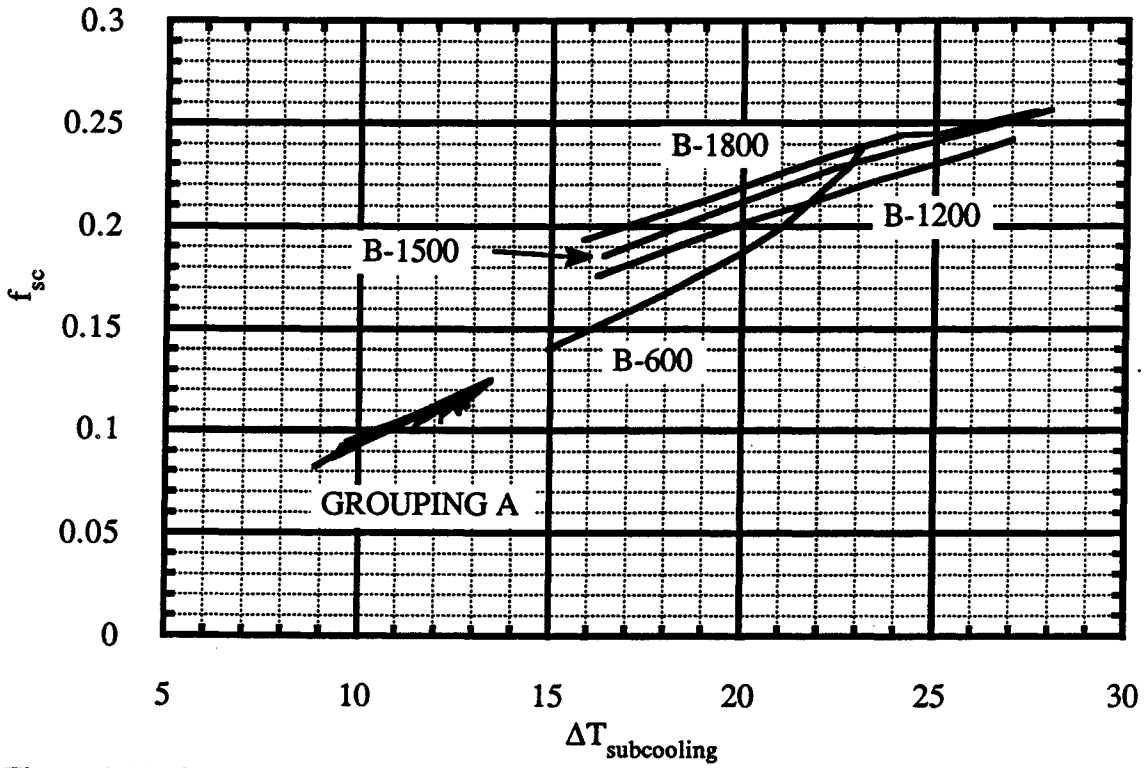

Figure 4.11. Subcooling Fraction of the Condenser Versus the Subcooling Temperature.

Table 4.2 summarizes the fractions of the condenser calculated for each of the three sections. The test number corresponds to the conditions specified in Table 4.1. The magnitude of the desuperheating fractions in comparison to the subcooling fractions may seem large at first for the low air flow group. But the desuperheating section is part of the parallel tube section of the condenser. Since the flow rate through each tube is half the total refrigerant flow rate, which also decreases the refrigerant heat transfer coefficient, a longer length of tube is required to obtain a larger amount of heat transfer without the large pressure drop. Also, the air flow across the condenser is extremely low for this system at the low air flow test points. The higher air flow group has a larger subcooling section since the air flow rate is higher and thus aiding in the subcooling process.

Table 4.2. Calculated Condenser Fractions for the Specified Test Run.

TEST NUMBER	f_{dsh}	f_{cond}	f_{sc}	Σf_i
A-590-1	0.158	0.757	0.083	0.997
A-590-2	0.210	0.714	0.102	1.026
A-590-3	0.243	0.692	0.097	1.032
A-590-4	0.266	0.683	0.093	1.042
A-590-5	0.274	0.665	0.087	1.027
A-710-1	0.154	0.751	0.087	0.991
A-710-2	0.191	0.697	0.117	1.005
A-710-3	0.220	0.677	0.107	1.004
A-710-4	0.233	0.670	0.105	1.008
A-710-5	0.247	0.652	0.100	0.999
A-825-1	0.151	0.745	0.093	0.989
A-825-2	0.183	0.691	0.122	0.997
A-825-3	0.209	0.676	0.112	0.997
A-825-4	0.219	0.669	0.108	0.997
A-825-5	0.234	0.648	0.105	0.987
A-945-1	0.150	0.746	0.092	0.988
A-945-2	0.178	0.689	0.126	0.993
A-945-3	0.204	0.672	0.117	0.994
A-945-4	0.212	0.664	0.111	0.987
A-945-5	0.226	0.648	0.109	0.983

Table 4.2. (cont.)

TEST NUMBER	f_{dsh}	f_{cond}	f_{sc}	Σf_i
A-1060-1	0.151	0.750	0.095	0.996
A-1060-2	0.180	0.704	0.111	0.994
A-1060-3	0.202	0.671	0.118	0.991
A-1060-4	0.208	0.665	0.112	0.985
A-1060-5	0.223	0.650	0.113	0.986
B-600-1	0.013	0.813	0.141	0.967
B-600-2	0.017	0.777	0.168	0.962
B-600-3	0.029	0.748	0.188	0.965
B-600-4	0.051	0.726	0.201	0.978
B-600-5	0.075	0.710	0.222	1.007
B-600-6	0.108	0.679	0.230	1.016
B-600-7	0.134	0.652	0.239	1.025
B-1200-1	0.015	0.831	0.177	1.023
B-1200-2	0.020	0.785	0.200	1.005
B-1200-3	0.031	0.748	0.213	0.992
B-1200-4	0.049	0.722	0.224	0.995
B-1200-5	0.068	0.690	0.233	0.992
B-1200-6	0.085	0.677	0.238	1.000
B-1200-7	0.097	0.661	0.243	1.001
B-1500-1	0.017	0.815	0.187	1.018
B-1500-2	0.023	0.775	0.211	1.010
B-1500-3	0.036	0.737	0.230	1.003
B-1500-4	0.053	0.711	0.238	1.002
B-1500-5	0.070	0.680	0.247	0.997
B-1500-6	0.084	0.665	0.252	1.000
B-1500-7	0.096	0.646	0.258	1.000
B-1800-1	0.017	0.827	0.195	1.039
B-1800-2	0.027	0.768	0.214	1.009
B-1800-3	0.041	0.727	0.234	1.002
B-1800-4	0.059	0.696	0.246	1.001
B-1800-5	0.080	0.673	0.247	1.000
B-1800-6	0.089	0.650	0.254	0.992
B-1800-7	0.101	0.633	0.258	0.992

Figures 4.12 shows the friction factor times the total tube length for the three sections of the condenser. Each of these friction factors decrease as the refrigerant mass flow rate increases and is not a function of the volumetric air flow rate. The magnitude of the subcooling friction

factor should be larger than the desuperheating section. Although this result holds true, the magnitude of the friction factor using a Moody chart analysis is an order of magnitude larger than the results shown here. The results of the condensing section can not be verified by the Moody chart since the process is two-phase.

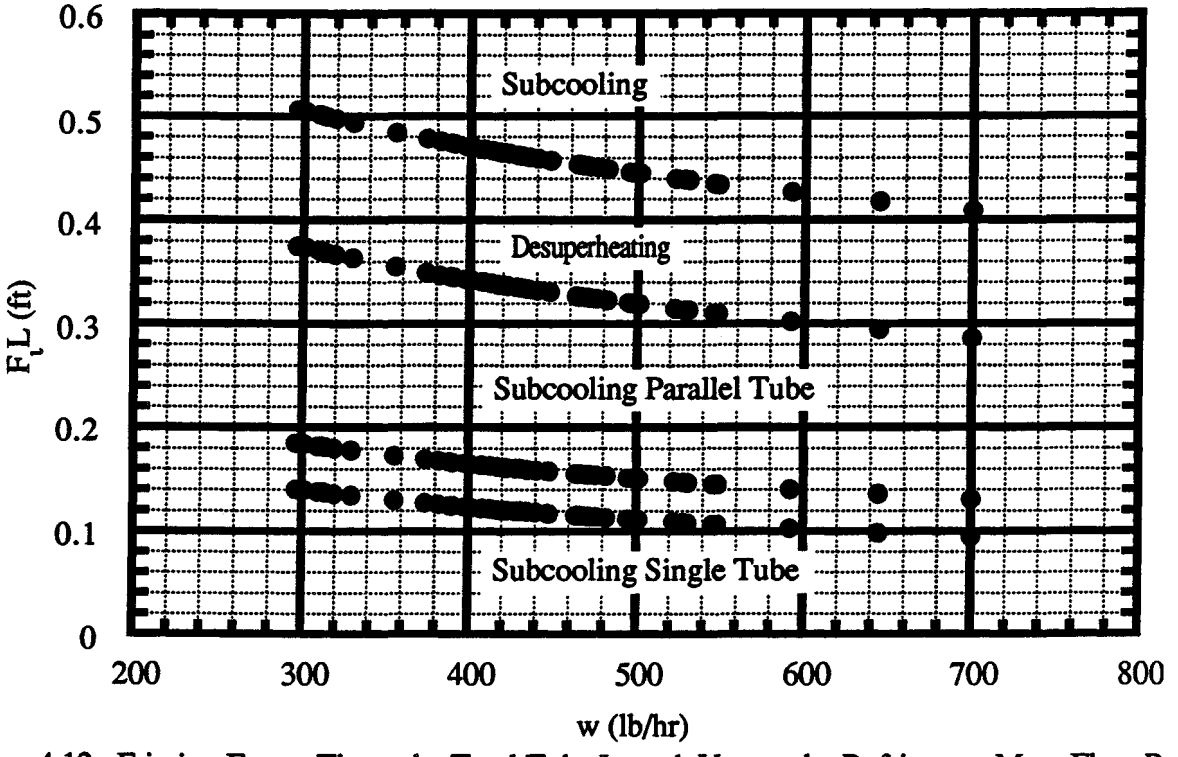

Figure 4.12. Friction Factor Times the Total Tube Length Versus the Refrigerant Mass Flow Rate.

Table 4.3 summarizes the pressure drops of the condenser calculated with the friction factors for each of the three sections. The test number corresponds to the conditions specified in Table 4.1. At the lower evaporator load (Grouping A), the condensing section has the largest pressure drop, then the desuperheating section and finally the subcooling section. In general, the condensing pressure drop is two to five times larger than the desuperheating section. The subcooling section is usually an order of magnitude smaller than the desuperheating section. At high evaporator loads (Grouping B), the pressure drop in the condensing section is the largest. The desuperheating and subcooling sections have pressure drops that are almost identical. These

pressures drops are an order of magnitude smaller to three times smaller than the condensing section.

Table 4.3. Calculated Pressure Drops for the Specified Test Run.

TEST NUMBER	ΔP_{dsh} psia	ΔP_{cond} psia	ΔP_{sc} psia	$\Sigma \Delta P_i$ psia	$\Delta P_{measured}$ psia
A-590-1	0.96	5.02	0.23	6.21	5.56
A-590-2	1.79	6.32	0.50	8.61	7.16
A-590-3	2.22	6.42	0.53	9.17	7.89
A-590-4	2.60	6.69	0.56	9.85	8.10
A-590-5	2.65	6.33	0.49	9.47	8.50
A-710-1	0.93	4.92	0.22	6.07	5.95
A-710-2	1.63	6.12	0.52	8.27	7.91
A-710-3	1.96	6.07	0.48	8.51	8.35
A-710-4	2.14	6.12	0.50	8.76	8.57
A-710-5	2.35	6.04	0.47	8.86	8.78
A-825-1	0.89	4.79	0.21	5.90	6.12
A-825-2	1.51	5.87	0.48	7.86	7.73
A-825-3	1.88	6.11	0.48	8.48	9.10
A-825-4	1.99	6.03	0.45	8.46	9.06
A-825-5	2.18	5.86	0.45	8.49	9.10
A-945-1	0.91	4.86	0.21	5.97	5.98
A-945-2	1.46	5.80	0.47	7.73	7.49
A-945-3	1.82	6.00	0.47	8.30	8.98
A-945-4	1.91	5.94	0.43	8.29	8.91
A-945-5	2.12	5.91	0.44	8.48	9.11
A-1060-1	0.92	4.95	0.21	6.09	6.18
A-1060-2	1.38	5.60	0.35	7.32	7.97
A-1060-3	1.79	5.93	0.45	8.17	8.47
A-1060-4	1.87	5.90	0.41	8.18	8.78
A-1060-5	2.11	5.94	0.44	8.49	9.29
B-600-1	0.07	5.63	0.35	6.05	6.00
B-600-2	0.12	6.41	0.64	7.16	7.49
B-600-3	0.27	6.90	0.98	8.15	8.48
B-600-4	0.51	7.30	1.32	9.13	9.16
B-600-5	0.81	7.70	1.80	10.32	9.66
B-600-6	1.24	7.76	2.22	11.22	10.49
B-600-7	1.62	7.85	2.74	12.20	10.64

Table 4.2. (cont.)

TEST NUMBER	ΔP_{dsh} psia	ΔP_{cond} psia	ΔP_{sc} psia	$\Sigma \Delta P_i$ psia	$\Delta P_{measured}$ psia
B-1200-1	0.08	6.75	0.41	7.24	5.98
B-1200-2	0.15	7.54	0.65	8.34	7.65
B-1200-3	0.29	7.89	0.87	9.05	9.14
B-1200-4	0.55	8.25	1.09	9.90	10.11
B-1200-5	0.83	8.26	1.29	10.39	10.65
B-1200-6	1.10	8.57	1.47	11.15	11.44
B-1200-7	1.29	8.53	1.62	11.45	12.18
B-1500-1	0.10	6.71	0.44	7.24	6.19
B-1500-2	0.19	7.66	0.71	8.57	7.98
B-1500-3	0.36	8.03	0.96	9.35	9.08
B-1500-4	0.61	8.29	1.16	10.06	10.38
B-1500-5	0.87	8.22	1.35	10.43	11.13
B-1500-6	1.10	8.42	1.53	11.05	11.55
B-1500-7	1.31	8.40	1.70	11.41	12.24
B-1800-1	0.09	6.69	0.41	7.20	5.97
B-1800-2	0.21	7.28	0.63	8.12	7.78
B-1800-3	0.40	7.65	0.86	8.91	8.85
B-1800-4	0.65	7.83	1.05	9.52	10.12
B-1800-5	0.97	8.05	1.19	10.20	10.95
B-1800-6	1.12	7.89	1.31	10.32	11.66
B-1800-7	1.33	7.94	1.44	10.71	11.68

4.4. Verification of the Condenser Model

To clarify how well the model predicts the outlet refrigerant pressure (P_{out}) and temperature ($T_{ref,out}$) and the outlet air temperature ($T_{air,out}$), a steady-state version of the transient condenser program was utilized. The air (w_{air}) and refrigerant (w_{in}) flow rates are inputs into the model. Also, the refrigerant temperature ($T_{ref,in}$) and pressure ($P_{ref,in}$) and the inlet air temperature ($T_{air,in}$) are known. The flow rates are used with the results from the least-squares analysis to predict the UL for the given section. The friction factor (FL) for the section is determined with the refrigerant mass flow rate.

A heat exchanger and refrigerant-side energy rate equation was used in conjunction with the momentum equation for each of the three sections. An air-side energy rate equation was used for the entire condenser to predict the outlet air temperature of the condenser. The program then used a

Newton-Raphson technique to solve for the six unknowns related to the two equations for each of the three condenser sections.

For the desuperheating section, an energy rate balance between the the heat exchanger and refrigerant-side results in an equation:

$$w_{in}(h_g - h_{in}) = f_{dsh}LU_{dsh}(T'_{air} - T'_{ref})_{dsh} \tag{4.3}$$

where

$$LU_{dsh} = f(\dot{V}, w_{in})$$

The unknowns are h_g, f_{dsh}, and $T_{air,out}$, which is used in the term T'_{air}. This equation is used in the solution technique to determine f_{dsh}. Since the refrigerant exiting the desuperheating section is a saturated vapor, the momentum equation is used to determine the outlet pressure (P_g) of this section which also specifies the outlet enthalpy (h_g).

$$P_{in} + \frac{\left(\frac{w_{in}}{2}\right)^2}{A^2\rho_{in}} = P_g + \frac{\left(\frac{w_{in}}{2}\right)^2}{A^2\rho_g} + F_{dsh}L\,\frac{f_{dsh}}{d}\,\frac{\left(\frac{w_{in}}{2}\right)^2}{2\rho_{in}A^2} \tag{4.4}$$

where

$$F_{dsh}L = f(w_{in})$$

A similar method is used for the condensing section. The energy rate balance between the heat exchanger and the refrigerant-side is used in the Newton-Raphson solution method to solve for the fraction of the condenser in the condensing region (f_{cond}).

$$w_{in}(h_f - h_g) = f_{cond}LU_{cond}(T'_{air} - T'_{ref})_{cond} \tag{4.5}$$

where

$$LU_{cond} = f(\dot{V}, w_{in})$$

The outlet enthalpy (h_f) of this section is determined with the momentum equation. By determing the saturation pressure, the enthalpy is also known.

$$P_g + \frac{\left(\frac{w_{in}}{2}\right)^2}{A^2\rho_g} = P_f + \frac{w_{in}^2}{A^2\rho_f} + F_{cond}L \frac{(\frac{1}{3} - f_{dsh})}{d} \frac{\left(\frac{w_{in}}{2}\right)^2}{2\rho_g A^2} + \tag{4.6}$$

$$F_{cond}L \frac{(f_{cond} - (\frac{1}{3} - f_{dsh}))}{d} \frac{w_{in}^2}{2\rho_g A^2}$$

where

$$F_{cond}L = f(w_{in})$$

In the subcooling section, the fraction (f_{sc}) can be determined explicitly since the sum of the condenser fractions must equate to 1:

$$f_{sc} = 1 - f_{dsh} - f_{cond} \tag{4.7}$$

The energy rate equation and the momentum equation must be used together to detemine the outlet refrigerant state in the subcooling section since the subcooled liquid is a function of pressure and temperature:

$$w_{in}(h_{out} - h_f) = f_{sc}LU_{sc}(T'_{air} - T'_{ref})_{sc} \tag{4.8}$$

where

$$LU_{sc} = f(\dot{V}, w_{in})$$

$$P_f + \frac{w_{in}^2}{A^2\rho_f} = P_{out} + \frac{w_{in}^2}{A^2\rho_{out}} + F_{sc}L\frac{f_{sc}}{d}\frac{w_{in}^2}{2\rho_f A^2} \tag{4.9}$$

where

$$F_{sc}L = f(w_{in})$$

Only the calculation of the outlet air temperature remains ($T_{air,out}$). This is determined with an air-side and refrigerant-side energy rate balance:

$$T_{air,out} = T_{air,in} - \frac{w_{in}(h_{out} - h_{in})}{(w_{air}C_{p,air})} \tag{4.10}$$

The results are shown in Table 4.4. The quantity is displayed as the measured test value and the error between the measured and predicted values. To obtain a better understanding of the relative outlet air temperature error, the total heat exchange was calculated instead of showing the outlet air temperature. The calculated error for this quantity is between ±1.8% or a difference of about ±493 Btu/hr. The pressure drop for the entire section is within ±20% or a difference of ±1.2 psid. The amount of subcooling has a maximum positive error of 34% or a predicted subcooling temperature higher by 3.2°F and a maximum negative error of 20% or a predicted subcooling temperature lower by 2.5-3.5°F. The change in air temperature is within 3% or about 0.4°F.

Table 4.4. Condenser Model Predictions.

TEST NUMBER	Q_{ref} Test	Q_{ref} Error	ΔP_{ref} Test	ΔP_{ref} Error	ΔT_{sc} Test	ΔT_{sc} Error	ΔT_{air} Test	ΔT_{air} Error
	Btu/hr	%	psid	%	°F	%	°F	%
A-590-1	24671	-0.33	5.6	-11.78	8.8	-4.92	39.4	1.11
A-590-2	33458	1.05	7.2	-18.12	10.5	20.98	52.8	1.76
A-590-3	36415	1.19	7.9	-13.48	10.0	24.23	57.7	2.26
A-590-4	38928	1.60	8.1	-17.88	9.5	33.80	60.9	2.79
A-590-5	39262	0.84	8.5	-9.10	9.3	19.32	62.5	2.34

Table 4.4. (cont.)

TEST NUMBER	Q_{ref} Test Btu/hr	Q_{ref} Error %	ΔP_{ref} Test psid	ΔP_{ref} Error %	ΔT_{sc} Test °F	ΔT_{sc} Error %	ΔT_{air} Test °F	ΔT_{air} Error %
A-710-1	24150	-0.59	6.0	-1.94	9.2	-12.49	32.0	1.06
A-710-2	33048	0.07	7.9	-4.12	12.4	1.74	43.5	0.97
A-710-3	35090	-0.07	8.3	-1.47	11.7	-0.91	46.1	1.20
A-710-4	36413	0.11	8.6	-1.27	11.5	2.11	48.6	1.47
A-710-5	38021	-0.32	8.8	-0.51	11.3	-5.95	50.2	1.38
A-825-1	23729	-0.69	6.1	3.80	9.8	-15.59	27.3	1.11
A-825-2	31907	-0.29	7.7	-1.67	13.1	-4.27	36.1	0.82
A-825-3	34866	-0.37	9.1	7.22	12.3	-7.77	39.5	1.07
A-825-4	35391	-0.40	9.1	7.03	12.1	-8.65	40.4	1.14
A-825-5	37053	-0.81	9.1	6.64	12.1	-16.40	42.5	1.08
A-945-1	23757	-0.67	6.0	0.09	9.5	-15.18	23.6	1.23
A-945-2	31440	-0.43	7.5	-3.35	13.4	-6.13	31.3	0.84
A-945-3	34424	-0.50	9.0	7.89	12.8	-10.02	34.4	1.10
A-945-4	34950	-0.74	8.9	6.99	12.5	-14.96	34.8	0.95
A-945-5	36874	-0.95	9.1	6.70	12.5	-19.13	36.8	1.08
A-1060-1	23887	-0.38	6.2	2.02	9.6	-9.02	21.4	1.60
A-1060-2	29634	-0.44	8.0	8.43	11.7	-10.15	26.4	0.97
A-1060-3	34051	-0.57	8.5	3.63	12.7	-10.76	30.4	1.16
A-1060-4	34572	-0.79	8.8	6.72	12.5	-16.33	30.6	1.03
A-1060-5	36848	-0.80	9.3	8.67	12.7	-16.97	32.8	1.36
B-600-1	22514	-1.44	6.0	-2.10	14.8	-18.83	35.1	0.27
B-600-2	27374	-1.73	7.5	2.52	17.8	-18.60	42.4	-0.25
B-600-3	31555	-1.63	8.5	1.73	19.7	-14.94	48.8	-0.38
B-600-4	35069	-1.12	9.2	-1.25	20.7	-9.11	53.9	-0.04
B-600-5	38597	0.14	9.7	-6.09	21.9	1.63	59.2	0.95
B-600-6	41940	0.58	10.5	-5.29	22.4	4.64	64.1	1.26
B-600-7	45021	0.98	10.6	-11.79	22.7	7.71	68.4	1.58
B-1200-1	23261	0.65	6.0	-20.81	16.1	12.49	18.2	2.74
B-1200-2	28006	0.03	7.6	-8.79	19.3	1.80	21.9	2.03
B-1200-3	31642	-0.47	9.1	1.19	21.5	-4.87	24.8	1.47
B-1200-4	35059	-0.39	10.1	2.45	23.2	-3.97	27.4	1.47
B-1200-5	37978	-0.50	10.7	2.59	24.9	-4.68	29.6	1.28
B-1200-6	40662	-0.21	11.4	3.15	25.7	-2.25	31.5	1.50
B-1200-7	42522	-0.20	12.2	6.68	26.6	-2.62	33.0	1.46
B-1500-1	23643	0.49	6.2	-16.89	16.2	9.65	14.8	2.59
B-1500-2	28702	0.17	8.0	-6.81	19.4	3.10	18.1	2.20
B-1500-3	32502	-0.07	9.1	-2.50	22.1	-0.29	20.4	1.91
B-1500-4	35586	-0.13	10.4	3.87	23.7	-1.87	22.4	1.78
B-1500-5	38215	-0.31	11.1	6.85	25.4	-3.75	24.1	1.56
B-1500-6	40734	-0.18	11.5	5.00	26.3	-2.29	25.6	1.63
B-1500-7	42945	-0.22	12.2	7.50	27.5	-2.88	27.0	1.54

Table 4.4. (cont.)

TEST NUMBER	Q_{ref} Test	Q_{ref} Error	ΔP_{ref} Test	ΔP_{ref} Error	ΔT_{sc} Test	ΔT_{sc} Error	ΔT_{air} Test	ΔT_{air} Error
	Btu/hr	%	psid	%	°F	%	°F	%
B-1800-1	22626	1.06	6.0	-20.15	15.7	18.75	11.7	3.19
B-1800-2	27193	0.13	7.8	-3.71	18.8	2.19	14.1	2.37
B-1800-3	31061	-0.10	8.8	-0.15	21.7	-1.01	16.1	2.10
B-1800-4	34127	-0.18	10.1	6.81	23.7	-2.93	17.7	1.99
B-1800-5	37012	-0.23	11.0	7.75	24.7	-3.45	19.1	1.89
B-1800-6	38865	-0.49	11.7	12.14	26.2	-6.39	20.2	1.59
B-1800-7	40926	-0.46	11.7	8.70	27.2	-5.31	21.2	1.59

CHAPTER 5

SUMMARY AND RECOMMENDATIONS

The condenser can be modeled as three sections: desuperheating, condensing, and subcooling. With steady-state data and using a least-squares analysis, the overall heat transfer coefficient and friction factor of each section can be determined. An energy balance determined the overall heat transfer coefficient and the momentum balance determined the friction factors. Since the friction factors are determined, the pressure drops within each section can be calculated. Realizing that the condenser operates within a certain range of thermodynamic states, the calculation procedure to compute the overall heat transfer coefficients and the friction factors is simplified. The overall heat transfer coefficient for each section was expressed in terms of the refrigerant mass flow rate and the volumetric air flow rate. The friction factor for each section was expressed in terms of the refrigerant mass flow rate and a constant.

The energy balance model determined the fractions of each section within the condenser within ±5%. Determining the pressure drop with the momentum balance resulted in errors as high as -22% but the majority of the data was within ±10%. For all sections, the overall heat transfer coefficient times the tube length increases as the refrigerant mass flow rate and the air volume flow rate increases. The magnitudes of the overall heat transfer coefficient times the tube length show the condensing section being the largest, then the desuperheating section, and finally the subcooling section being the smallest.

The fraction of the desuperheating region versus the desuperheating temperature increases as the air volumetric flow rate decreases. Also, as the desuperheating temperature increases, the fraction also increases. For the subcooling fraction versus the subcooling temperature, at the low entering air evaporator temperatures, the subcooling fraction appears to be independent of the volumetric air flow rate and increases as the subcooling temperature increases. The high entering air evaporator temperatures shows the subcooling fraction increasing with increasing volumetric air flow and increasing with the subcooling temperature.

With the fractions known, the pressures drops were calculated for each of the three sections. In general, the friction factor decreases as the refrigerant mass flow rate increases. The results show the subcooling section being the largest, then the desuperheating section, and finally the condensing section being the smallest. To increase the accuracy of the pressure drop model, the friction as a result of the return bends should be included into the model.

The transient program contained in Appendix B has not been used in this paper. Although the theory is believed to be sound, time limitations prevented the use of the program. Additional time should be invested in incorporating the findings of this project into the transient computer program.

All the results in this paper are based on an exact energy balance between the air and refrigerant sides. It is believed that the theory would work for actual test conditions but the data collected and used in this analysis were believed to be suspect as a result of the refrigerant flow rate readings. Additional time needs to be invested in determining if this is the actual error in the measurements or if other errors persist.

APPENDIX A

PROPERTY DATA

McLinden et al. [29] have determined the property data for R-134a. The property information needed to evaluate the governing equations was curve-fit over the range of operating conditions for a typical automotive condenser. The information that follows is in SI units. Therefore, temperature is in K, pressure in kPa, density in kg/m^3, and enthalpy in kJ/kg. To convert between the SI units and the IP units a conversion table is provided at the end of this appendix.

The saturated properties were curve-fitted to a polynomial function based on temperature. The temperature range is 273 K to 373 K for all of the saturated properties in terms of temperature. The saturated liquid density in terms of saturated liquid temperature was written:

$$\rho_f = 19970 - 177.85T_f + 0.57787T_f^2 - 63.806\times10^{-5}T_f^3 \qquad (A.1)$$

The saturated vapor density in terms of saturated vapor temperature was written:

$$\rho_g = 12.132\times10^4 - 1569.7T_g + 7.6036T_g^2 - 16.351\times10^{-3}T_g^3 + 13.183\times10^{-6}T_g^4 \qquad (A.2)$$

The saturated liquid enthalpy in terms of the saturated liquid temperature was written:

$$h_f = 91.189 - 1.4507T_f + 47.693\times10^{-4}T_f^2 \qquad (A.3)$$

The saturated vapor enthalpy in terms of saturated vapor temperature was written:

$$h_g = -16456 + 215.19T_g - 1.0431T_g^2 + 22.526x10^{-4}T_g^3 - 18.248x10^{-7}T_g^4 \quad (A.4)$$

The saturated pressure in terms of the saturated temperature was written:

$$P_{sat} = -26797 + 299.89T_{sat} - 1.1504T_{sat}^2 + 15.212x10^{-4}T_{sat}^3 \quad (A.5)$$

The saturated temperature in terms of the saturated pressure was written:

$$T_{sat} = 255.77 + 73.663x10^{-3}P_{sat} - 19.727x10^{-6}P_{sat}^2 + 21.909x10^{-10}P_{sat}^3 \quad (A.6)$$

The saturated vapor enthalpy in terms of the saturated vapor pressure was written:

$$h_g = 233.1 + 61.095x10^{-3}P_g - 33.361x10^{-6}P_g^2 + 89.853x10^{-10}P_g^3 - 10.125x10^{-13}P_g^4 \quad (A.7)$$

Since the superheated refrigerant state requires two properties to define the state, in this case pressure and temperature, property information was curve fittted at seven different pressures in the range of 689 to 2757 kPa based on a temperature range of 300 to 425 K. At a given pressure and temperature, two fitted property equations, based on a lower and higher pressure value than the given pressure, were determined based on the temperature. These two equations would then be used in a linear interpolation to determine the property data of the given state. The subscript in the following equations denotes the pressure (kPa) at which the curve fit was evaluated. For enthalpy

$$h_{689.29} = -39.522 + 1.0073T \quad (A.8)$$

$$h_{1033.93} = -58.884 + 1.0480T \quad (A.9)$$

$$h_{1378.57} = -79.136 + 1.0904T \quad (A.10)$$

$$h_{1723.21} = -100.10 + 1.1340T \quad (A.11)$$

$$h_{2067.86} = -126.61 + 1.1909T \quad (A.12)$$

$$h_{2412.5} = -149.90 + 1.2392T \quad (A.13)$$

$$h_{2757.14} = -182.03 + 1.3087T \quad (A.14)$$

To determine the enthalpy for a given pressure, P, and a temperature, T, the following linear relation was used

$$h = \frac{(h_{PH} - h_{PL})\,(P-PL)}{PH - PL} + h_{PL} \quad (A.15)$$

where

PL = the largest pressure from the curve fits below the given pressure

PH = the smallest pressure from the curve fits above the given pressure

A similar method was used to determine the density of the superheat refrigerant:

$$\rho_{689.29} = 121.62 - 0.43669T + 46.996x10^{-5}T^2 \quad (A.16)$$

$$\rho_{1033.93} = 224.63 - 0.84782T + 92.859x10^{-5}T^2 \quad (A.17)$$

$$\rho_{1378.57} = 380.25 - 1.5068T + 16.823x10^{-4}T^2 \quad (A.18)$$

$$\rho_{1723.21} = 597.18 - 2.4487T + 27.652x10^{-4}T^2 \quad (A.19)$$

$$\rho_{2067.86} = 987.75 - 4.2365T + 48.824x10^{-4}T^2 \quad (A.20)$$

$$\rho_{2412.5} = 1407.0 - 6.1108T + 70.455x10^{-4}T^2 \quad (A.21)$$

$$\rho_{2757.14} = 2249.8 - 10.054T + 11.739x10^{-3}T^2 \quad (A.22)$$

To determine the density for a given pressure, P, and a temperature, T, the following linear relation was used

$$\rho = \frac{(\rho_{PH} - \rho_{PL})\,(P-PL)}{PH - PL} + \rho_{PL} \quad (A.23)$$

Conversion Factors:

$$1\,\frac{lbf}{in^2} = 6.895\ kPa \quad (A.24)$$

$$1\,\frac{lb_m}{ft^3} = 16.0185\,\frac{kg}{m^3} \quad (A.25)$$

$$1\,\frac{Btu}{lb_m} = 2.3260\,\frac{kJ}{kg} \quad (A.26)$$

$$T_F = \frac{9}{5}T_C + 32 \quad (A.27)$$

$$T_K = T_C + 273.16 \quad (A.28)$$

APPENDIX B

TRANSIENT CONDENSER PROGRAM

```
! VARIABLE DEFINITIONS

! AX = INNER CROSS-SECTIONAL AREA OF THE TUBE {M^2}
! C(I) = CAPACITANCE FOR TUBE AND REFRIGERANT IN SECTION I {KJ/(KG-K)}
! CPA = AVERAGE OF THE INLET AND OUTLET AIR SPECIFIC HEATS {KJ/(KG-K)}
! DELT = TIME STEP {S}
! DELTA = FRACTIONAL INCREMENT OF X(I)
! DIAM = INNER TUBE DIAMETER {M}
! ENTER2SECT = MARKER FOR CHANGE BETWEEN THE THREE SECTON AND TWO
! SECTION CONDENSER
!       1 = CHANGE BETWEEN THREE AND TWO SECTIONS
!       0 = NO CHANGE
! F(I) = FRACTION OF TOTAL TUBE LENGTH OF SECTION I {-}
! FF(I) = FRICTION FACTOR FOR SECTION I
! FIRST = MARKER FOR FIRST ITERATION
!     0 = FIRST TIME THROUGH
!     1 = NOT FIRST TIME THROUGH
! h# = REFRIGERANT ENTHALPY STATE # {KJ/KG}
! L = TOTAL CONDENSER TUBE LENGTH {M}
! NUMDATA = NUMBER OF DATA POINTS COLLECTED FROM THE EXPERIMENTAL
!RUN
! P# = REFRIGERANT PRESSURE STATE # {KPa}
! PTEST = OUTLET CONDENSER REFRIGERANT PRESSURE DATA WRT TIME {PSIG}
! RHOA = AVERAGE OF THE INLET AND OUTLET AIR DENSITIES {KG/M^3}
! RHOR = AVERAGE OF THE INLET AND OUTLET REFRIGERANT DENSITIES
!{KG/M^3}
! STOR(I,J) = TIME DEPENDENT TERM FROM THE PREVIOUS TIME STEP
!       I = DESUPERHEATING (1), 2-PHASE (2) OR LIQUID SECTION (3)
!       J = EQUATION FOR THE GIVEN SECTION
! T# = REFRIGERANT TEMPERATURE STATE # {K}
! TA = AVERAGE OF THE INLET AND OUTLET AIR TEMPERATURES {K}
! TATEST = OUTLET CONDENSER AIR TEMPERATURE DATA WRT TIME {F}
! TA# = AIR TEMPERATURE STATE # {K}
! TR = AVERAGE OF THE INLET AND OUTLET REFRIGERANT TEMPERATURES {K}
! TRTEST = OUTLET CONDENSER REFRIGERANT TEMPERATURE DATA WRT TIME
!{F}
! TWOSECT = MARKER FOR PARTIAL CONDENSING SONDITION
!       1 = TWO SECTION CONDENSER
!       0 = THREE SECTION CONDENSER
! U(I) = OVERALL HEAT-TRANSFER COEFFICIENT FOR SECTION I {KW/(M-K)}
! WA = MASS FLOW RATE OF AIR {KG/S}
! W# = MASS FLOW RATE STATE # {KG/S}
! WR = AVERAGE OF THE INLET AND OUTLET REFRIGERANT MASS FLOW RATES
!{KG/S}
```

```
!FOR REFRIGERANT STATES
!       1 = DESUPERHEATING INLET
!       2 = DESUPERHEATING OUTLET AND CONDENSING INLET
!       3 = CONDENSING OUTLET AND SUBCOOLING INLET
!       4 = SUBCOOLING OUTLET
!
!FOR AIR STATES
!       1 = DESUPERHEATING SECTION
!       2 = CONDENSING SECTION
!       3 = SUBCOOLING SECTION

!OBTAIN REFRIGERANT PROPERTIES IN PROGRAM WITH THE LIBRARY COMMAND
LIBRARY "R134a FITS.LIB*"

!DECLARE GLOBAL VARIABLES
DIM PTEST(200,2),TRTEST(200,2),TATEST(200,2),R(4),DX(4),RO(4)
DIM X(4),FPRIME(4,4),INVFPRIME(4,4)
DECLARE PUBLIC AX,C1,C2,C3,C4,C5,C(),CPA
DECLARE PUBLIC FIRST,DELT,DIAM,F(),FF()
DECLARE PUBLIC h1,h2,h3,h4,L,P1,P2,P3,P4,RHOR1,RHOR2,RHOR3,RHOR4,STOR(,)
DECLARE PUBLIC TAi,TA1,TA2,TA3,TR1,TR2,TR3,TR4,U(),WA
DECLARE DEF WR1,WR2,WR3,WR4,X3,hpt,dpt,cppt

! INPUT ESTIMATION PARAMETERS FROM FILE "PARAM"
OPEN #1: NAME "PARAM", CREATE OLD
INPUT #1: L
INPUT #1: DIAM
INPUT #1: FF(1),FF(2),FF(3)
INPUT #1: U(1),U(2),U(3)
INPUT #1: C(1),C(2),C(3)
CLOSE #1

! INPUT EXPERIMENTAL DATA FROM FILE "TEST" WHICH ARE TO BE COMPARED
!WITH THE OUTPUTS OF THE COMPUTER MODEL
OPEN #2: NAME "TEST", CREATE OLD
INPUT #2: NUMDATA
!HIGH AND LOW SET THE HIGHER AND LOWER BOUNDS OF THE Y-AXIS FOR
!PLOTTING ONTO THE SCREEN
INPUT #2: HIGHA,HIGHB,HIGHC
INPUT #2: LOWA,LOWB,LOWC
MAT PTEST = ZER(NUMDATA,2)
MAT TRTEST = ZER(NUMDATA,2)
MAT TATEST = ZER(NUMDATA,2)
FOR I = 1 TO NUMDATA
   INPUT #2: TIMESTEP,PTEST(I,2),TRTEST(I,2),TATEST(I,2)
   LET PTEST(I,1)=TIMESTEP
   LET TRTEST(I,1)=TIMESTEP
   LET TATEST(I,1)=TIMESTEP
NEXT I
CLOSE #2
```

```
!DISPLAY THE BORDERS OF THE FIRST GRAPH
OPEN #11: SCREEN 0.0,.98,0.66,.98
SET WINDOW -20,180,LOWA-(HIGHA-LOWA)/18,HIGHA+(HIGHA-LOWA)/18
BOX LINES 0,180,LOWA,HIGHA+(HIGHA-LOWA)/18
FOR I = 0 TO 6
   SET TEXT JUSTIFY "CENTER","TOP"
   PLOT TEXT, AT I*30,LOWA: STR$(I*30)
   SET TEXT JUSTIFY "RIGHT","HALF"
   PLOT TEXT, AT 0,LOWA+I*(HIGHA-LOWA)/6: STR$(ROUND(LOWA+I*(HIGHA-
LOWA)/6,1))
NEXT I

!DISPLAY THE BORDERS OF THE SECOND GRAPH
OPEN #12: SCREEN 0.0,.98,0.33,.65
SET WINDOW -20,180,LOWB-(HIGHB-LOWB)/18,HIGHB+(HIGHB-LOWB)/18
BOX LINES 0,180,LOWB,HIGHB+(HIGHB-LOWB)/18
FOR I = 0 TO 6
   SET TEXT JUSTIFY "CENTER","TOP"
   PLOT TEXT, AT I*30,LOWB: STR$(I*30)
   SET TEXT JUSTIFY "RIGHT","HALF"
   PLOT TEXT, AT 0,LOWB+I*(HIGHB-LOWB)/6: STR$(ROUND(LOWB+I*(HIGHB-
LOWB)/6,1))
NEXT I

!DISPLAY THE BORDERS OF THE THIRD GRAPH
OPEN #13: SCREEN 0.0,.98,0.0,0.32
SET WINDOW -20,180,LOWC-(HIGHC-LOWC)/18,HIGHC+(HIGHC-LOWC)/18
BOX LINES 0,180,LOWC,HIGHC+(HIGHC-LOWC)/18
FOR I = 0 TO 6
   SET TEXT JUSTIFY "CENTER","TOP"
   PLOT TEXT, AT I*30,LOWC: STR$(I*30)
   SET TEXT JUSTIFY "RIGHT","HALF"
   PLOT TEXT, AT 0,LOWC+I*(HIGHC-LOWC)/6: STR$(ROUND(LOWC+I*(HIGHC-
LOWC)/6,1))
NEXT I

!DISPLAY THE LABELS FOR EACH GRAPH
WINDOW #11
SET TEXT JUSTIFY "RIGHT","BASE"
PLOT TEXT, AT 180,LOWA : "PRESSURE (PSIG) VS TIME (SEC)"
MAT PLOT LINES: PTEST
WINDOW #12
SET TEXT JUSTIFY "RIGHT","BASE"
PLOT TEXT, AT 180,LOWB : "TEMPERATURE REFRIG (F) VS TIME(SEC)"
MAT PLOT LINES: TRTEST
WINDOW #13
SET TEXT JUSTIFY "RIGHT","BASE"
PLOT TEXT, AT 180,LOWC : "TEMPERATURE AIR (F) VS TIME (SEC)"
MAT PLOT LINES: TATEST
```

```
! CALCULATE AND SET NEEDED CONSTANTS
LET AX=PI/4*(DIAM)^2
LET DELT=1
LET DELTA=.001
LET ENTER2SECT=0
LET FIRST=0
LET TWOSECT=0
LET TIMER=0
LET X3=1

! OPEN REQUIRED INPUT AND OUTPUT FILES
OPEN #3: NAME "INITIAL", CREATE OLD
OPEN #4: NAME "RESULTS", CREATE NEWOLD
ERASE #4
OPEN #5: NAME "MODEL", CREATE NEWOLD
ERASE #5

!CHECK FOR END OF DATA  AND INCREMENT TIME STEP
DO WHILE TIMER<=NUMDATA
LET TIMER=TIMER+1

! READ "INITIAL" FILE FOR A GIVEN TIME STEP
INPUT #3: TR1,P1,WR4,WA,TAi
! CONVERT DATA TO SI SYSTEM
LET TR1 = 5/9*(TR1-32) + 273.16
LET P1 = 6.895*(P1+14.7)
LET WR4 = 0.4536/3600*WR4
LET WA = 0.072/60*0.4536*WA
LET TAi = 5/9*(TAi-32) + 273.16

!ASSUME CONDENSER IS NOT TWO SECTIONS, DESUPERHEATING, CONDENSING
!AND SUBCOOLING (TWOSECT=0)
IF TWOSECT=0 THEN
  LET NVAR=12
  MAT R=ZER(NVAR)
  MAT DX=ZER(NVAR)
  MAT RO=ZER(NVAR)
  MAT X=CON(NVAR)
  MAT FPRIME=ZER(NVAR,NVAR)
  MAT INVFPRIME=ZER(NVAR,NVAR)

  !IF FIRST ITERATION (FIRST=0), THEN GUESS UNKNOWNS BASED ON KNOWN
  !EXPERIMENTAL INLET CONDITIONS
  IF FIRST=0 THEN
   !DESUPERHEATING SECTION
    LET X(1)=WR4
    LET X(2)=P1
    LET X(3)=.1
    LET X(4)=TAi
   !CONDENSING SECTION
    LET X(5)=WR4
    LET X(6)=P1
    LET X(7)=.7
    LET X(8)=TAi
```

```
    !SUBCOOLING SECTION
     LET X(9)=WR4
     LET X(10)=P1
     LET X(11)=330
     LET X(12)=TAi
   !IF NOT FIRST ITERATION (FIRST=1), THEN GUESS UNKNOWNS BASED ON
   !VALUES DETERMINED DURING THE LAST TIME INTERVAL
   ELSE
    !DESUPERHEATING SECTION
     LET X(1)=WR1
     LET X(2)=P2
     LET X(3)=F(1)
     LET X(4)=TA1
    !CONDENSING SECTION
     LET X(5)=WR2
     LET X(6)=P3
     LET X(7)=F(2)
     LET X(8)=TA2
    !SUBCOOLING SECTION
     LET X(9)=WR3
     LET X(10)=P4
     LET X(11)=TR4
     LET X(12)=TA3
   END IF

   !PERFORM NEWTON-RAPHSON ROUTINE UNTIL THE OVERALL ERROR IS SMALL
   !OR 13 ITERATIONS HAVE BEEN COMPLETED
   LET COUNT=0
   DO
     LET COUNT=COUNT+1
     CALL CALFP
     CALL CALCR(R,X)
     MAT INVFPRIME=INV(FPRIME)
     MAT DX=INVFPRIME*R
     MAT X=X-DX
     LET ERR=DOT(DX,DX)
     LET XNORM=DOT(X,X)
     LET CHECK=0
     FOR K=1 TO NVAR
        LET CHECK=CHECK + ABS(R(K))
     NEXT K
     IF COUNT=13 THEN EXIT DO
   LOOP WHILE CHECK >.01

   !IF 13 ITERATIONS WERE COMPLETED, ASSUME CONDENSER IN TWO SECTIONS,
   !DESUPERHEATING AND PARTIAL CONDENSING (TWOSECT=1)
   IF COUNT=13 THEN
     LET TWOSECT=1
     LET ENTER2SECT=1
   ELSE
     LET TWOSECT=0
   END IF

END IF
```

```
!IF FIRST ITERATION (FIRST=0), THEN GUESS UNKNOWNS BASED ON KNOWN
!EXPERIMENTAL INLET CONDITIONS OR IF SUBCOOLING SECTION IS SMALL AFTER
!THE THREE SECTION CALCULATION, PERFROM THE TWO SECTION CALCULATION
IF TWOSECT=1 OR F(3)<>ABS(F(3)) THEN
  LET NVAR=8
  MAT R=ZER(NVAR)
  MAT DX=ZER(NVAR)
  MAT RO=ZER(NVAR)
  MAT X=CON(NVAR)
  MAT FPRIME=ZER(NVAR,NVAR)
  MAT INVFPRIME=ZER(NVAR,NVAR)
  LET WR3=WR4

  !IF FIRST ITERATION (FIRST=0), THEN GUESS UNKNOWNS BASED ON KNOWN
  !EXPERIMENTAL INLET CONDITIONS
  IF FIRST=0 OR ENTER2SECT=1 THEN
   !DESUPERHEATING SECTION
    LET X(1)=WR4
    LET X(2)=P1
    LET X(3)=.3
    LET X(4)=310
   !PARTIAL CONDENSING SECTION
    LET X(5)=WR4
    LET X(6)=P1
    LET X(7)=.1
    LET X(8)=310
    LET ENTER2SECT=0
  !IF NOT FIRST ITERATION (FIRST=1), THEN GUESS UNKNOWNS BASED ON
  !VALUES DETERMINED DURING THE LAST TIME INTERVAL
  ELSE
   !DESUPERHEATING SECTION
    LET X(1)=WR1
    LET X(2)=P2
    LET X(3)=F(1)
    LET X(4)=TA1
   !PARTIAL CONDENSING SECTION
    LET X(5)=WR2
    LET X(6)=P3
    LET X(7)=X3
    LET X(8)=TA2
  END IF
```

```
!PERFORM NEWTON-RAPHSON ROUTINE UNTIL THE OVERALL ERROR IS SMALL
 DO
  CALL CALFP2
  CALL CALCR2(R,X)
  MAT INVFPRIME=INV(FPRIME)
  MAT DX=INVFPRIME*R
  MAT X=X-DX
  LET ERR=DOT(DX,DX)
  LET XNORM=DOT(X,X)
  LET CHECK=0
  FOR K=1 TO NVAR
    LET CHECK=CHECK + ABS(R(K))
  NEXT K
 LOOP WHILE CHECK >.01

 LET TWOSECT=1

END IF


!DETERMINE IF TWO SECTION CONDENSER IS A THREE SECTION CONDENSER BY
!MONITORING THE EXIT QUALITY OF THE TWO SECTION CONDENSER
IF X3<=.0001 THEN
 LET TWOSECT=0
 LET X3=1
END IF

!STORE THE TIME DEPENDENT TERMS FOR EACH SECTION
LET STOR(1,1)=(RHOR1+RHOR2)/2
LET STOR(1,2)=(RHOR1+RHOR2)/2*C(1)*(TR1+TR2)/2
LET STOR(1,3)=(WR1+WR2)/2
LET STOR(2,1)=(RHOR2+RHOR3)/2
LET STOR(2,2)=(RHOR2+RHOR3)/2*C(2)*(TR2+TR3)/2
LET STOR(2,3)=(WR2+WR3)/2
LET STOR(3,1)=(RHOR3+RHOR4)/2
LET STOR(3,2)=(RHOR3+RHOR4)/2*C(3)*(TR3+TR4)/2
LET STOR(3,3)=(WR3+WR4)/2

!WRITE INFORMATION TO A FILE
MAT PRINT #4: STOR
PRINT #4: TIMER;CHR$(9);TR1;CHR$(9);TR2;CHR$(9);TR3;CHR$(9);TR4;CHR$(9);
PRINT #4: WR1;CHR$(9);WR2;CHR$(9);WR3;CHR$(9);WR4;CHR$(9);
PRINT #4: P1;CHR$(9);P2;CHR$(9);P3;CHR$(9);P4;CHR$(9);
PRINT #4: h1;CHR$(9);h2;CHR$(9);h3;CHR$(9);h4;CHR$(9);
PRINT #4: F(1);CHR$(9);F(2);CHR$(9);F(3)
PRINT #5: TR4,P4,TA1,TA2,TA3
```

```
!PLOT INFORMATION ON THE SCREEN
WINDOW #11
PLOT TIMER,P4/6.895 - 14.7;
WINDOW #12
PLOT TIMER,9/5*(TR4-273.16) + 32;
WINDOW #13
LET THIS = 9/5*(F(1)*TA1+F(2)*TA2+F(3)*TA3-273.16) + 32
PLOT TIMER,THIS;
LET FIRST=1
LOOP

!CLOSE THE OPEN FILES
CLOSE #3
CLOSE #4
CLOSE #5

SUB CALFP
  ! INTERNAL SUBROUTINE TO FILL PARTIAL DERIVATIVE MATRIX FOR THE
  !THREE SECTION CONDENSER
  CALL CALCR(RO,X)
  FOR I=1 TO NVAR
    LET  DELTAX=DELTA*X(I)
    LET X(I)=X(I)+DELTAX
    CALL CALCR(R,X)
    FOR  J=1 TO NVAR
      LET FPRIME(J,I)=(R(J)-RO(J))/(DELTAX)
    NEXT J
    LET X(I)=X(I)-DELTAX
  NEXT I
END SUB

SUB CALFP2
  ! INTERNAL SUBROUTINE TO FILL PARTIAL DERIVATIVE MATRIX FOR THE
  !TWO SECTION CONDENSER
  CALL CALCR2(RO,X)
  FOR I=1 TO NVAR
    LET  DELTAX=DELTA*X(I)
    LET X(I)=X(I)+DELTAX
    CALL CALCR2(R,X)
    FOR  J=1 TO NVAR
      LET FPRIME(J,I)=(R(J)-RO(J))/(DELTAX)
    NEXT J
    LET X(I)=X(I)-DELTAX
  NEXT I
END SUB

END


MODULE COMMON
PUBLIC AX,C(3),DELT,DIAM,F(3),FF(3),h1,h2,h3,h4,L,P1,P2,P3,P4
PUBLIC RHOR,RHOR1,RHOR2,RHOR3,RHOR4,STOR(3,3),TAi,TA1,TA2,TA3
PUBLIC TR,TR1,TR2,TR3,TR4,U(3),WA,WR,WR1,WR2,WR3,WR4,X3
PUBLIC FIRST
```

```
SUB CALCR(R(),X())
! DEFINE RESIDUAL EQUAITONS FOR THREE SECTION CONDENSER NR METHOD
! DESUPERHEAT SECTION
! R(1) = MASS
! R(2) = MOMENTUM
! R(3) = ENERGY RATE EQUATION WITH RESPECT TO AIR
! R(4) = ENERGY RATE EQUATION WITH RESPECT TO REFRIGERANT
! TWO-PHASE SECTION
! R(5) = MASS
! R(6) = MOMENTUM
! R(7) = ENERGY RATE EQUATION WITH RESPECT TO AIR
! R(8) = ENERGY RATE EQUATION WITH RESPECT TO REFRIGERANT
! SUBCOOLING SECTION
! R(9) = MASS
! R(10) = MOMENTUM
! R(11) = ENERGY RATE EQUATION WITH RESPECT TO AIR
! R(12) = ENERGY RATE EQUATION WITH RESPECT TO REFRIGERANT

DECLARE DEF cpat,cppt,dgt,dlt,dpt,hgt,hlt,hpt,pst,tsp
LET WR1=X(1)
LET P2=X(2)
LET F(1)=X(3)
LET TA1=X(4)
LET WR2=X(5)
LET P3=X(6)
LET F(2)=X(7)
LET TA2=X(8)
LET WR3=X(9)
LET P4=X(10)
LET TR4=X(11)
LET TA3=X(12)

LET h1=hpt(P1,TR1)
LET RHOR1=dpt(P1,TR1)

! DESUPERHEATING
LET TR2=tsp(P2)
LET TRS1=(TR1+TR2)/2
LET RHOR2=dgt(TR2)
LET RHORS1=(RHOR1+RHOR2)/2
LET h2=hgt(TR2)
LET TAS1=(TAi+TA1)/2
LET WRS1=(WR1+WR2)/2
LET CPAS1=(cpat(TA1)+cpat(TAi))/2
IF FIRST=0 THEN
 LET STOR(1,1)=RHORS1
 LET STOR(1,2)=RHORS1*C(1)*TRS1
 LET STOR(1,3)=WRS1
END IF
```

```
! TWO-PHASE
 LET TR3=tsp(P3)
 LET TRS2=(TR2+TR3)/2
 LET RHOR3=dlt(TR3)
 LET RHORS2=(RHOR2+RHOR3)/2
 LET h3=hlt(TR3)
 LET TAS2=(TAi+TA2)/2
 LET WRS2=(WR2+WR3)/2
 LET CPAS2=(cpat(TA2)+cpat(TAi))/2
 IF FIRST=0 THEN
  LET STOR(2,1)=RHORS2
  LET STOR(2,2)=RHORS2*C(2)*TRS2
  LET STOR(2,3)=WRS2
 END IF

! SUBCOOLING
 LET F(3)=1 - F(1) - F(2)
 LET TRS3=(TR3+TR4)/2
 LET RHOR4=dlt(TR4)
 LET RHORS3=(RHOR3+RHOR4)/2
 LET h4=hlt(TR4) + 1/RHOR4*(P4 - pst(TR4))
 LET TAS3=(TAi+TA3)/2
 LET WRS3=(WR3+WR4)/2
 LET CPAS3=(cpat(TA3)+cpat(TAi))/2
 IF FIRST=0 THEN
  LET STOR(3,1)=RHORS3
  LET STOR(3,2)=RHORS3*C(3)*TRS3
  LET STOR(3,3)=WRS3
 END IF

!RESIDUAL EQUATIONS
 LET R(1)=WR1 - WR2 - AX*L*F(1)*(RHORS1 - STOR(1,1))/DELT
 LET Q=WR2*h2 - WR1*h1 + AX*L*F(1)*(RHORS1*C(1)*TRS1 - STOR(1,2))/DELT
 LET R(2)=Q - F(1)*WA*CPAS1*(TAi-TA1)
 LET R(3)=Q - F(1)*U(1)*L*(TAS1-TRS1)
 LET FR=P1*1000*AX + WR1^2/RHOR1/AX - P2*1000*AX - WR2^2/RHOR2/AX
 LET R(4)=FR-FF(1)*F(1)*L/2/DIAM/AX*WRS1^2/RHORS1-L*F(1)*(WRS1 -
STOR(1,3))/DELT

 LET R(5)=WR2 - WR3 - AX*L*F(2)*(RHORS2 - STOR(2,1))/DELT
 LET Q=WR3*h3 - WR2*h2 + AX*L*F(2)*(RHORS2*C(2)*TRS2 - STOR(2,2))/DELT
 LET R(6)=Q - F(2)*WA*CPAS2*(TAi-TA2)
 LET R(7)=Q - F(2)*U(2)*L*(TAS2-TRS2)
 LET FR=P2*1000*AX + WR2^2/RHOR2/AX - P3*1000*AX - WR3^2/RHOR3/AX
 LET R(8)=FR-FF(2)*F(2)*L/2/DIAM/AX*WRS2^2/RHORS2-L*F(2)*(WRS2 -
STOR(2,3))/DELT
```

```
 LET R(9)=WR3 - WR4 - AX*L*F(3)*(RHORS3 - STOR(3,1))/DELT
 LET Q=WR4*h4 - WR3*h3 + AX*L*F(3)*(RHORS3*C(3)*TRS3 - STOR(3,2))/DELT
 LET R(10)=Q - F(3)*WA*CPAS3*(TAi-TA3)
 LET R(11)=Q - F(3)*U(3)*L*(TAS3-TRS3)
 LET FR=P3*1000*AX + WR3^2/RHOR3/AX - P4*1000*AX - WR4^2/RHOR4/AX
 LET R(12)=FR-FF(3)*F(3)*L/2/DIAM/AX*WRS3^2/RHORS3-L*F(3)*(WRS3 -
STOR(3,3))/DELT
END SUB


SUB CALCR2(R(),X())
 ! DEFINE RESIDUAL EQUAITONS FOR TWO SECTION CONDENSER NR METHOD
 ! DESUPERHEAT SECTION
 ! R(1) = MASS
 ! R(2) = MOMENTUM
 ! R(3) = ENERGY RATE EQUATION WITH RESPECT TO AIR
 ! R(4) = ENERGY RATE EQUATION WITH RESPECT TO REFRIGERANT
 ! PARTIAL CONDENSING SECTION
 ! R(5) = MASS
 ! R(6) = MOMENTUM
 ! R(7) = ENERGY RATE EQUATION WITH RESPECT TO AIR
 ! R(8) = ENERGY RATE EQUATION WITH RESPECT TO REFRIGERANT

 DECLARE DEF cpgt,cplt,cpat,cppt,dgt,dlt,dpt,hgt,hlt,hpt,pst,tsp
 LET WR1=X(1)
 LET P2=X(2)
 LET F(1)=X(3)
 LET TA1=X(4)
 LET WR2=X(5)
 LET P3=X(6)
 LET X3=X(7)
 LET TA2=X(8)

 LET h1=hpt(P1,TR1)
 LET RHOR1=dpt(P1,TR1)

 ! DESUPERHEATING
 LET TR2=tsp(P2)
 LET TRS1=(TR1+TR2)/2
 LET RHOR2=dgt(TR2)
 LET RHORS1=(RHOR1+RHOR2)/2
 LET h2=hgt(TR2)
 LET TAS1=(TAi+TA1)/2
 LET WRS1=(WR1+WR2)/2
 LET CPAS1=(cpat(TA1)+cpat(TAi))/2
 IF FIRST=0 THEN
  LET STOR(1,1)=RHORS1
  LET STOR(1,2)=RHORS1*C(1)*TRS1
  LET STOR(1,3)=WRS1
 END IF
```

```
 ! PARTIAL CONDENSING
 LET F(2)=1-F(1)
 LET TR3=tsp(P3)
 LET TRS2=(TR2+TR3)/2
 LET RHOR3=dlt(TR3) + X3*(RHOR2-dlt(TR3))
 LET RHORS2=(RHOR2+RHOR3)/2
 LET h3=hlt(TR3) + X3*(h2-hlt(TR3))
 LET TAS2=(TAi+TA2)/2
 LET WRS2=(WR2+WR3)/2
 LET CPAS2=(cpat(TA2)+cpat(TAi))/2
 IF FIRST=0 THEN
  LET STOR(2,1)=RHORS2
  LET STOR(2,2)=RHORS2*C(2)*TRS2
  LET STOR(2,3)=WRS2
 END IF

 !RESIDUAL EQUTIONS
 LET R(1)=WR1 - WR2 - AX*L*F(1)*(RHORS1 - STOR(1,1))/DELT
 LET Q=WR2*h2 - WR1*h1 + AX*L*F(1)*(RHORS1*C(1)*TRS1 - STOR(1,2))/DELT
 LET R(2)=Q - F(1)*WA*CPAS1*(TAi-TA1)
 LET R(3)=Q - F(1)*U(1)*L*(TAS1-TRS1)
 LET FR=P1*1000*AX + WR1^2/RHOR1/AX - P2*1000*AX - WR2^2/RHOR2/AX
 LET R(4)=FR-FF(1)*F(1)*L/2/DIAM/AX*WRS1^2/RHORS1-L*F(1)*(WRS1 -
STOR(1,3))/DELT

 LET R(5)=WR2 - WR3 - AX*L*F(2)*(RHORS2 - STOR(2,1))/DELT
 LET Q=WR3*h3 - WR2*h2 + AX*L*F(2)*(RHORS2*C(2)*TRS2 - STOR(2,2))/DELT
 LET R(6)=Q - F(2)*WA*CPAS2*(TAi-TA2)
 LET R(7)=Q - F(2)*U(2)*L*(TAS2-TRS2)
 LET FR=P2*1000*AX + WR2^2/RHOR2/AX - P3*1000*AX - WR3^2/RHOR3/AX
 LET R(8)=FR-FF(2)*F(2)*L/2/DIAM/AX*WRS2^2/RHORS2-L*F(2)*(WRS2 -
STOR(2,3))/DELT

 LET F(3)=0
 LET WR4=WR3
 LET TR4=TR3
 LET P4=P3
 LET TA3=TA2
 LET h4=h3
 LET CPR4=CPR3
 LET RHOR4=RHOR3
END SUB

END MODULE
```

APPENDIX C

TEST STAND FOR TRANSIENT STUDIES

The design of the test stand, Michael [35], to perform transient studies of mobile air conditioning systems and components is described in this chapter. Included in this description are the refrigerant loop design, condenser air loop design, and evaporator air loop design. The instrumentation and data acquisition of the test stand are described. Included in this description are the pressure, temperature, dew point, air velocity, refrigerant mass flow rate, torque, and speed instrumentation. Appendix D is a list of the parts that have been acquired. All of those parts are located in the Air Conditioning and Refrigeration Center laboratory in the Mechanical Engineering Laboratory. This chapter is intended to serve as a growing documentation recording the improved and newly purchased items installed into the test stand at the distribution time of this document.

C.1. Refrigerant Loop

The refrigerant loop will initially consist of a refrigerant 134a air conditioning system from a 1989 Ford Taurus. Figure C.1 is a schematic of the refrigerant loop of the test stand. The refrigerant loop is located between the condenser air loop and the evaporator air loop. The two air loops are connected by "Unistrut," which will support the refrigerant lines and components between the air loops. The compressor stand fits between the two air loops. The components in the refrigerant loop are the compressor, condenser, control devices, evaporator, accumulator-dehydrator, refrigerant lines, and refrigerant. The following seven sections describe each component.

C.1.1. Compressor Stand

The compressor stand was used to mount the compressor and the associated hardware to obtain torque and speed data from the compressor as well as allowing for variable speed operation. The compressor stand was a "Unistrut" structure consisting of a variable speed drive, electric

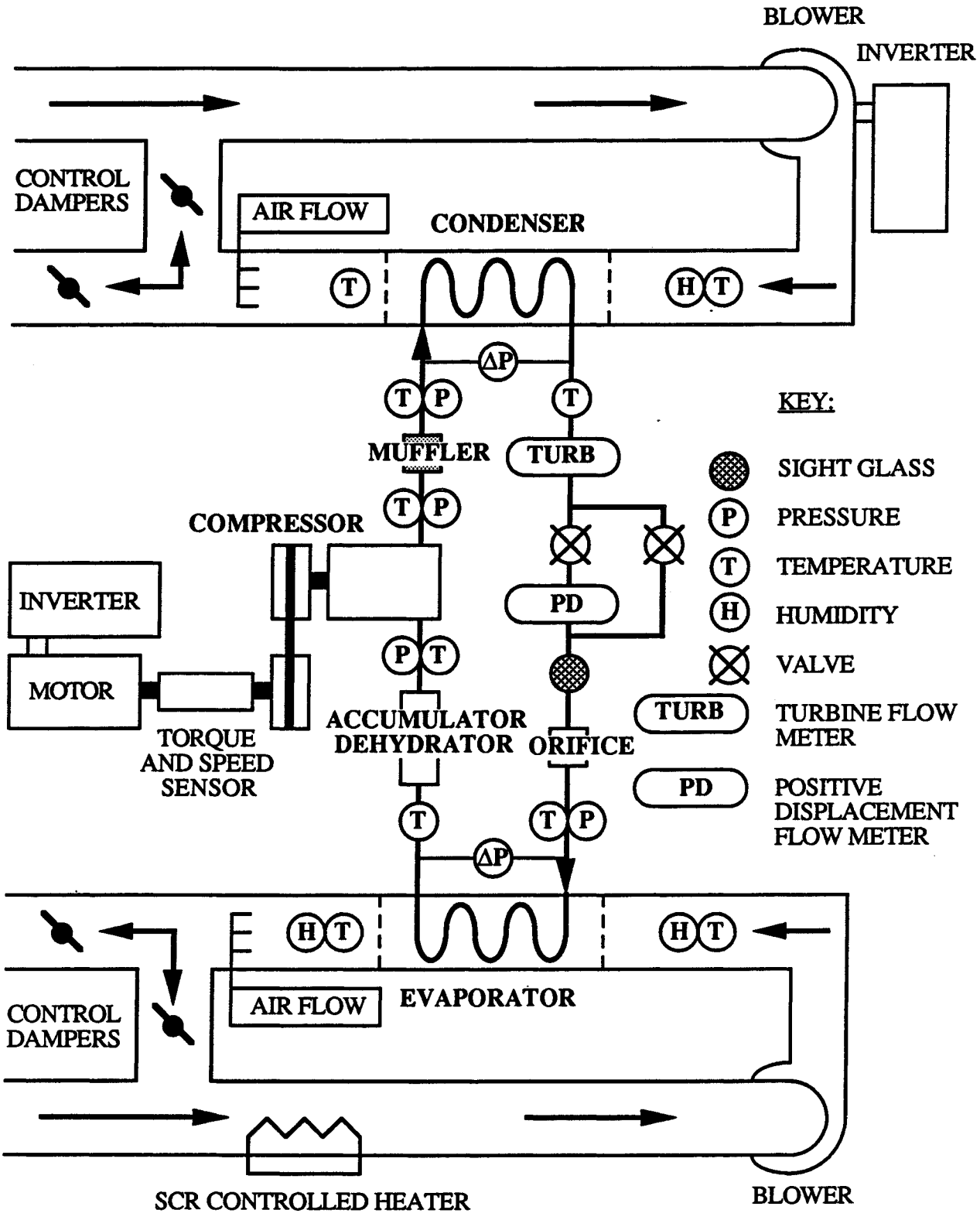

Figure C.1. Schematic of Transient Test Stand

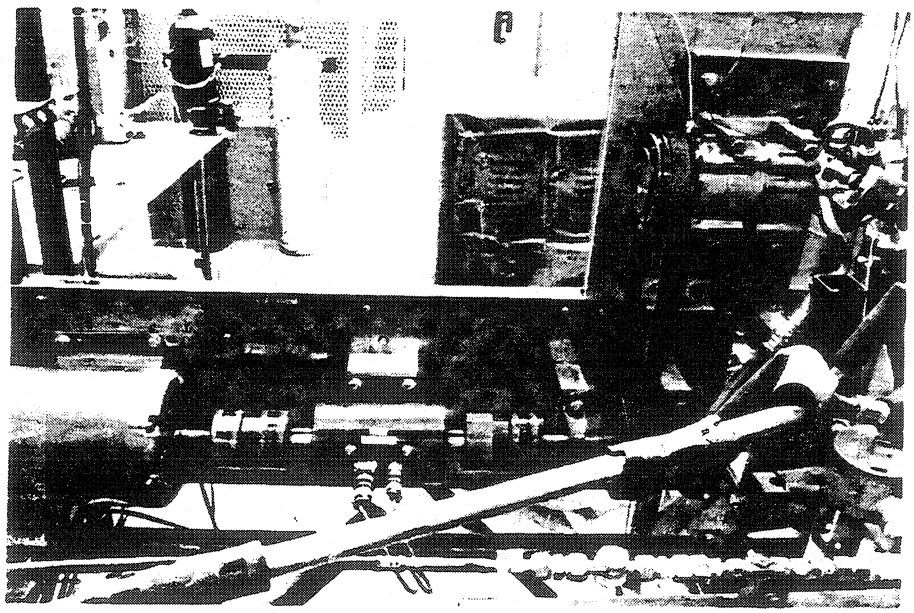

Figure C.2. Photograph of Compressor Stand.

motor, torque sensor, jackshaft, compressor, and compressor mounting plate. Figure C.2 is a photograph of the compressor stand.

A speed controller along with an electric motor were used to provide the variable speed drive for the compressor. The speed controller used was an IDM Controls, Inc. 36 Amp 3-Phase 230 VAC inverter (Model No. CIMR-7.5 G2). It produced a variable frequency output from 230 VAC, 60 Hz input. The electric motor used was a 7-1/2 Hp @ 3450 RPM, 240 VAC, 3-phase Baldor electric motor (Model No. M3219T). The motor had a No. 184T frame and an open enclosure. The team of the speed controller and electric motor allowed for variable speed operation from 0 to 3450 RPM. The electric motor was coupled to the torque sensor through the use of a Lovejoy collar (Model No. L110 x 1.125). A rubber spider fit between the collar on the electric motor and the collar on the torque sensor to form a flexible coupling which was tolerant to misalignment of the two shafts. The shaft diameter of the electric motor was 1.125" (28.6 mm) with a 0.25" (6.4 mm) keyway.

A Lebow torque sensor (Model No. 1805-2K-04) was used to measure the torque input and speed of the jackshaft that powered the compressor. The unit was a high accuracy rotary transformer strain gage bridge torque sensor with an integral magnetic pick-up speed sensor. The torque sensor was coupled to the electric motor and jackshaft through the use of Lovejoy collar (Model No. L110 x 1.5). The shaft diameter of the torque sensor was 1.5" (38.1 mm) with a 0.375" (9.5 mm) keyway.

The jackshaft consisted of a shaft, pulley, and two pillow blocks. The shaft was 1.0" (25.4 mm) in diameter and had a 0.25" (6.4 mm) keyway. It was coupled to the torque sensor through the use of a Lovejoy collar (Model No. L110 x 1.0). As before, a rubber spider fit between the collar on the jackshaft and the collar on the torque sensor formed a flexible coupling. A serpentine pulley from the crankshaft of a 1989 Ford Taurus was purchased and modified to fit on the 1" (25.4 mm) jackshaft. The ratio of the jackshaft pulley diameter to the compressor pulley diameter will be the same as the production ratio because the pulleys used are production pulleys. The serpentine belt that is required to drive the compressor has a belt width of 27/32" (21.4 mm). Two Dodge pillow blocks (Model No. 1" SC P.B.) with 1.0" (25.4 mm) inner diameter ball bearings located and supported the jackshaft.

The compressor mounting plate attached the compressor to the compressor stand and allowed for tensioning of the serpentine belt. Figure C.3 is a drawing of the compressor mounting plate and the mounting feet that support the compressor. A Schrader valve was located on the suction side of the compressor. This valve was used to charge the system with refrigerant.

The compressor was a ten-cylinder swash plate compressor with a 12 VDC electromagnetic clutch. The electromagnetic clutch was energized to form a coupling between the compressor and the serpentine drive. A 12 VDC supply was connected to the electromagnetic clutch and controlled with a manual switch. This same supply could also be connected to the control computer to switch the power on and off electronically.

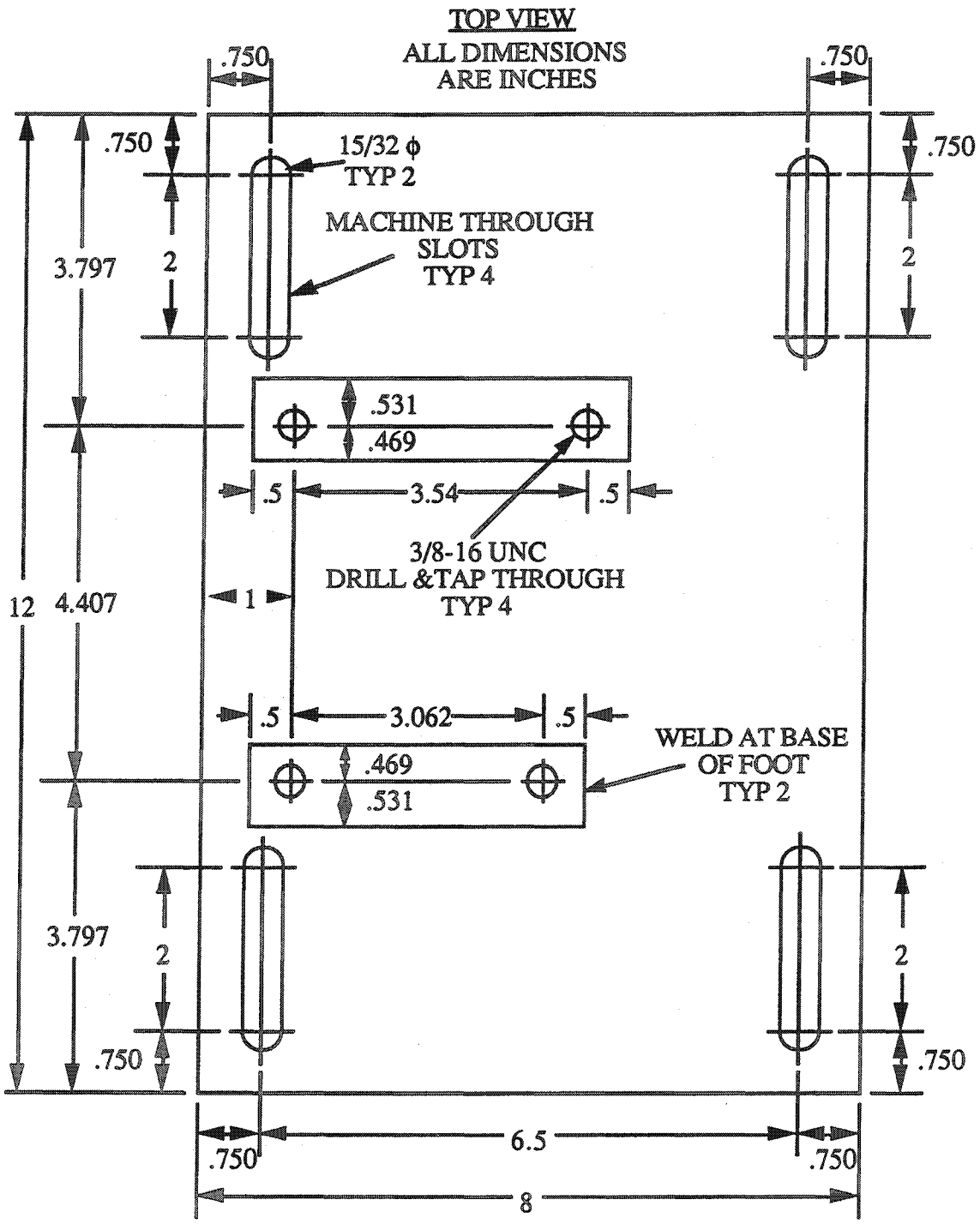

PLATE MATERIAL: 1/4" ALUMINUM PLATE
FEET MATERIAL: 1" X 1" BAR STOCK

Figure C.3. Ford Compressor Mounting Plate.

C.1.2. Condenser

The condenser was a tube and fin condenser shown in Figure C.4. It consists of tubes that run through plate fins. The tubes are brazed to the plate fins. The condenser face dimensions are 15-3/8" x 24-5/8" (39.1 cm x 62.6 cm) resulting in a condenser face area of 2.63 ft^2 (0.244 m^2). The condenser was mounted in the condenser box in crossflow with the airstream in the condenser air loop. The 1989 Taurus has a two speed fan that pulls air through the radiator and the condenser. The fan is rated at 745 scfm (0.352 m^3/s) on LO and 880 scfm (0.415 m^3/s) on HI.

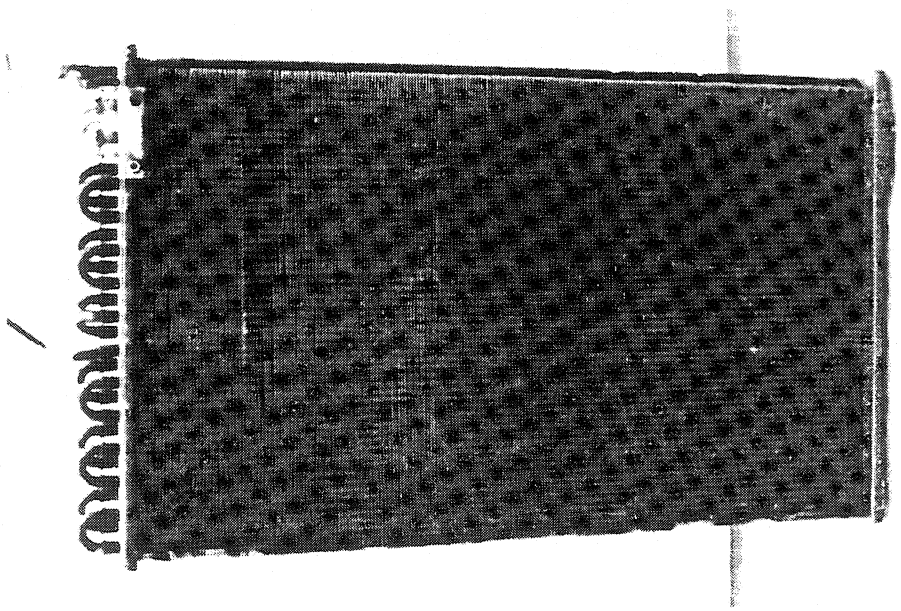

Figure C.4. Photograph of Condenser.

C.1.3. Control Devices

The expansion device was an orifice tube. The orifice tube was located in the refrigerant line between the condenser outlet and evaporator inlet.

C.1.4 Evaporator

The evaporator used was a plate/fin evaporator. A typical plate/fin evaporator is shown in Figure C.5. It consists of aluminum plates and fins alternately sandwiched together. The face dimensions of the evaporator are 7-1/2" x 8" (19.0 cm x 20.3 cm) resulting in an evaporator face area of 0.42 ft^2 (0.039 m^2). The evaporator was mounted in the evaporator box in crossflow with the airstream in the evaporator air loop. Water condensate from the face of the evaporator fell into the downstream mixing box in the evaporator air loop and remained there until removal by a drain located on the bottom of the mixing box. The 1989 Taurus is rated for a maximum evaporator air flow of 215 scfm (0.101 m^3/s).

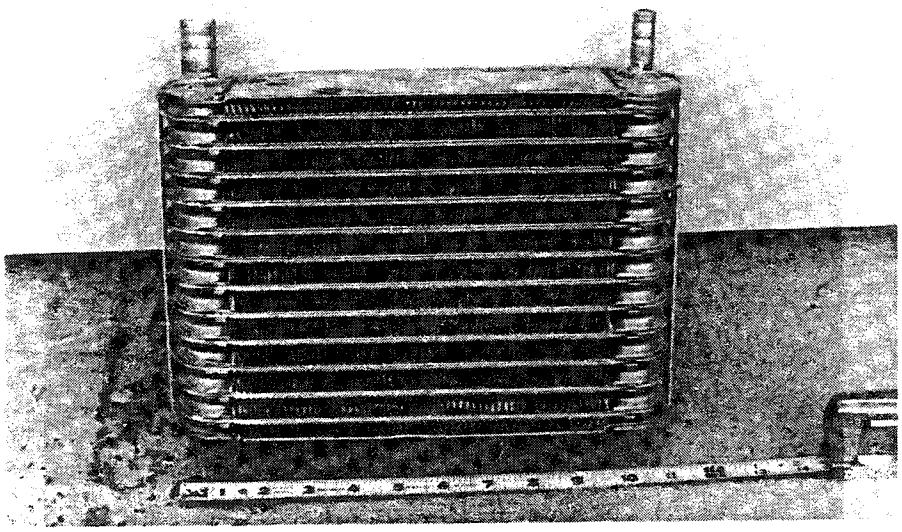

Figure C.5. Photograph of Evaporator.

C.1.5. Accumulator-Dehydrator

An accumulator-dehydrator was used in the refrigerant loop and is shown in Figure C.6. The accumulator-dehydrator serves several purposes. First, it serves as reservoir for excess refrigerant in the system during any transients that might occur. Second, integral to the accumulator-dehydrator is a filter that removes particulate from the refrigerant and a desiccant to remove any moisture in the refrigerant. Lastly, the accumulator-dehydrator is designed such that it will deliver only vapor to the compressor. The accumulator-dehydrator was located between the outlet of the evaporator and the inlet of the compressor.

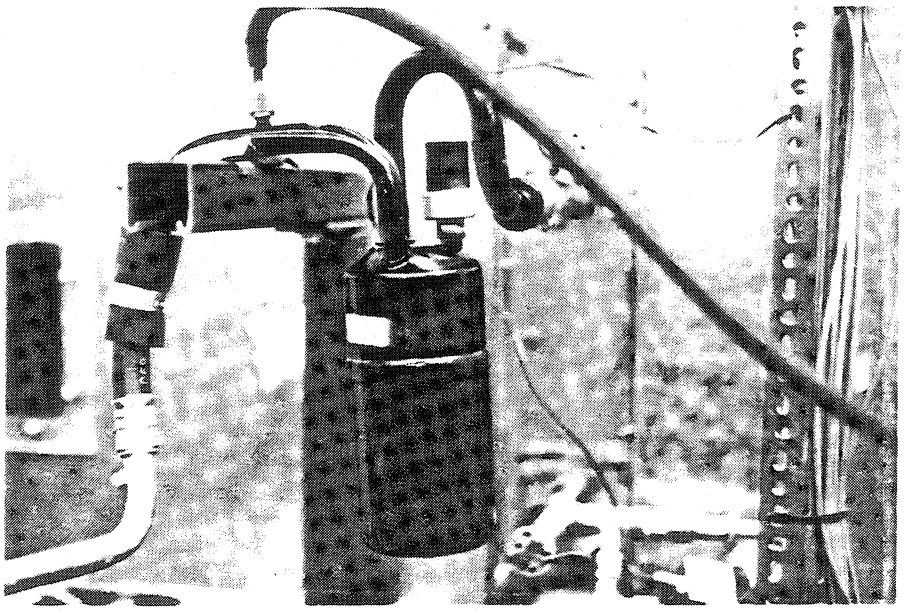

Figure C.6. Photograph of Accumulator-Dehydrator.

C.1.6. Refrigerant Lines

The Ford air conditioning system is comprised of the following three refrigerant lines: the A/C accumulator & hose assembly, the A/C tube assembly and the A/C manifold & tube assembly.

They are elastomer hoses that connect to the compressor, condenser, and evaporator though the use of spring lock couplings. The spring lock couplings provide for easy attachment of the heat exchangers to the refrigerant lines. Four different sizes of spring lock couplings were used on the refrigerant lines. Ford has supplied spring lock tools that allow the couplings to be easily disassembled. The three refrigerant production lines were not modified but their connections were changed to include the refrigerant sensors in the refrigerant lines. These modifications are discussed in the remainder of this section.

The A/C accumulator & hose assembly attaches the outlet of the evaporator to the inlet of the compressor. The accumulator-dehydrator is on one end of the hose assembly, and it is connected by an elastomer hose to a metal tube on the other end. There is a spring lock coupling on each end of the hose assembly. The connection to the compressor was made with the spring lock coupling.

The accumulator-dehydrator was connected to the outlet of the evaporator with a copper block. The block, shown in Figure C.7, is intended to hold one end of the spring lock couplings with a Gyrolok fitting. This allows for easy assembly of the accumulator-dehydrator to the block. Connected to the block were a temperature probe mounted so that the probe is in the center of the refrigerant stream and the pressure difference reference port. The other end of the block has the male spring lock coupling connected to the block with a Gyrolok. The coupling on the block was attached to the mating coupling on the outlet of the evaporator.

The A/C tube assembly attaches the outlet of the condenser to the inlet of the evaporator. The orifice tube is located on one end of the hose assembly, and it is connected by an elastomer hose to a metal tube on the other end. There is a spring lock coupling on each end of the hose assembly.

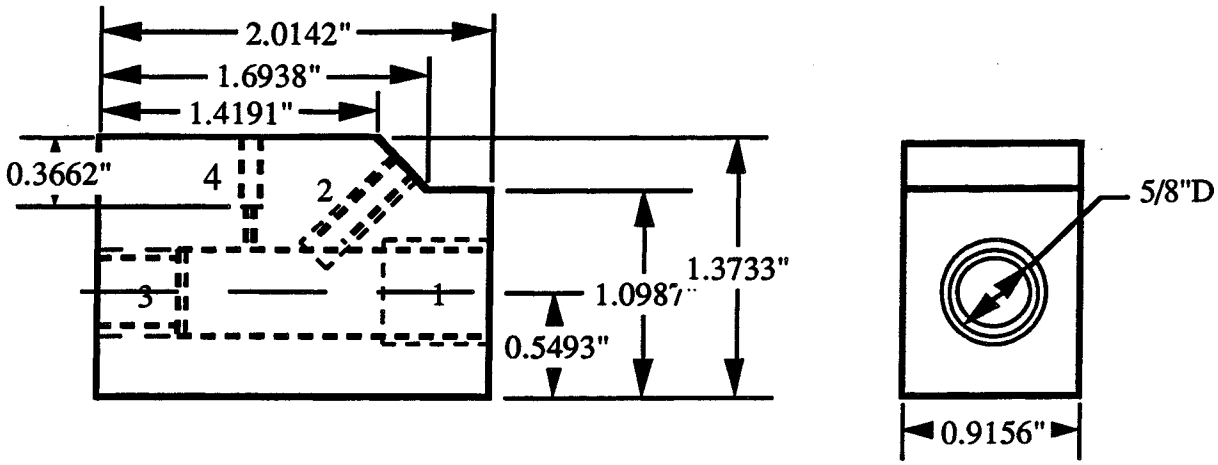

1 OUTLET REFRIG 3/4" PT

2 TEMP PROBE 1/8" PT

3 INLET REFRIG 1/2" PT

4 DEL P TAP 1/8" & 1/16" DRILL

Figure C.7. Copper Block Connection.

The evaporator end of the A/C tube assembly was attached to a spring lock coupling which is attached to a Gyrolok fitting. The absolute and difference pressure transducers were attached to the Gyrolok fittings. Once again, the temperature probe is connected to the Gyroloks fittings so that the probe is in the center of the refrigerant fluid stream and just entering the evaporator housing. A Gyrolok fitting holds the spring lock connector which is inserted into the evaporator spring lock fitting.

The A/C tube assembly was cut just before the entrance to the orifice tube. A Gyrolok fitting was attached to the orifice tube. This fitting allowed for the connection of the sight glass and the flow meters within the refrigerant line. The spring lock connector on the original assembly was attached to the new refrigerant line with a Gyrolok fitting.

The A/C tube assembly to the condenser was made with a spring lock connector were the connector on the condenser side was cut and flared. This allowed instrumentation to be inserted

between the condenser connector and the condenser outlet. A pressure reference port for the pressure difference sensor was constructed with a tee pipe fitting. The temperature probe was inserted into the tubing so that it would be in the center section of the fluid flow. A flare fitting was attached to the condenser tubing to allow the assembly described above to be attached to the condenser.

The A/C manifold & tube assembly consists of a manifold that provides the spring lock coupling to the inlet of the compressor and the hose assembly forming the outlet of the compressor. A muffler is located in the hose assembly to quiet the discharge of the compressor. A high pressure relief valve is located in the portion of the manifold connected to the compressor outlet. The valve is designed to vent off abnormally high pressures in the system if they should occur during operation. The manifold was bolted to the compressor with one screw which requires an installation torque of 18 to 27 lb_f•ft (24 to 37 N•m). The spring lock coupling forming the compressor inlet on the manifold was connected to the metal tube from the A/C accumulator & hose assembly mentioned above.

To attach the pressure and temperature sensors onto the manifold, the manifold was machined so that the pressure and temperature sensors would be inserted as close to the output and input ports as physically possible. The temperature probes were inserted into the compressor chamber no more than an inch (2.54cm).

A sight glass was placed in the refrigerant line leaving the condenser. The sight glass provided a visual check on the state of the refrigerant exiting the condenser. During normal operation of the system, the refrigerant should be subcooled liquid.

C.1.7. Refrigerant

Since the oil used with a CFC-12 system is not compatible with the oil used with a HFC-134a system, two entire air conditioning systems will be needed to perform the tests. Ford Motor Company has donated two entire air conditioning systems from their 1989 Ford Taurus. All

of the components are identical with the exception of the compressor and the accumulator-dehydrator.

The difference in the compressors is that one of them is filled with seven ounces of mineral oil that is compatible with CFC-12. The other compressor is filled with seven ounces of Allied oil "A" that is compatible with HFC-134a. The difference in the accumulator-dehydrators is that one of them is filled with a desiccant that is compatible with CFC-12. The other is filled with an experimental desiccant that is compatible with HFC-134a.

C.2. Condenser Air Loop

The condenser air loop provided the ability to control the inlet air conditions of the condenser. The condenser air loop allowed both the mass flow rate and temperature of the condenser inlet air to be controlled. Figure C.8 is a schematic of the condenser air loop. A "Unistrut" structure was constructed to support the condenser air loop and is shown in Figure C.9. The components in the condenser air loop are the blower, inverter, condenser box, mixing boxes, air velocity flow station, dampers, and ducting. The following four sections describe these components.

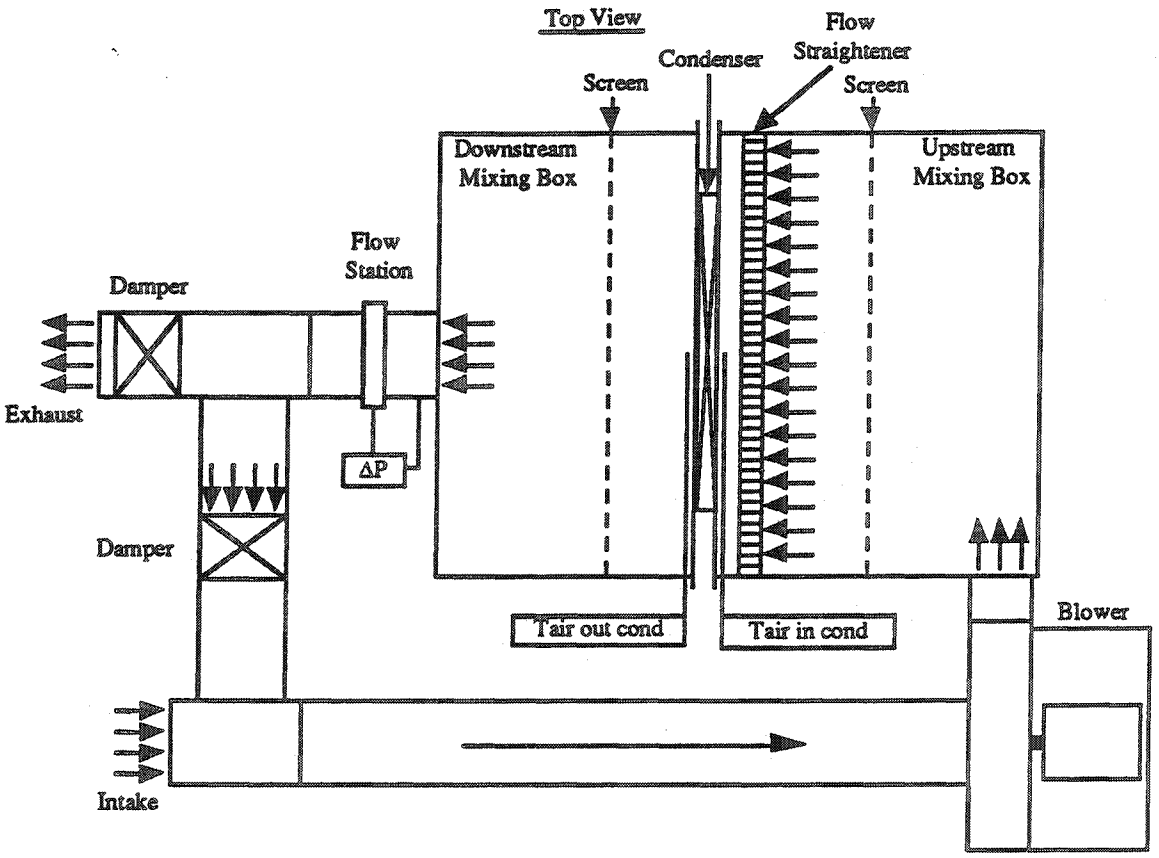

Figure C.8. Test Stand Condenser Air Loop.

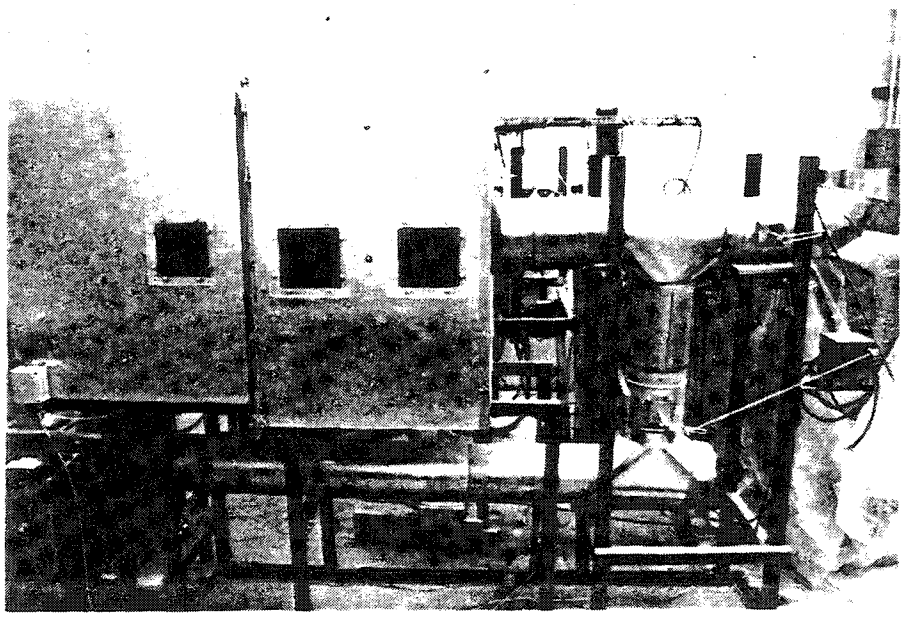

Figure C.9. Photograph of Condenser Air Loop.

C.2.1. Blower and Inverter

The blower used in the condenser air loop is a Dayton high pressure direct-drive blower (Model No. 4C330). The blower supplied the pumping power to move the air through the condenser air loop. The blower consists of a blower wheel, blower housing, and electric motor. The blower wheel is 13-1/2" (34.3 cm) in diameter and has self-cleaning radial blades. The wheel is made from cast aluminum and is balanced. It fits in the housing and is attached to the electric motor shaft by two set screws. The housing supports the electric motor and blower wheel and is made from welded 16 gauge steel. The electric motor is a 5 Hp @ 3450 RPM, 240 VAC, 3-phase Dayton electric motor (Model No. 3N669). The motor has a No. 182T frame and an open enclosure. Figure C.10 is the performance curve of the blower.

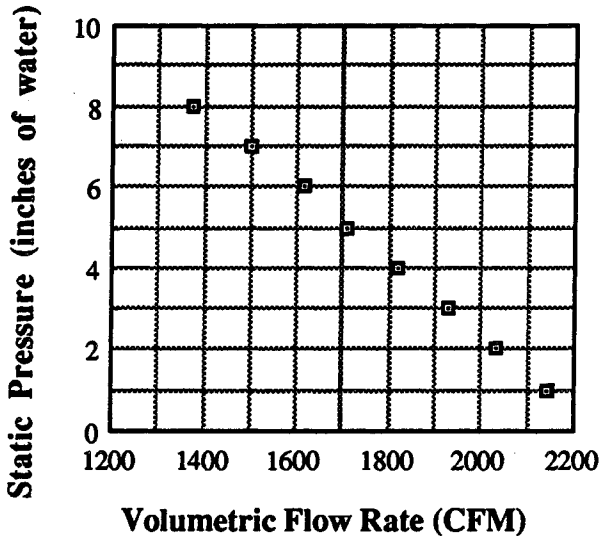

Figure C.10. Dayton Model 4C330 Blower Performance Curve.

An Asea Brown Boveri model M01712A00 Parajust M speed controller rated at 17 Amps for a 240 VAC 3-phase output was connected to the direct-drive blower. This inverter allowed the flow of air across the condenser to be controlled either manually or with a 0-5 Volt signal. A stand

constructed of "Unistrut" was designed to support the inverter and the Dayton high pressure direct-drive blower.

C.2.2. Condenser Box and Mixing Boxes

The condenser box, made of 22 gage sheet metal, supported the condenser as well as the temperature instrumentation. The physical design of the condenser box was that of a sheet metal box with open ends. The box has a face dimension of 27 1/2" x 16" (0.70m x 0.41m) and a depth of 2" (5.1 cm). The open ends have flanges on them. The ends of the box are flat sheet metal plates with the same cross-sectional area as the upstream and downstream mixing boxes. Each end has a rectangular hole; the downstream end in its center with the same cross-sectional area as the condenser being tested and the other end offset to allow for the additional space required by the instrumentation. The ends were bolted to the flanges on the condenser box. The entire condenser box assembly was bolted to the flanges on the upstream and downstream mixing boxes.

This design facilitates the testing of condensers that have different physical dimensions. The only modification to the condenser air loop when testing a different condenser will be to fabricate a condenser box to house the particular condenser.

There are two mixing boxes in the condenser air loop, the upstream mixing box and the downstream mixing box. The face dimensions of the two mixing boxes are 44" x 38" (1.1m x 0.97m). The upstream box is 2' (0.61m) deep while the downstream mixing box is 2' 6" (0.76m) deep. The two mixing boxes made of 22 gage sheet metal are described below.

The upstream mixing box conditioned the turbulent air leaving the blower and helped to ensure a uniform velocity profile entering the condenser. The physical design of the upstream mixing box was that of a sheet metal box with open ends. The open ends have flanges on them. The ends of the mixing box are flat pieces of sheet metal bolted to the flanges. The inlet end plate has no holes in it so the plate can serve as an end to the upstream mixing box. The condenser blower discharged into the bottom of the upstream mixing box through a square duct 5 7/8" x 7 1/4" (14.9cm x 18.4cm). The square ducting connecting the blower to the upstream mixing box

has the same cross section as the outlet of the blower. The upstream mixing box also has a square hole the same cross section as the outlet of the blower on its side to allow the air to enter. A screen with 1/8" (0.32cm) diameter holes, four holes per inch (2.54cm), was placed in the center of the box to provide a uniform pressure drop and straightening effect on the air. The air flowed through a 1/4" (0.64cm) honeycomb cell structure flow straightener with a 1" (2.54cm) depth. The flow straightener was an additional device to ensure a uniform velocity profile entering the condenser. The outlet end plate was the same plate that forms the inlet of the condenser box mentioned previously.

The downstream mixing box collected the air that passed over the condenser and provided a mounting point for the air velocity flow station. The physical design of the downstream mixing box was that of a sheet metal box with flanges on the open ends. A screen was placed in the box to provide a uniform pressure drop and to ensure a constant velocity profile through the condenser. The ends of the mixing box were flat pieces of sheet metal bolted to the flanges. The inlet end plate was the same plate that forms the outlet of the condenser box mentioned previously. The outlet end plate has a circular hole cut into it with the same cross section as the air velocity flow station to provide for mounting of the station and an exit for the air from the box.

C.2.3. Air Velocity Flow Station

The air velocity flow station used was a Air Monitor 8" Lo-Flo pitot traverse station (Model No. P). The air velocity flow station was mounted to the outlet of the downstream mixing box of the condenser air loop. Doved tails formed in a circle on the box were compressed against the flow station with a rubber hose and a hose clamp to form the air seal. The flow station was supported with the "Unistrut" structure. The flow station is a cylindrical device with a inner diameter of 8.407" (21.4 cm) and a length of 12" (30.5 cm). The volumetric air flow range of the station is 150 to 2160 cfm (0.071 to 1.019 m^3/s) with an accuracy of 1% of the actual volumetric flow rate. The air flow to be measured flows though the inside of the station. Once inside, the air is straightened by an air straightener-equalizer consisting of an open cell honeycomb structure with a

minimum cell size to length ratio of 36 to 1. The equalizer helps to eliminate turbulent and rotational flows before they encounter the pressure taps. Next, the total pressure averaging manifold in the shape of an "X" is located concentrically in the station. This manifold has several total pressure taps that allow the averaged total pressure of the flow to be measured through a external 1/4" FPT fitting on the outside of the station. Next, the air flows over several static pressure taps that are located concentrically around the inside of the station. The taps allow the averaged static pressure of the flow to be measured through a external 1/4" FPT fitting on the outside of the station. The air flow then exits the station. A differential pressure transducer was connected to the total pressure fitting and the static pressure fitting to provide a velocity pressure reading of the condenser air flow.

C.2.4. Dampers and Ducting

The two dampers that were used in the condenser air loop are Ruskin round dampers (Model No. CDRS25). The two dampers provided 0 to 100% recirculation of the condenser loop air. Each damper is 8" (20 cm) in diameter with a neoprene blade seal on the control blade. The blade seal provides for less than 0.1% leakage. The blade has a locking quadrant handle for manual operation.

A Johnson Controls non-spring return motor actuator with a 24VAC floating control input (Model No. M120AGA-1) was used to control the dampers. This control was performed by a Honeywell single loop controller (Model No. DC3002-0-01A-2-00-0111). This controller allows for an input signal in the form of a thermocouple voltage and then switches relays based upon a specified band width. By setting the temperature desired for the air entering the condenser, the controller would control the damper openings and thus control the amount of heated air entering the condenser by controlling the amount of recirculated heated air. The two dampers were connected in parallel so that the dampers would move simultaneously.

The rest of the ducting in the air loop was comprised of round duct, tee fittings, and any other connections necessary to connect the components. The ducting was made from sheet metal. The round ducting that connects the flow station, dampers and blower was 8" (20.3 cm) round duct. The two tees in the loop were 8" (20 cm) tees. The square ducting connecting the blower to the upstream mixing box has the same cross section as the outlet of the blower.

C.3. Evaporator Air Loop

The evaporator air loop provided the ability to control the inlet air conditions of the evaporator. The evaporator air loop allowed the mass flow rate, temperature and relative humidity of the evaporator inlet air to be controlled. It allowed for testing of the evaporator at conditions it would see in its normal operating environment by providing 0 to 100% recirculation of the air in the loop along with reheat and steam injection. Figure C.11 is a schematic of the evaporator air loop. A "Unistrut" structure was constructed that will support the evaporator air loop and is shown in Figure C.12. The components in the evaporator air loop are the blower, evaporator box, mixing boxes, air velocity flow station, dampers, duct heater, and steam injection unit. The following six sections describe these components.

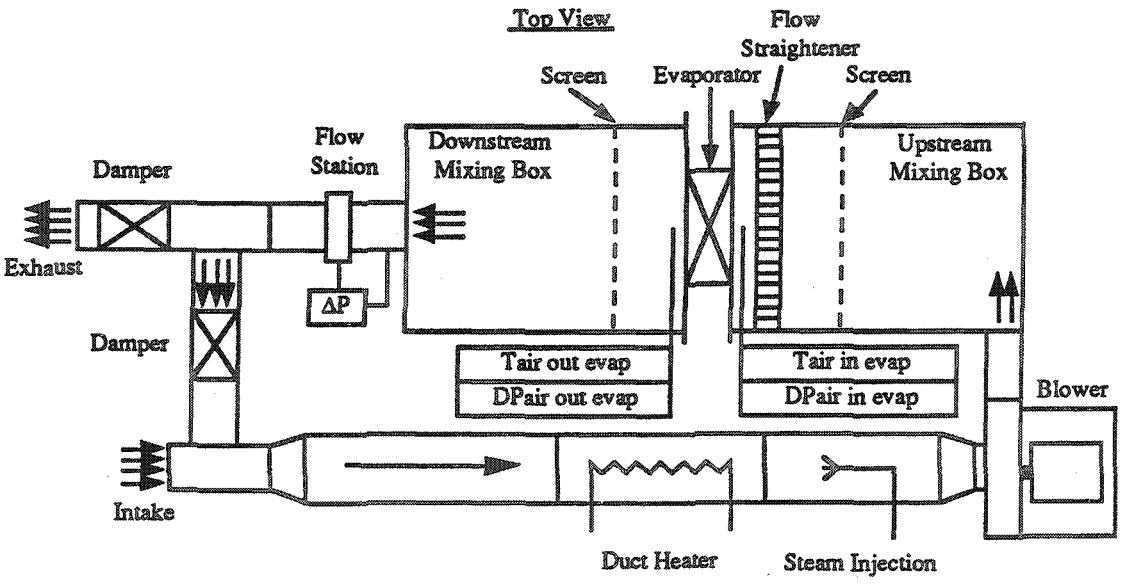

Figure C.11. Test Stand Evaporator Air Loop.

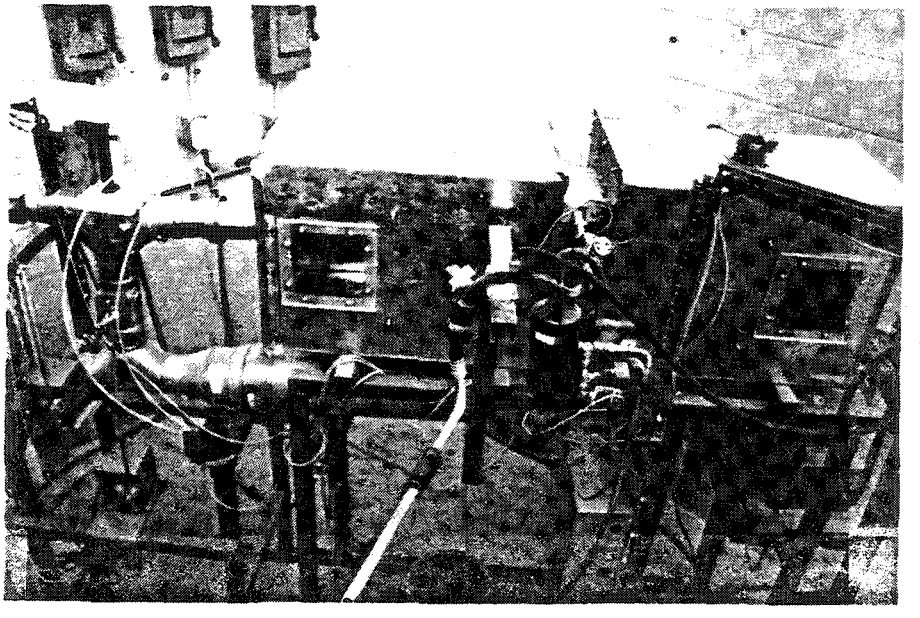

Figure C.12. Photograph of Evaporator Air Loop.

C.3.1. Blower

The blower used in the evaporator air loop is a Dayton high pressure direct-drive blower (Model No. 2C820). The blower used in the evaporator air loop is similar to the one used in the condenser air loop with the following exceptions. The blower wheel is 9" (22.9 cm), and the electric motor is a 1/3 Hp @ 3450 RPM, 115 VAC, 1-phase Dayton electric motor (Model No.

2k5868). The motor has a No. 48 frame and an open enclosure. Figure C.13 is the performance curve of the blower.

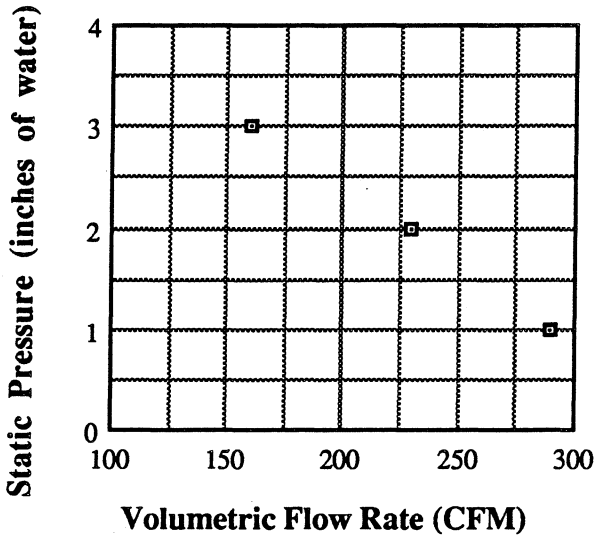

Figure C.13. Dayton Model 2C940 Blower Performance Curve.

C.3.2. Evaporator Box and Mixing Boxes

The evaporator box was similar in design to the condenser box. The only differences were that the evaporator box is smaller in size, 18" x 15" (46cm x 38cm) face dimensions and 4" (10cm) deep, and will support dew point as well as temperature instrumentation. As before, this design facilitates the testing of evaporators that have different physical dimensions. The only modification to the evaporator air loop when testing a different evaporator will be to fabricate a evaporator box to house the particular evaporator.

The upstream and downstream mixing boxes were similar in design to those in the condenser air loop. The only differences are that the boxes will be smaller in size, face dimensions of 20" x 17" (51cm x 43cm) at a depth of 24" (61cm), and that provisions for condensate removal were included in the downstream mixing box. A positive shut-off valve drain was attached to the

bottom of the downstream mixing box. This allowed for condensate removal when the test was completed and a leak free downstream mixing box during the testing.

C.3.3. Air Velocity Flow Station

The air velocity flow station that was used is a Air Monitor 3" Lo-Flo pitot traverse station (Model No. P). It is similar in function to the air velocity station in the condenser air loop. The air velocity flow station was mounted to the outlet of the downstream mixing section of the evaporator air loop. The flow station is a cylindrical device with an inner diameter of 3.334" (8.5 cm) and a length of 12" (30.5 cm). The volumetric air flow range of the station is 24 to 340 cfm (0.0113 to 0.160 m^3/s) with an accuracy of 1% of the actual volumetric flow rate.

C.3.4. Dampers and Ducting

The two dampers that were used in the evaporator air loop are Ruskin round dampers (Model No. CDRS25). They are identical in design to the dampers in the condenser air loop except that they are 4" (10 cm) in diameter.

A Johnson Controls non-spring return motor actuator with a 24VAC floating control input (Model No. M120AGA-1) was purchased to control the dampers. Currently, these dampers are being controlled manually. The mixing damper was used to control the humidity by controlling the amount of dry air recirculating from the evaporator outlet. The exit damper controlled the flow across the evaporator by restricting the air flow.

The rest of the ducting in the air loop was comprised of round duct, tee fittings, and any other connections necessary to connect the components. The ducting was made from sheet metal. The round ducting that connects the flow station to the dampers was 4" (10 cm) round duct. The two tees in the loop were 4" (10 cm) tees. To facilitate the duct heater and steam injection unit, 8" (20 cm) round duct was used for the two components This required one 6" (15 cm) to 4" (10 cm) reducer to connect the intake tee to the 8" (20cm) to 6" (15cm) reducer. Another 8" (20cm) to 6" (15cm) reducer was required to connect the 8" (20cm) round duct to the blower. The

square ducting connecting the blower to the upstream mixing box had the same cross section as the outlet of the blower 3 1/8" x 3 1/8" (7.9cm x 7.9cm).

C.3.5. Duct Heater

A duct heater was installed in a 8" (20 cm) round section of ducting in front of the steam injection ducting. The duct heater provided the reheat necessary to achieve inlet evaporator temperatures above ambient, which is analogous to the non-ventilated interior of a car on a sunny day. The duct heater was constructed from the heating elements out of small 1500 Watt Sears space heaters (Model No. 42F36240) with circular heating elements. Two of the heating elements were wired in series. Another set was connected to this existing set resulting in an equivalent circuit of two resister in series in two different branches wired parallel to each other. A 220VDC supply was wired across this circuit.

To control the amount of heat added to the air stream, an Omega 240 Volt 30Amp single phase SCR power controller (Model No. SCR71Z-230) was added to the system. With the Omega single loop controller (Model No. Cn-2001-T-FI-DI), the temperature into the evaporator was monitored and the SCR would be fired by a controller signal to adjust for the desired temperature set point programmed into the controller.

C.3.6. Steam Injection

A steam injection unit will be installed in a 8" (20 cm) round section of ducting in front of the blower. The steam injection unit will provide the steam necessary to raise the relative humidity of the evaporator inlet air. The steam injection unit will consist of a steam head aimed into the air flow connected to a valve that will control the amount of steam released. The worst case relative humidity requirement for evaporator inlet air during the operation of the air conditioning system will be calculated. This will determine the amount of steam that will need to be injected into the system, and thus the size of the steam head and lines.

C.4. Instrumentation And Data Acquisition

The test stand was fitted with instrumentation that will allow data to be taken for the transient studies. Fast response time was critical for all components so the transients can be recorded. The next seven sections describe the instrumentation and data acquisition of the test stand. Included in Appendix D are the instruments that have been acquired. Figure C.1 shows the type and location of data that will be recorded from the stand.

C.4.1. Temperature Instrumentation

Two types of temperature instrumentation were required: (1) air temperatures and (2) refrigerant temperatures. Four air temperature and six refrigerant temperatures were measured.

The inlet air temperatures of the condenser and the evaporator were measured using a handmade copper-constantan thermocouple circuit. Four thermocouples were placed on the screen located in the downstream mixing boxes and wired in parallel to obtain an average inlet air temperature.

The outlet air temperatures were measured using a nine point thermocouple array. By setting up a series of sensing and reference junctions, an average temperature difference across the heat exchanger was measured. With nine points measuring the temperature difference, the signal received by the measuring device is amplified nine times. This temperature difference was then added or subtracted from the inlet air temperatures to obtain the outlet air temperature. Figure C.14 shows a schematic of a three point thermocouple array and the general pattern was used to construct the nine point array.

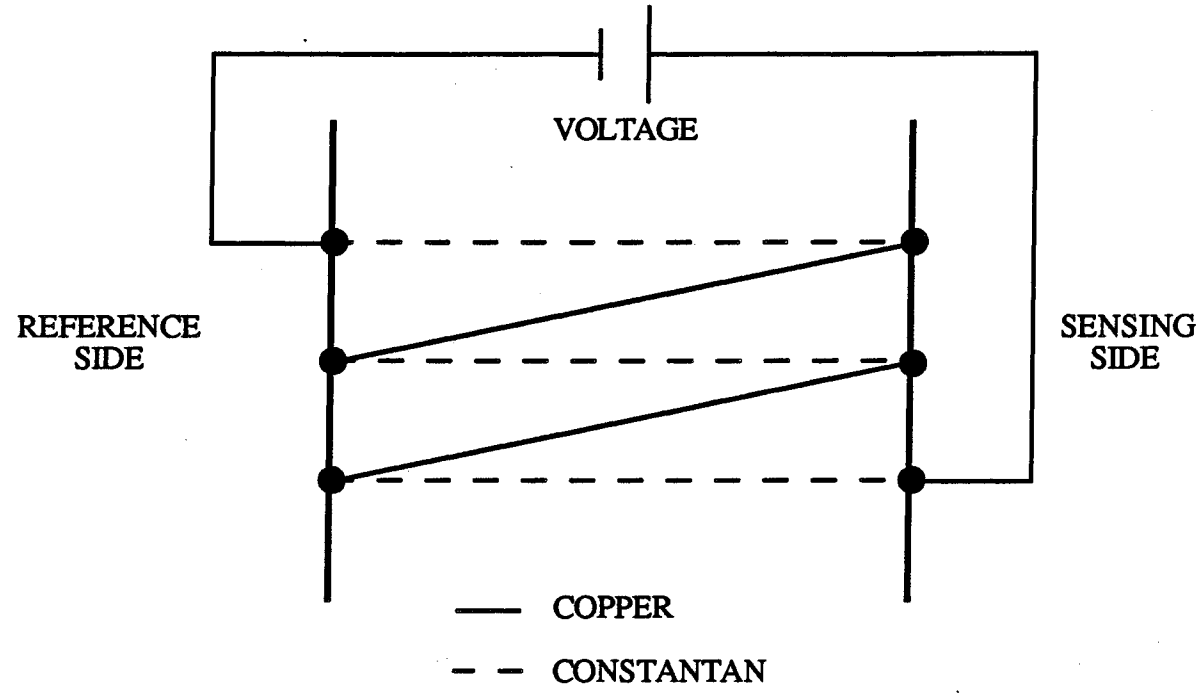

Figure C.14. Three Point Thermocouple Array.

The six refrigerant temperatures were measured using Omega 3" (7 cm) long thermocouple probes (Model No. TB-CPSS-116U). The thermocouple probes are copper-constantan with a 1/16" (1.6 mm) 306 stainless steel sheath. The thermocouple probes were mounted into a tee in the refrigerant line with a compression fitting. This enabled the end of the probe to be in the center of the refrigerant flow and result in an accurate temperature measurement of the refrigerant..

C.4.2. Pressure Instrumentation

Two types of pressure instrumentation were required: (1) air pressures and (2) refrigerant pressures. One ambient pressure and six refrigerant pressures were required

The only ambient pressure required is a absolute pressure of the ambient air. This pressure is necessary to convert the gauge refrigerant pressure transducer outputs to absolute pressures and to serve as an atmospheric pressure measurement for the calculation of the density of air. This measurement was determined by a Setra pressure transducer (Model No. 280E) with a range of 0 to 25 psia (0 to 172 kPa absolute). It has a operating temperature range of 0 to 175°F (-17.8 to

79.4°C) and a dynamic response time of 1 to 5 ms. The output of the transducer is linear with pressure and ranges from 0 to 5 VDC. The accuracy is ±0.11 percent of full scale. The excitation voltage required is 15 to 32 VDC unregulated, and a power supply will be purchased to supply the voltage. The transducer draws 10 mA @ 24 VDC. The transducer has a 1/4-18 NPT internal fitting. The transducer was mounted close to the data acquisition system with the pressure fitting open to the ambient air.

Four gauge pressure transducers along with two differential pressure transducers were used to determine the six refrigerant pressures.

The output refrigerant pressure of the compressor, P2, and the inlet refrigerant pressure of the condenser, P3, were measured using two Setra gauge pressure transducers (Model No. 207) with a range of 0 to 500 psig (0 to 3447 kPa gauge). The output of the transducer is linear with pressure and ranges from 0.1 to 5.1 VDC. They have an operating temperature range of -40 to 260°F (-40 to 126.7°C) and a dynamic response time of 1 to 5 ms. Their accuracy is ±0.13 percent of full scale. The excitation voltage required is 12 to 28 VDC unregulated, and a power supply was purchased to supply the voltage for each transducer. Each transducer draws 5 mA @ 24 VDC. The transducer has a 1/4"-18 NPT external fitting. Each transducer was mounted close to its respective measurement location with the pressure fitting screwing into a tee in the refrigerant line.

The inlet refrigerant pressure of the compressor, P1, and the inlet refrigerant pressure of the evaporator, P6, were measured using two Setra gauge pressure transducers (Model No. 207) with a range of 0 to 100 psig (0 to 689 kPa gauge). The pressure transducers are the same as those described above but with a different range. A power supply was purchased to supply the voltage for each transducer. Each transducer was mounted close to its respective measurement location with the pressure fitting screwing into a tee in the refrigerant line.

The pressure drop of the condenser and the pressure drop of the evaporator was measured using two Setra high accuracy differential pressure transducers (Model No. C228-1) with a range of 0 to 25 psid (0 to 172 kPa differential). The output of the transducer is linear with pressure and

ranges from 4 to 20mA. They have an operating temperature range of 0 to 175°F (-17.8 to 79.4°C) and a dynamic response time of less than 40 ms. Their accuracy is ±0.15 percent of full scale. The excitation voltage required is 24 VDC unregulated. Each transducer draws 10 mA @ 24 VDC. Each transducer has two 1/8"-27 NPT internal positive pressure fittings. Each transducer was mounted close to its respective measurement location with the reference pressure fitting screwing onto a tee in the heat exchanger outlet refrigerant line and the positive pressure fitting screwing onto a tee in the heat exchanger inlet refrigerant line.

All of the pressure sensors mentioned above are manufactured by Setra Systems, Inc. Their operation is based on Setra's patented variable capacitance design. The design features a 17-PH stainless steel pressure body and an insulated electrode plate that is fastened to the center of a diaphragm in the sensor, creating a variable capacitor between the sensor body and the electrode plate. When the pressure in the body is increased, a slight deformation of the diaphragm changes the capacitance. This change in capacitance is detected and converted to a linear DC electric signal by the electronic circuit in the pressure sensor. This design makes for an accurate unit with fast dynamic response and low hysteresis. The pressure sensor is very stable under transient temperatures and is compensated for both zero and sensitivity shifts due to temperature variations.

C.4.3. Dew Point Instrumentation

Two dew point sensor measurements will be required. The two sensors will be used to record the evaporator air inlet and outlet dew points. The dew point measurements will allow properties such as the relative humidity and humidity ratio of the moist air to be obtained from moist air tables and the psychrometric chart. A third sensor could be installed in the upstream mixing box of the condenser air loop if it is ever deemed necessary to record the condenser air inlet dew point.

The dew point sensors that will be used are General Eastern dew point transmitters (Model No. 655). They use a type 611-A saturated-salt lithium chloride dew point sensor to determine the dew point. The operating dew point range of the sensors is 0 to 100°F (-17.8 to 37.8°C) with an

accuracy of ±1°F (±0.55°C). The sensor can provide three simultaneous outputs: 0 to 5 VDC, 4 to 20 mA and a field-adjustable alarm relay. The 0 to 5 VDC output of each sensor will be used. The response time of the sensors is typically 3 to 5 minutes in an airstream with a velocity of 10 fpm. The input voltage of the sensors is 115 VAC and the nominal operating input current is 8.7 mA. The sensors will be mounted in their respective locations to the upstream and downstream mixing boxes in the evaporator air loop.

C.4.4. Air Velocity Instrumentation

The air velocity flow stations have two pressure ports on them that when measured and subtracted give the velocity pressure of the flow. The volumetric flow rate was calculated from the velocity pressure. The velocity pressure of the condenser air flow station and the velocity pressure of the evaporator was measured using two Setra very low differential pressure transducers (Model No. 264) with a range of 0 to 2.5 inches water column differential. The output of the transducers is linear with pressure and ranges from 0 to 5 VDC. They have an operating temperature range of 0 to 175°F (-17.8 to 79.4°C) and a dynamic response time of 1 to 5 ms. Their accuracy is ±1.0 percent of full scale. The excitation voltage required is 12 to 28 VDC unregulated, and a power supply was purchased to supply the voltage for each transducer. Each transducer draws 10 mA @ 24 VDC. Each transducer has two 3/16" (4.6 mm) barbed brass pressure fittings for 1/4" (6.4 mm) push-on tube. Each transducer was mounted close to its respective air flow station with the LOW pressure fitting attached to the static pressure fitting on the station by 1/4" (6.4 mm) tubing and the HI pressure fitting attached to the stagnation pressure fitting on the station by 1/4" (6.4 mm) tubing.

C.4.5. Refrigerant Flow Rate Instrumentation

Two flow meters were located at the outlet of the condenser. Through conversations with automotive air conditioning engineers at Chrysler and Ford, the typical CFC-12 mass flow rate range of their systems is 200 to 600 lb_m/hr (0.0252 to 0.0756 kg/s). A positive displacement

meter was selected since this meter was independent of the liquid viscosity. Since the system uses R134a and probably other refrigerants that are not even in production, it was believed that this meter would handle all the flow measuring requirements. Then it was discovered that the positive displacement meter would not handle vapor. Since transients were being studied, it was believed that vapor may exist at the outlet of the condenser. So a turbine meter, unaffected by vapor, was selected that could only be calibrated for R12. By placing the two meters in series with a bypass on the positive displacement meter, steady state runs would allow the turbine meter to be calibrated with the information from the positive displacement meter.

The Emco positive displacement flow meter (Model No. PDP-3-1000) is rated for 0 to 95gph (0 to 6000cc/min). The 4-piston displacement flow meter has an accuracy ±0.5 percent of the reading within the linear range and a repeatability of ±0.10 percent. It has a process temperature limit of -40 to 500°F (-40 to 260°C) and a response time of 1 second. The power required for the analog output is 18-30VDC. The analog output is a 2-wire 4-20mA signal. The meter is connected to the refrigerant lines with a female 3/8" NPT. The pressure drop across the flow meter is less than 2 psi (14 KPa). A 10 microns filtration device (Model No. 3-3/8") was insert at the entrance of the meter to assure that a clean liquid would enter the meter.

The Sponsler precision turbine flow meter (Model No. SP1/4-353B-A-RF) has a flow range of 0.1 - 1.5 gpm (0.0063 - 0.0946 L/s). A Sponsler modulated carrier amplifier (Model No. SP717) was attached to the flow meter to generate a proportional 12-35 VDC squarewave output based on the carrier frequency from the RF pickup coil in the turbine meter. The Sponsler multi-fuction rate indicator totalizer (Model No. SP2900) was connected to the amplifier to convert the squarewave pulse to a two-wire 4-20mA output. The meter has a linearity of ±0.25 percent over the specified flow range and a repeatability of ±0.1 percent or better over the nominal rated flow range. It has a temperature range up to 750°F (399°C). The meter was connected to the refrigerant line with 1/2" NPT male end fittings. The pressure drop across the flow meter is less than 2 psi (14 KPa).

C.4.6. Torque and Speed Instrumentation

The torque sensor used was a Lebow high accuracy rotary transformer strain gage bridge torque sensor (Model No. 1805-2K-04) with an integral magnetic pick-up speed sensor. The range of the torque measurement was 0 to 2000 lb_f•in. (0 to 226 N•m), and the torque sensor speed range was 0 to 15000 RPM. The torque sensor's nonlinearity, hysteresis, and repeatability were ±0.1%, ±0.1%, and ±0.05%, respectively. The torque sensor was connected to a Daytronics strain gage conditioner (Model No. 3278) with LED display. The conditioner provided the input excitation signal to the torque sensor and the compensating circuitry to provide a 0 to 5 VDC linear output with torque. A Lebow precision calibration reference (Model No. 7927) was connected in series with the torque sensor and the strain gage conditioner. The precision calibration reference utilized an isolated bridge reference creating a quasi torque sensor output signal so the frequency conditioner could be calibrated. The calibration quasi torque sensor output signal was 1150 lb_f•in. (130 N•m).

The magnetic speed sensor was connected to a Daytronics frequency conditioner (Model No. 3240) with LED display. The frequency conditioner was a frequency counter that determined the frequency of the magnetic speed sensor output signal and displayed the frequency in Hz. Since the output of the speed sensor had a one to one relationship with the rotational speed of the shaft in RPM, the display was also a direct RPM reading.

C.4.7. Data Acquisition

All measurements were sent to the data acquisition boards located in the expansion slots of an Apple Macintosh II™ personal computer. The computer in team with the software supplied with the boards allowed for the display, output, storage, and/or analysis of the data. Three boards were purchased and filled the data acquisition needs of the test stand. They are described below.

A Strawberry Tree model ACM2-16-16 16-bit data acquisition board along with two T-21 thermocouple panels were used to read the thermocouple inputs. The data acquisition board and the thermocouple panels were purchased as a matched pair. The data acquisition board has 16

differential analog inputs and 16 digital input/outputs. Each thermocouple panel provided terminals for attaching the 16 differential analog inputs and 16 digital input/outputs. They have an isothermal plate with integral cold junction sensor for accurate temperature measurements. Each panel can accept eight differential analog (thermocouple) inputs.

Two Strawberry Tree model ACM2-12-8A 12-bit data acquisition boards along with two T-21 general purpose panels were used to read the other analog inputs from the test stand. The data acquisition board and the thermocouple panel were purchased as a matched pair. The data acquisition board has 8 differential analog inputs, 8 digital input/outputs and two analog outputs. The general purpose panel provides the terminals for attaching the 8 differential analog inputs, 8 digital input/outputs and two analog outputs. They also have room for up to eight optically isolated I/O modules. The two dew point, six refrigerant pressure, and two velocity pressure transducers were attached to the two general purpose panels. The two analog output capabilities of each board were selected so the speed controller and electrically actuated damper controllers could be controlled by the computer.

A data acquisition program was written using the software supplied by Strawberry Tree. The software is called "Analog Connection ACM2™, Data Acquisition and Control System for the Macintosh II™." The program will display a schematic of the test stand on the screen as well as the data in real time. The program will also contain provisions for sampling all of the data at predetermined time intervals and storing it in a file.

APPENDIX D

TEST STAND FOR TRANSIENT STUDIES PARTS LIST

Part Number	Quantity	Description/Requirements	Supplier
E9DH-19C913-AB	1	Accumulator & hose assembly, desiccant is compatible with CFC-12	Ford Motor Company
XE9DH-19C913-AB	1	Accumulator & hose assembly, experimental desiccant is compatible with HFC-134a, S/N CH-11384-01	Ford Motor Company
7C562	1	Blower, high pressure, direct-drive, 13-1/2" diameter wheel, 230/460 VAC, 3-phase, Dayton	Grainger
7C504	1	Blower, high pressure, direct-drive, 9" diameter wheel, 115/230 VAC, 1-phase, Dayton	Grainger
1610-1"	1	Bushing, Taper-Lock, 1.0 inch shaft diameter, Dodge	Berry Bearing
60-2702	1	Cabinet, louvered series 60, BUDD	Klaus Industries Electronics
E9DH-19D629-AA	1	Compressor & clutch assembly, FX 15, filled with 7 oz. mineral oil for CFC-12	Ford Motor Company
E9DH-19D629-AA	1	Compressor & clutch assembly, FX 15, filled with 7 oz. Allied oil "A" for HFC-134a, S/N 10832-08	Ford Motor Company
E8DH-19710-AA	2	Condenser, fin-tube	Ford Motor Company
3240	1	Conditioner, frequency with RPM display, Daytronic	Comtel-Midwest
3278	1	Conditioner, strain gage with lbf•in display, Daytronic	Comtel-Midwest
L110x1.0	1	Coupling, flexible, 1.0 inch shaft diameter, Lovejoy	Berry Bearing
L110x1.125	1	Coupling, flexible, 1.125 inch shaft diameter, Lovejoy	Berry Bearing
L110x1.5	2	Coupling, flexible, 1.5 inch shaft diameter, Lovejoy	Berry Bearing
CDRS25	2	Damper, control, 4 inch round with neoprene blade seal and locking hand quadrant, Ruskin	W. John Bowman & Associates
CDRS25	2	Damper, control, 8 inch round with neoprene blade seal and locking hand quadrant, Ruskin	W. John Bowman & Associates
M120AGA-1	4	Damper actuators, non-spring return, 35 lb-in, 24 VAC, two-position. Damper linkage assembly (Y20DAB-2)	Johnson Controls
655	2	Dew Point Transmitters	General Eastern
CN-2001-T-FI-DI	1	Digital controller, non-alarm controller, 4-20mA output, type T thermocouple, Omega input, remote 0-5 VDC setpoint, Omega	Omega
DC-3002-0-	1	Digital controller, two-alarm controller, 4-20 mA output, thermocouple input, Honeywell	Honeywell
	4	Disassembly Tools, spring lock refrigerant line coupling	Ford Motor Company
E8DH-19860-AA	2	Evaporator, plate/fin	Ford Motor Company

Part Number	Quantity	Description/Requirements	Supplier
SCR71Z-230	1	Heat controller, 240 Volt, single phase, SCR controller, Omega	Omega
42F36240	4	Heaters, 1500 Watts	Sears
CIMR-7.5 G2	1	Inverter, 36 Amp, 230 VAC, 3 Phase	IDM Controls Inc.
M01712A00	1	Inverter, 17 Amp, 240 VAC, 3-Phase input, NEMA 1 enclosure, Parajust M. Options include input conditioning card (680828G03), expansion potentiometer card (680832G03), display card (680829), and insert with operator devices and display window (680836)	Flolo Corporation
E9DH-19D734-CB	2	Manifold & tube assembly, provides spring lock coupling for compressor inlet and a refrigerant line to connect compressor outlet to condenser inlet	Ford Motor Company
M3219T	1	Motor, electric, 7-1/2 Hp @ 3450 RPM, 240 VAC, 3-phase, open, 184T frame, Baldor	Cox Electric Motor Service, Inc.
1" SC P.B.	2	Pillow Block, ball bearing, 1 inch shaft diameter, Dodge	Berry Bearing
Model P	1	Pitot Traverse Station, Lo-Flo, Size 3", stainless steel, 24-340 cfm, Air-Monitor	Air Filter and Equipment Corp.
Model P	1	Pitot Traverse Station, Lo-Flo, Size 8", stainless steel, 150-2160 cfm, Air-Monitor	Air Filter and Equipment Corp.
PDP-3-1000	1	Positive displacement flow meter, 0 to 95 GPH, 4-20 mA output, female 3/8" NPT, Emco. 10 microns filtration device (3-3/8")	Delta
Model 264	2	Pressure Transducer, very low differential, 0-2.5 inch wcd, 0-5 VDC output, Setra	Setra Systems, Inc.
Model C228-1	2	Pressure Transducer, high accuracy differential, 0-25 psid, 4-20 mA output, Setra	Setra Systems, Inc.
Model 207	2	Pressure Transducer, gage, 0-100 psig, 0.1-5.1 VDC output, Setra	Setra Systems, Inc.
Model 207	2	Pressure Transducer, gage, 0-500 psig, 0.1-5.1 VDC output, Setra	Setra Systems, Inc.
Model 280E	1	Pressure Transducer, absolute, 0-25 psia 0-5 VDC output, Setra	Setra Systems, Inc.
E8D26A312A	1	Pulley, serpentine, from crankshaft of 1988 3.0L V-6 Taurus	Hill Ford
1" A4.2 B4.6	1	Pulley, V-belt, 1/2", uses 1610 bushing, Dodge	Berry Bearing
N850334-S	1	Screw, connects manifold & tube assembly to compressor	Ford Motor Company
L110 SOX	2	Spiders, Lovejoy	Berry Bearing
TB-CPSS-116U	7	Thermocouple Probes, 1/16" dia., 3 inches long, copper-constantan	Omega
1805-2K-04	1	Torque sensor, high accuracy rotary transformer with speed sensor and foot mount, 0-2000 lb-in, Lebow	Comtel-Midwest
E8OH-19N651-AC	2	Tube assembly, connects condenser outlet to evaporator inlet, also houses orifice tube	Ford Motor Company

Part Number	Quantity	Description/Requirements	Supplier
SP1/4-353B-A-RF	1	Turbine flow meter, 0.1 to 1.5 GPM, 4-20 mA output, 1/2" NPT, R12 calibration, Sponsler. Sponsler modulated carrier amplifier (SP717). Sponsler multifunction rate indicator totalizer (SP2900)	Sponsler Co., Inc.

APPENDIX E

ENERGY BALANCE LEAST-SQUARES ANALYSIS PROGRAM

```
! VARIABLE UNITS
! DENSITY: LBm/FT^3
! ENTHALPY: BTU/LBm
! LENGTHS: FT
! MASS FLOW RATE: LBm/HR
! PRESSURE: PSIA
! TEMPERATURE: F

!DIMENSIONING OF THE ARRAYS
DIMPin(20),Tin(20),Pout(20),Tout(20),wr(20),Tain(20),Taout(20),wa(20)
DIM PTf(20),PTg(20),Rin(20),hin(20),Rout(20),hout(20),ERROR(20)
DIM f(20,3),Y(20),ft(3,20),ftf(3,3),ftfi(3,3),fty(3),c(3),yc(3)

!SET THE NUMBER OF TEST RUNS (NTEST) AND THE NUMBER OF COEFFICIENTS
!FOR THE LEAST-SQUARES ANALYSIS
LET NTEST = 53
LET NCOEF = 4

!ZERO AND SET ARRAY DIMENSIONS
MAT Pin = ZER(NTEST)
MAT Tin = ZER(NTEST)
MAT Pout = ZER(NTEST)
MAT Tout = ZER(NTEST)
MAT wr = ZER(NTEST)
MAT Tain = ZER(NTEST)
MAT Taout = ZER(NTEST)
MAT wa = ZER(NTEST)
MAT Rin = ZER(NTEST)
MAT hin = ZER(NTEST)
MAT Rout = ZER(NTEST)
MAT hout = ZER(NTEST)
MAT ERROR = ZER(NTEST)
MAT f = ZER(NTEST,NCOEF)
MAT Y = ZER(NTEST)
MAT ft = ZER(NCOEF,NTEST)
MAT ftf = ZER(NCOEF,NCOEF)
MAT ftfi = ZER(NCOEF,NCOEF)
MAT fty = ZER(NCOEF)
MAT c = ZER(NCOEF)
MAT yc = ZER(NTEST)
MAT PTf = ZER(NTEST)
MAT PTg = ZER(NTEST)

! OPEN TEST DATA FILE (SSDATA) AND SATURATION PRESSURE FILE (press.*)
OPEN #1: NAME "SSDATA", CREATE OLD
OPEN #2: NAME "press.2", CREATE OLD
```

```
FOR I = 1 TO NTEST

! READ IN STEADY-STATE DATA
INPUT #1: wa(I),Tain(I),Taout(I),Tin(I),Pin(I),Tout(I),Pout(I),wr(I),mcalc
INPUT #2: PTg(I),PTf(I)
LET wr(I)=mcalc

! ENTHALPY AND DENSITY CALCULATION FOR INLET REFRIGERANT
IF Pin(I) => 100 AND Pin(I) < 150 THEN
  LET P1=93.604 + 0.24060*Tin(I)
  LET P2=89.753 + 0.25033*Tin(I)
  LET hin(I) = (P2-P1)/50*(Pin(I)-100) + P1
  LET R1=2.5438 - 6.8205E-3*Tin(I) + 9.0551E-6*Tin(I)^2
  LET R2=4.2874 - 1.2955E-2*Tin(I) + 1.7892E-5*Tin(I)^2
  LET Rin(I) = (R2-R1)/50*(Pin(I)-100) + R1
END IF
IF Pin(I) => 150 AND Pin(I) < 200 THEN
  LET P1=89.753 + 0.25033*Tin(I)
  LET P2=85.697 + 0.26045*Tin(I)
  LET hin(I) = (P2-P1)/50*(Pin(I)-150) + P1
  LET R1=4.2874 - 1.2955E-2*Tin(I) + 1.7892E-5*Tin(I)^2
  LET R2=6.5649 - 2.2460E-2*Tin(I) + 3.2415E-5*Tin(I)^2
  LET Rin(I) = (R2-R1)/50*(Pin(I)-150) + R1
END IF
IF Pin(I) => 200 AND Pin(I) < 250 THEN
  LET P1=85.697 + 0.26045*Tin(I)
  LET P2=81.469 + 0.27086*Tin(I)
  LET hin(I) = (P2-P1)/50*(Pin(I)-200) + P1
  LET R1=6.5649 - 2.2460E-2*Tin(I) + 3.2415E-5*Tin(I)^2
  LET R2=9.5003 - 3.5946E-2*Tin(I) + 5.3279E-5*Tin(I)^2
  LET Rin(I) = (R2-R1)/50*(Pin(I)-200) + R1
END IF
IF Pin(I) => 250 AND Pin(I) < 300 THEN
  LET P1=81.469 + 0.27086*Tin(I)
  LET P2=76.317 + 0.28445*Tin(I)
  LET hin(I) = (P2-P1)/50*(Pin(I)-250) + P1
  LET R1=9.5003 - 3.5946E-2*Tin(I) + 5.3279E-5*Tin(I)^2
  LET R2=14.001 - 6.0446E-2*Tin(I) + 9.4074E-5*Tin(I)^2
  LET Rin(I) = (R2-R1)/50*(Pin(I)-250) + R1
END IF
IF Pin(I) => 300 AND Pin(I) < 350 THEN
  LET P1=76.317 + 0.28445*Tin(I)
  LET P2=71.607 + 0.29599*Tin(I)
  LET hin(I) = (P2-P1)/50*(Pin(I)-300) + P1
  LET R1=14.001 - 6.0446E-2*Tin(I) + 9.4074E-5*Tin(I)^2
  LET R2=19.099 - 8.7135E-2*Tin(I) + 1.3575E-4*Tin(I)^2
  LET Rin(I) = (R2-R1)/50*(Pin(I)-300) + R1
END IF
```

```
 IF Pin(I) => 350 AND Pin(I) < 400 THEN
   LET P1=71.607 + 0.29599*Tin(I)
   LET P2=65.426 + 0.31259*Tin(I)
   LET hin(I) = (P2-P1)/50*(Pin(I)-350) + P1
   LET R1=19.099 - 8.7135E-2*Tin(I) + 1.3575E-4*Tin(I)^2
   LET R2=27.963 - .14074*Tin(I) + 2.2618E-4*Tin(I)^2
   LET Rin(I) = (R2-R1)/50*(Pin(I)-350) + R1
 END IF
 IF Pin(I) => 400 AND Pin(I) < 450 THEN
   LET P1=65.426 + 0.31259*Tin(I)
   LET P2=58.297 + 0.33226*Tin(I)
   LET hin(I) = (P2-P1)/50*(Pin(I)-400) + P1
   LET R1=27.963 - .14074*Tin(I) + 2.2618E-4*Tin(I)^2
   LET R2=41.792 - .22881*Tin(I) + 3.7711e-4*Tin(I)^2
   LET Rin(I) = (R2-R1)/50*(Pin(I)-400) + R1
 END IF
 IF Pin(I) => 450 AND Pin(I) < 500 THEN
   LET P1=58.297 + 0.33226*Tin(I)
   LET P2=51.013 + 0.35200*Tin(I)
   LET hin(I) = (P2-P1)/50*(Pin(I)-450) + P1
   LET R1=41.792 - .22881*Tin(I) + 3.7711e-4*Tin(I)^2
   LET R2=63.146 - .36937*Tin(I) + 6.2032e-4*Tin(I)^2
   LET Rin(I) = (R2-R1)/50*(Pin(I)-450) + R1
 END IF

 ! ENTAHLPY AND DENSITY CALCULATION FOR OUTLET REFRIGERANT
 LET hout(I)=9.3046 + 0.3817*Tout(I) - 7.0954e-4*Tout(I)^2 + 3.6006e-6*Tout(I)^3
 LET Rout(I)=86.981 - 0.22507*Tout(I) + 1.3487e-3*Tout(I)^2 - 5.7360e-6*Tout(I)^3

 NEXT I

 ! DETERMINATION OF CONDENSER FRACTIONS

 FOR I = 1 TO NTEST
  ! INITIAL GUESS OF SAT LIQ TEMP (Tf) AND SAT VAP TEMP (Tg)
 !  LET Tf = -.67111 + .93499*Pout(I) - 1.7717e-3*Pout(I)^2 + 1.3892e-6*Pout(I)^3
 !  LET Tg = -.67111 + .93499*Pin(I) - 1.7717e-3*Pin(I)^2 + 1.3892e-6*Pin(I)^3
 !OTHERWISE USE PRESSURES FROM MOMENTUM ANALYSIS ITERATION
   LET Tf = -.67111 + .93499*PTf(I) - 1.7717e-3*PTf(I)^2 + 1.3892e-6*PTf(I)^3
   LET Tg = -.67111 + .93499*PTg(I) - 1.7717e-3*PTg(I)^2 + 1.3892e-6*PTg(I)^3
   LET hf = 9.3046 + .3817*Tf - 7.0954e-4*Tf^2 + 3.6006e-6*Tf^3
   LET hg = 99.087 + .30872*Tg - 3.0423e-3*Tg^2 + 2.1404e-5*Tg^3 - 5.8621e-8*Tg^4

 ! FILL f MATRIX BY COLUMNS
   LET Qsh = wr(I)/3600*(hg-hin(I))
   LET Qc = wr(I)/3600*(hf-hg)
   LET Qsc = wr(I)/3600*(hout(I)-hf)

 ! DESUPERHEATING SECTION BASED ON HALF THE REFRIGERANT MASS FLOW
 !RATE
   LET f(I,1)=Qsh/(  (Tain(I)+Taout(I))/2 - (Tin(I)+Tg)/2)/(wr(I)/2)^0.8
 ! CONDENSING SECTION BASED ON THE REFRIGERANT MASS FLOW RATE
   LET f(I,2)=Qc/( (Tain(I)+Taout(I))/2   - (Tg+Tf)/2)/wr(I)^0.8
```

```
! SUBCOOLING SECTION BASED ON THE REFRIGERANT MASS FLOW RATE
  LET f(I,3)=Qsc/( (Tain(I)+Taout(I))/2 - (Tf+Tout(I))/2)/wr(I)^0.8
! ALL SECTIONS BASED ON THE VOLUMETRIC AIR FLOW RATE
  LET f(I,4)=( f(I,1)*(wr(I)/2)^0.8+f(I,2)*wr(I)^0.8+f(I,3)*wr(I)^0.8 )/wa(I)^0.5

! DETERMINE Y MATRIX (SUMMATION OF THE FRACTIONS = 1)
  LET Y(I) = 1.0

 NEXT I

! CALCULATE COEFFICIENTS
MAT ft=TRN(f)
MAT ftf=ft*f
MAT fty=ft*Y
MAT ftfi=INV(ftf)
MAT c=ftfi*fty
MAT yc=f*c

!PRINT OUT COEFFICIENT MATRIX (C) AND SOLUTION MATRIX BASED ON
!LEAST-SQUARES ANALYSIS (YC)
MAT PRINT C,YC
END
```

APPENDIX F

MOMENTUM BALANCE LEAST-SQUARES ANALYSIS PROGRAM

```
! VARIABLE UNITS
! DENSITY: LBm/FT^3
! ENTHALPY: BTU/LBm
! LENGTHS: FT
! MASS FLOW RATE: LBm/HR
! PRESSURE: PSIA
! TEMPERATURE: F

!DIMENSIONING OF THE ARRAYS
DIM Pin(20),Tin(20),Pout(20),Tout(20),wr(20),Tain(20),Taout(20),wa(20),PTf(20),PTg(20)
DIM Rin(20),hin(20),Rout(20),hout(20)
DIM f(20,3),Y(20),ft(3,20),ftf(3,3),ftfi(3,3),fty(3),c(3),yc(3),FF(3)

!SET THE NUMBER OF TEST RUNS (NTEST) AND THE NUMBER OF
!COEFFICIENTS FOR THE LEAST-SQUARES ANALYSIS
LET NTEST = 53
LET NCOEF = 4

!ZERO AND SET ARRAY DIMENSIONS
MAT Pin = ZER(NTEST)
MAT Tin = ZER(NTEST)
MAT Pout = ZER(NTEST)
MAT Tout = ZER(NTEST)
MAT wr = ZER(NTEST)
MAT Tain = ZER(NTEST)
MAT Taout = ZER(NTEST)
MAT wa = ZER(NTEST)
MAT Rin = ZER(NTEST)
MAT hin = ZER(NTEST)
MAT Rout = ZER(NTEST)
MAT hout = ZER(NTEST)
MAT f = ZER(NTEST,NCOEF)
MAT Y = ZER(NTEST)
MAT ft = ZER(NCOEF,NTEST)
MAT ftf = ZER(NCOEF,NCOEF)
MAT ftfi = ZER(NCOEF,NCOEF)
MAT fty = ZER(NCOEF)
MAT c = ZER(NCOEF)
MAT yc = ZER(NTEST)
MAT PTf = ZER(NTEST)
MAT PTg = ZER(NTEST)
MAT FF = ZER(4)
```

```
!PLACE ENERGY COEFFICEINTS INTO ARRAY FF
MAT READ FF
!P=PRESS.2
DATA 213.202,110.892,458.155,115.349

! CALCULATE TUBE X-AREA
LET DIAM = 0.02083
LET AREA = PI*DIAM^2/4

! OPEN TEST DATA FILE (SSDATA) AND SATURATION PRESSURE FILE (press.*)
OPEN #1: NAME "SSDATA", CREATE OLD
OPEN #2: NAME "PRESS.2", CREATE OLD

FOR I = 1 TO NTEST

! READ IN STEADY-STATE DATA
INPUT #1: wa(I),Tain(I),Taout(I),Tin(I),Pin(I),Tout(I),Pout(I),wr(I),MCALC
INPUT #2: PTg(I),PTf(I)
LET wr(I)=MCALC

! ENTHALPY AND DENSITY CALCULATION FOR INLET REFRIGERANT
IF Pin(I) => 100 AND Pin(I) < 150 THEN
  LET P1=93.604 + 0.24060*Tin(I)
  LET P2=89.753 + 0.25033*Tin(I)
  LET hin(I) = (P2-P1)/50*(Pin(I)-100) + P1
  LET R1=2.5438 - 6.8205E-3*Tin(I) + 9.0551E-6*Tin(I)^2
  LET R2=4.2874 - 1.2955E-2*Tin(I) + 1.7892E-5*Tin(I)^2
  LET Rin(I) = (R2-R1)/50*(Pin(I)-100) + R1
END IF
IF Pin(I) => 150 AND Pin(I) < 200 THEN
  LET P1=89.753 + 0.25033*Tin(I)
  LET P2=85.697 + 0.26045*Tin(I)
  LET hin(I) = (P2-P1)/50*(Pin(I)-150) + P1
  LET R1=4.2874 - 1.2955E-2*Tin(I) + 1.7892E-5*Tin(I)^2
  LET R2=6.5649 - 2.2460E-2*Tin(I) + 3.2415E-5*Tin(I)^2
  LET Rin(I) = (R2-R1)/50*(Pin(I)-150) + R1
END IF
IF Pin(I) => 200 AND Pin(I) < 250 THEN
  LET P1=85.697 + 0.26045*Tin(I)
  LET P2=81.469 + 0.27086*Tin(I)
  LET hin(I) = (P2-P1)/50*(Pin(I)-200) + P1
  LET R1=6.5649 - 2.2460E-2*Tin(I) + 3.2415E-5*Tin(I)^2
  LET R2=9.5003 - 3.5946E-2*Tin(I) + 5.3279E-5*Tin(I)^2
  LET Rin(I) = (R2-R1)/50*(Pin(I)-200) + R1
END IF
IF Pin(I) => 250 AND Pin(I) < 300 THEN
  LET P1=81.469 + 0.27086*Tin(I)
  LET P2=76.317 + 0.28445*Tin(I)
  LET hin(I) = (P2-P1)/50*(Pin(I)-250) + P1
  LET R1=9.5003 - 3.5946E-2*Tin(I) + 5.3279E-5*Tin(I)^2
  LET R2=14.001 - 6.0446E-2*Tin(I) + 9.4074E-5*Tin(I)^2
  LET Rin(I) = (R2-R1)/50*(Pin(I)-250) + R1
END IF
```

```
IF Pin(I) => 300 AND Pin(I) < 350 THEN
  LET P1=76.317 + 0.28445*Tin(I)
  LET P2=71.607 + 0.29599*Tin(I)
  LET hin(I) = (P2-P1)/50*(Pin(I)-300) + P1
  LET R1=14.001 - 6.0446E-2*Tin(I) + 9.4074E-5*Tin(I)^2
  LET R2=19.099 - 8.7135E-2*Tin(I) + 1.3575E-4*Tin(I)^2
  LET Rin(I) = (R2-R1)/50*(Pin(I)-300) + R1
END IF
IF Pin(I) => 350 AND Pin(I) < 400 THEN
  LET P1=71.607 + 0.29599*Tin(I)
  LET P2=65.426 + 0.31259*Tin(I)
  LET hin(I) = (P2-P1)/50*(Pin(I)-350) + P1
  LET R1=19.099 - 8.7135E-2*Tin(I) + 1.3575E-4*Tin(I)^2
  LET R2=27.963 - .14074*Tin(I) + 2.2618E-4*Tin(I)^2
  LET Rin(I) = (R2-R1)/50*(Pin(I)-350) + R1
END IF
IF Pin(I) => 400 AND Pin(I) < 450 THEN
  LET P1=65.426 + 0.31259*Tin(I)
  LET P2=58.297 + 0.33226*Tin(I)
  LET hin(I) = (P2-P1)/50*(Pin(I)-400) + P1
  LET R1=27.963 - .14074*Tin(I) + 2.2618E-4*Tin(I)^2
  LET R2=41.792 - .22881*Tin(I) + 3.7711e-4*Tin(I)^2
  LET Rin(I) = (R2-R1)/50*(Pin(I)-400) + R1
END IF
IF Pin(I) => 450 AND Pin(I) < 500 THEN
  LET P1=58.297 + 0.33226*Tin(I)
  LET P2=51.013 + 0.35200*Tin(I)
  LET hin(I) = (P2-P1)/50*(Pin(I)-450) + P1
  LET R1=41.792 - .22881*Tin(I) + 3.7711e-4*Tin(I)^2
  LET R2=63.146 - .36937*Tin(I) + 6.2032e-4*Tin(I)^2
  LET Rin(I) = (R2-R1)/50*(Pin(I)-450) + R1
END IF

! ENTAHLPY AND DENSITY CALCULATION FOR OUTLET REFRIGERANT
LET hout(I)=9.3046 + 0.3817*Tout(I) - 7.0954e-4*Tout(I)^2 + 3.6006e-6*Tout(I)^3
LET Rout(I)=86.981 - 0.22507*Tout(I) + 1.3487e-3*Tout(I)^2 - 5.7360e-6*Tout(I)^3

NEXT I

! DETERMINATION OF PRESSURE DROPS IN EACH CONDENSER SECTION
FOR I = 1 TO NTEST
! INITIAL GUESS OF SAT LIQ TEMP (Tf) AND SAT VAP TEMP (Tg)
!  LET Tf = -.67111 + .93499*Pout(I) - 1.7717e-3*Pout(I)^2 + 1.3892e-6*Pout(I)^3
!  LET Tg = -.67111 + .93499*Pin(I) - 1.7717e-3*Pin(I)^2 + 1.3892e-6*Pin(I)^3
!OTHERWISE USE PRESSURES FROM MOMENTUM ANALYSIS ITERATION
 LET Tf = -.67111 + .93499*PTf(I) - 1.7717e-3*PTf(I)^2 + 1.3892e-6*PTf(I)^3
 LET Tg = -.67111 + .93499*PTg(I) - 1.7717e-3*PTg(I)^2 + 1.3892e-6*PTg(I)^3
 LET RHOf = 86.981 - 0.22507*Tf + 1.3487e-3*Tf^2 - 5.7360e-6*Tf^3
 LET RHOg = 3.6627 - 0.16724*Tg + 3.3187e-3*Tg^2 - 2.3166e-5*Tg^3 + 6.1405e-8*Tg^4
 LET hf = 9.3046 + .3817*Tf - 7.0954e-4*Tf^2 + 3.6006e-6*Tf^3
 LET hg = 99.087 + .30872*Tg - 3.0423e-3*Tg^2 + 2.1404e-5*Tg^3 - 5.8621e-8*Tg^4
```

```
! FILL f MATRIX BY COLUMNS
!CALCULATE FRACTIONS OF EACH SECTION BASED ON ENERGY LEAST-SQUARES
!ANALYSIS
  LET Qsh = wr(I)/3600*(hg-hin(I))
  LET Qc = wr(I)/3600*(hf-hg)
  LET Qsc = wr(I)/3600*(hout(I)-hf)

  LET z1=Qsh/(  (Tain(I)+Taout(I))/2 - (Tin(I)+Tg)/2)/(wr(I)/2)^0.8
  LET z2=Qc/( (Tain(I)+Taout(I))/2   - (Tg+Tf)/2)/wr(I)^0.8
  LET z3=Qsc/( (Tain(I)+Taout(I))/2 - (Tf+Tout(I))/2)/wr(I)^0.8

LET Fsh = FF(1)*z1 + FF(4)*z1/wa(I)^0.5*(wr(I)/2)^0.8
LET Fc  = FF(2)*z2 + FF(4)*z2/wa(I)^0.5*wr(I)^0.8
LET Fsc = FF(3)*z3 + FF(4)*z3/wa(I)^0.5*wr(I)^0.8

!CALCULATE PRESSURE DROPS FOR EACH OF THE THREE SECTIONS

!DESUPERHEATING SECTION AT HALF THE MASS FLOW RATE
LET f(I,1)=Fsh*(wr(I)/2/3600)^2/DIAM/2/Rin(I)/AREA^2 *(1/(wr(I)/2/3600)^0.237)
!CONDENSING SECTION AT HALF THE MASS FLOW RATE
LET f(I,2)=(1/3-Fsh)*(wr(I)/2/3600)^2/DIAM/2/RHOg/AREA^2 *(1/(wr(I)/2/3600)^0.237)
!CONDENSING SECTION AT THE MASS FLOW RATE
LET f(I,2)=f(I,2)+(Fc-(1/3-Fsh))*(wr(I)/3600)^2/DIAM/2/RHOg/AREA^2
*(1/(wr(I)/3600)^0.237)
!SUBCOOLING SECTION AT THE MASS FLOW RATE
LET f(I,3)=Fsc*(wr(I)/3600)^2/DIAM/2/RHOf/AREA^2 *(1/(wr(I)/3600)^0.25)
!CONSTANT FOR THE DESUPERHEATING AND CONDENSING SECTIONS
LET f(I,4)=Fsh*(wr(I)/2/3600)^2/DIAM/2/Rin(I)/AREA^2
LET f(I,4)=f(I,4)+(1/3-Fsh)*(wr(I)/2/3600)^2/DIAM/2/RHOg/AREA^2
LET f(I,4)=f(I,4)+(Fc-(1/3-Fsh))*(wr(I)/3600)^2/DIAM/2/RHOg/AREA^2

! DETERMINE Y MATRIX (INLET AND OUTLET PRESSURE DROP AND MOMENTUM
!TERMS)

  LET xx = Pin(I)*32.2*144 + (wr(I)/2/3600)^2/AREA^2/Rin(I)
  LET Y(I) = xx - Pout(I)*32.2*144 - (wr(I)/3600)^2/AREA^2/Rout(I)

NEXT I

! CALCULATE COEFFICIENTS
MAT ft=TRN(f)
MAT ftf=ft*f
MAT fty=ft*Y
MAT ftfi=INV(ftf)
MAT c=ftfi*fty
MAT yc=f*c

!PRINT OUT COEFFICIENT MATRIX (C) AND SOLUTION MATRIX BASED ON
!LEAST-SQUARES ANALYSIS (YC)
MAT PRINT C,YC

!OPEN FILE TO STORE THE NEW SATURATION PRESSURES
OPEN #3: NAME "press.*", CREATE NEWOLD
ERASE #3
```

```
! CHECK PRESSURE DROP CALCULATION WITH SECTIONAL MOMENTUM
!EQUATIONS
FOR I = 1 TO NTEST
! INITIAL GUESS OF SAT LIQ TEMP (Tf) AND SAT VAP TEMP (Tg)
!  LET Tf = -.67111 + .93499*Pout(I) - 1.7717e-3*Pout(I)^2 + 1.3892e-6*Pout(I)^3
!  LET Tg = -.67111 + .93499*Pin(I) - 1.7717e-3*Pin(I)^2 + 1.3892e-6*Pin(I)^3
!OTHERWISE USE PRESSURES FROM MOMENTUM ANALYSIS ITERATION
  LET Tf = -.67111 + .93499*PTf(I) - 1.7717e-3*PTf(I)^2 + 1.3892e-6*PTf(I)^3
  LET Tg = -.67111 + .93499*PTg(I) - 1.7717e-3*PTg(I)^2 + 1.3892e-6*PTg(I)^3
  LET RHOf = 86.981 - 0.22507*Tf + 1.3487e-3*Tf^2 - 5.7360e-6*Tf^3
  LET RHOg = 3.6627 - 0.16724*Tg + 3.3187e-3*Tg^2 - 2.3166e-5*Tg^3 + 6.1405e-8*Tg^4
  LET hf = 9.3046 + .3817*Tf - 7.0954e-4*Tf^2 + 3.6006e-6*Tf^3
  LET hg = 99.087 + .30872*Tg - 3.0423e-3*Tg^2 + 2.1404e-5*Tg^3 - 5.8621e-8*Tg^4

!CALCULATE FRACTIONS OF EACH SECTION BASED ON ENERGY LEAST-SQUARES
!ANALYSIS
  LET Qsh = wr(I)/3600*(hg-hin(I))
  LET Qc = wr(I)/3600*(hf-hg)
  LET Qsc = wr(I)/3600*(hout(I)-hf)

  LET z1=Qsh/(  (Tain(I)+Taout(I))/2 - (Tin(I)+Tg)/2)/(wr(I)/2)^0.8
  LET z2=Qc/( (Tain(I)+Taout(I))/2   - (Tg+Tf)/2)/wr(I)^0.8
  LET z3=Qsc/( (Tain(I)+Taout(I))/2 - (Tf+Tout(I))/2)/wr(I)^0.8

  LET Fsh = FF(1)*z1 + FF(4)*z1/wa(I)^0.5*(wr(I)/2)^0.8
  LET Fc  = FF(2)*z2 + FF(4)*z2/wa(I)^0.5*wr(I)^0.8
  LET Fsc = FF(3)*z3 + FF(4)*z3/wa(I)^0.5*wr(I)^0.8

  LET FFsh = c(1)*1/(wr(I)/2/3600)^0.237 + c(4)
  LET FFc = c(2)*1/(wr(I)/2/3600)^0.237 +c(4)
  LET FFsc = c(3)*1/(wr(I)/3600)^0.25

!CALCULATE DESUPERHEATING PRESSURE DROP AT HALF THE MASS FLOW RATE
LET dPsh = -(wr(I)/3600/2)^2/AREA^2*(1/Rin(I)-1/RHOg-Fsh/DIAM/2/Rin(I)*(c(4)+c(1)*
(1/(wr(I)/2/3600)^0.237)))
!CALCULATE CONDENSING PRESSURE DROP AT HALF THE MASS FLOW RATE
LET dPc = (wr(I)/3600/2)^2/AREA^2*(-1/RHOg+(1/3-fsh)/DIAM/2/RHOg*(c(4)+c(2)*
(wr(I)/3600/2)^(-0.237)))
!CALCULATE CONDENSING PRESSURE DROP AT THE MASS FLOW RATE
LET dPc = dPc+(wr(I)/3600)^2/AREA^2*(1/RHOf+(fc-(1/3-fsh))/DIAM/2/RHOg*(c(4)+c(2)*
(wr(I)/3600)^(-0.237)))
!CALCULATE SUBCOOLING PRESSURE DROP AT THE MASS FLOW RATE
LET dPsc = (wr(I)/3600)^2/AREA^2*(1/Rout(I)-1/RHOf+(c(3)*(1/(wr(I)/3600)^0.25))
*Fsc/DIAM/2/RHOf)

!DETERMINE PRESSURE DROP FROM TEST RUNS
LET delPtest = Pin(I)-Pout(I)
!CONVERT PRESSURE DROP TO psia AND DETERMINE THE TOTAL PRESSURE DROP
LET dPsh = dPsh/32.2/144
LET dPc  = dPc/32.2/144
LET dPsc = dPsc/32.2/144
LET Ptot = dPsh + dPc + dPsc
```

```
!PRINT THE NEW VAPOR AND LIQUID PRESSURE TO THE FILE
PRINT #3: Pin(I)-dPsh/Ptot*delPtest;",";Pout(I)+dPsc/Ptot*delPtest

NEXT I
END
```

REFERENCES

1. Ellison, R.D., F.A. Creswick, C.K. Rice, W.L. Jackson, and S.K. Fischer, "Heat Pump Modeling: A Progress Report," 4th Annual Heat Pump Technology Conference, Oklahoma State University, April 1979.

2. Davis, G.L., and T.C. Scott, "Component Modeling Requirements for Refrigeration System Simulation," Proceedings of the 1976 Purdue Compressor Technology Conference, Purdue University, pp. 401-408.

3. Davis, G.L., F. Chianese Jr., and T.C. Scott, "Computer Simulation of Automotive Air Conditioning - Components, System, and Vehicle," 1972 SAE Congress Paper 720077.

4. Martin, D.L., Digital Computer Simulation of Water-Source Heat Pump Performance, University of Illinois at Urbana-Champaign, 1981.

5. Kays, W.M., and A.L. London, Compact Heat Exchangers, 3rd Edition, McGraw-Hill, New York, 1984.

6. Dusinberre, G.M., "Calculation of Transients in a Cross-Flow Heat Exchanger," ASME Journal of Heat Transfer, Vol. 81, Feb. 1959, pp. 61-67.

7. Myers, G.E., J.W. Mitchell, and R.F. Norman, "The Transient Response of Crossflow Heat Exchangers, Evaporators, and Condensers," ASME Journal of Heat Transfer, Vol. 89, Feb. 1967, pp.75-80.

8. Myers, G.E., J.W. Mitchell, and C.F. Lindeman Jr., "The Transient Response of Heat Exchangers Having an Infinite Capacitance Rate Fluid," ASME Journal of Heat Transfer, Vol. 92, May 1970, pp. 269-275.

9. Yamashita, H., R. Izumi, and S. Yamaguchi, "Analysis of the Dynamic Characteristics of Cross-flow Heat Exchangers With Both Fluids Unmixed," Bulletin of the JSME, Vol. 21, No. 153, March 1978, pp. 479-485.

10. Romie, F.E., "Transient Response of Gas-to-Gas Crossflow Heat Exchangers With Neither Gas Mixed," ASME Journal of Heat Transfer, Vol. 105, Aug 1983, pp. 563-570.

11. Gvozdenac, D.D., "Analytical Solution of the Transient Response of Gas-to-Gas Crossflow Heat Exchanger With Both Fluids Unmixed," ASME Journal of Heat Transfer, Vol. 108, Nov. 1986, pp. 722-727.

12. Spiga, G., and M. Spiga, "Two-Dimensional Transient Solutions for Crossflow Heat Exchangers With Neither Gas Mixed," ASME Journal of Heat Transfer, Vol. 109, May 1987, pp.281-286.

13. Wedekind, G.L., B.L. Bhatt, and B.T. Beck, "A System Mean Void Fraction Model for Predicting Various Transient Phenomena Associated With Two-Phase Evaporating and Condensing Flows," International Journal of Multiphase Flow, Vol. 4, 1978, pp. 97-114.

14. Gartner, J.R., and H.L. Harrison, "Dynamic Characteristics of Water-to-Air Crossflow Heat Exchangers," ASHRAE Transactions, Vol. 71, 1965, pp. 212-224.

15. Schoenberg, A. A., "Mathematical Model With Experimental Verification for the Dynamic Behavior of a Single-Tube Condenser," Nasa Tech Note, 1966, D-3453, pp. 1-51.

16. Neckowicz, T.S., W.E. Murphy, V.W. Goldschmidt, and R.C.R. Johnston, "A Note on One Aspect of the Transient Response of Package Air Conditioners: Flooding of the Liquid Line," ASHRAE Transactions, Vol. 90, Part 1A, 1984, pp. 179-184.

17. Tanaka, N., M. Ikeuchi, and G. Yamanaka, "Experimental Study on the Dynamic Characteristics of a Heat Pump," ASHRAE Transactions, Vol. 88, Part 2, 1982, pp. 323-330.

18. Mulroy, W.J., and D.A. Didion, "Refrigeration Migration in a Split-Unit Air Conditioner," ASHRAE Transactions, Vol. 91, Part 1A, 1985, pp. 193-206.

19. Miller, W.A., "The Laboratory Evaluation of the Heating Mode Part-Load Operation of an Air-to-Air Heat Pump," ASHRAE Transactions, Vol. 91, Part 2A, 1985, pp. 524-535.

20. Belth, M.I., and D.R. Tree, "Design and Preliminary Analysis for Measuring Transient Mass Rate of Flow in Unitary Heat Pumps," ASHRAE Transactions, Vol. 92, Part 1B, 1986, pp. 843-853.

21. Josiassen, N.J., "Simulation of Condition Sequence During Start-Up of an Evaporation Refrigerating System," Proceedings of the 1978 Purdue Compressor Technology Conference, Purdue University, pp. 309-316.

22. Murphy, W.E., and V.W. Goldschmidt, "Cyclic Characteristics of a Typical Residential Air Conditioner - Modeling of Start-Up Transients," ASHRAE Transactions, Vol. 91, Part 2a, 1985, pp. 427-444.

23. Murphy, W.E., and V.W. Goldschmidt, "Cycling Characteristics of a Residential Air Conditioner - Modeling of Shutdown Transients," ASHRAE Transactions, Vol. 92, Part 1A, 1986, pp. 186-202.

24. Dhar, M., and W. Sodel, "Transient Analysis of a Vapor Compression Refrigeration System: Part 1 - The Mathematical Model," 15th International Congress of Refrigeration, Vol. 2, Venice, Sept. 23-29, 1979.

25. Dhar, M., and W. Sodel, "Transient Analysis of a Vapor Compression Refrigeration System: Part 2 - Computer Simulation and Results," 15th International Congress of Refrigeration, Vol. 2, Venice, Sept. 23-29, 1979.

26. Chi, J., and D. Didion, "A Simulation Model of the Transient Performance of a Heat Pump," International Journal of Refrigeration, Vol. 5, No. 3, May 1982, pp 176-184.

27. MacArthur, J.W., "Analytical Representation of the Transient Interactions in Vapor Compression Heat Pumps," ASHRAE Transactions, Vol. 90, Part 1B, 1984, pp.982-996.

28. White, F.M., Fluid Mechanics, 2nd Edition, McGraw-Hill, New York, 1986.

29. McLinden, M.O., J.S. Gallagher, L.A. Weber, G. Morrison, D. Ward, A.R.H. Goodwin, M.R. Moldover, J.W. Schmidt, H.B. Chae, T.J. Bruno, J.F. Ely, M.L. Huber, "Measurement and Formulation of the Thermodynamic Properties of Refrgierants 134a

(1,1,1,2 - Tetraflouroethane) and 123 (1,1 - Dichloro - 2,3,2 - Triflourethane)," ASHRAE Transactions, Vol. 96, Part 1, 1990.

30. "Condensers," *1983 ASHRAE Handbook and Product Directory - Equipment Handbook*, American Society of Heating, Refrigerating, and Air Conditioning Engineers, Atlanta, 1982.

31. Stoecker, W.F., Design of Thermal Systems, McGraw-Hill, New York, 1980, pp. 115-123.

32. Stoecker, W.F. and Jones, J.W., Refrigeration and Air Conditioning, McGraw-Hill, New York, 1986, pp. 233-252.

33. Eckels, S.J. and Pate, M.B., "A Comparison of R-134a and R-12 In-Tube Heat Transfer Coefficients Based on Existing Correlations," ASHRAE Transactions, Vol. 96, Part1, 1990.

34. "Fluid Flow," *1989 ASHRAE Handbook and Product Directory - Fundamentals Handbook*, American Society of Heating, Refrigerating, and Air Conditioning Engineers, Atlanta, 1989.

35. Michael, T.A., Design of an Automotive Air Conditioning Test Stand for Screening and Transient Studies, University of Illinois at Urbana-Champaign, 1989.